Numerical Simulations of Atherosclerotic Plaque Growth Using Experimental Data

Carolina Brites Ramos

Thesis to obtain the Master of Science Degree in

Biomedical Engineering

Supervisors: Dr. Jorge Filipe Duarte Tiago and Dr. Ana Rosa Miranda dos Santos Silva Herdade

Examination Committee

Chairperson: Dr. Maria do Rosário De Oliveira Silva
Supervisor: Dr. Jorge Filipe Duarte Tiago
Members of the Committee: Dr. Ana Leonor Mestre Vicente Silvestre

November 2018

Resumo

Palavras-Chave: Placa aterosclerótica, modelação matemática, equações adveção-reação-difusão, análise de sensibilidade, microscopia intravital

A aterosclerose é uma doença cardiovascular caracterizada pela formação e progressão de uma placa lipídica na camada interna da parede arterial (íntima). Originada por uma longa inflamação crónica, a lesão aterosclerótica é protagonizada por diferentes agentes biológicos consoante a fase de desenvolvimento. Para uma melhor compreensão desta patologia, o presente estudo combina métodos matemáticos, experimentais e computacionais.

De modo a visualizar o crescimento da placa, é sugerido um novo modelo matemático baseado em estudos anteriores para descrever, através de equações diferenciais parciais (EDPs), as células e espécies que intervêm na aterosclerose. O nosso foco reside na forma como a acumulação contínua das células massivas (macrófagos, células espumosas e musculares lisas) e fibras de colagéno é modelada na íntima.

Para determinar parâmetros do modelo, realizou-se um procedimento experimental em ratinhos saudáveis. Recorreu-se a microscopia intravital para avaliar a aderência ao endotélio dos monócitos circulantes e posterior transmigração (evento determinante na aterogénese). Assim, a metodologia descrita pode ser objeto de estudo de trabalho futuro na monitorização de estenose arterial em ratinhos ateroscleróticos.

Para observar o crescimento da placa em geometrias simplificadas durante tempos biológicos relevantes, implementou-se o modelo proposto na secção longitudinal idealizada da coronária descendente anterior esquerda (DAE) e, posteriormente, numa geometria mais realista da bifurcação coronária esquerda. Finalmente, para além do estudo da sua origem (experimental ou estimada), procedeu-se a uma análise de sensibilidade aos parâmetros utilizados no modelo. Os resultados revelam consistência com os observados na literatura, porém, a utilização de parâmetros fisiológicos humanos ainda permanece um desafio.

Abstract

Keywords: Atherosclerotic plaque, mathematical modelling, advection-reaction-diffusion equations, sensitivity analysis, intravital microscopy

Atherosclerosis is a cardiovascular disease (CVD) characterized by the formation and progression of a lipid plaque inside the arterial wall innermost layer (intima). Originated by a long chronic inflammation, the atherosclerotic lesion is starred by different biological agents according to the stage of plaque development. For a better understanding of this pathology, the present study combines mathematical, experimental and computational approaches.

Aiming at visualizing plaque growth, a novel mathematical approach is suggested, starting from previous studies to describe, through partial differential equations (PDEs), cells and species which intervene in atherosclerosis. Our focus regards the way the continuous accumulation of massive cells (macrophages, foam cells and smooth muscle cells) and collagen fibres are modeled inside the intima.

To access model parameters, an experimental approach was performed on healthy mice models. We resorted to intravital microscopy to record luminal monocytes endothelial adherence and posterior transmigration (a crucial event during atherogenesis). Thus, the described procedure should be the subject for future work on arterial stenosis monitorization in atherosclerotic mice.

Besides, to evaluate plaque growth on simplified geometries during relevant biological lifetimes, the proposed model was implemented in an idealized longitudinal section of a left anterior descending (LAD) artery and, afterward, in a more realistic geometry of left coronary bifurcation. Finally, apart from accessing their origin (experimental or estimated), a sensitivity analysis of our model parameters is also provided. Results show robust consistency with literature; however, the use of accurate human physiological parameters still remains a challenge.

Acknowledgments

I must start by expressing my sincere gratitude towards Doctor Jorge Tiago, for the tireless help, even when my little doubts meant long meetings. Thank you for teaching me so much about numerical and computational methods but, most important, thank you for training me to think out of the box. That is something I will carry throughout my life.

Secondly, I would like to thank Professor Adélia Sequeira for all the encouragement and for the availability in giving me new ideas, thus, guiding me during this investigation. Collaborating with Professor Adélia and Doctor Jorge Tiago was a real privilege.

I also want to thank Doctor Ana Herdade, for all the kindness and availability in helping me on this experimental procedure, as well as for her care and sympathy. I am sincerely grateful for having worked with you.

I want to thank my amazing course colleagues, in particular, Teresa Cardoso, for your help and friendship. I would like to thank my boyfriend for always believing in me and for teaching me to believe in myself. Also, I must thank my brother not only because he begged me but also because he deserves it.

Finally, I must thank my parents for being my best friends, for supporting and advising me during this troubled journey but, above all, for the rigorous education, always prioritizing excellence in our academic and personal formation.

Contents

Resumo ..... **ii**

Abstract ..... **iv**

Acknowledgments ..... **vi**

Contents ..... **viii**

List of Figures ..... **x**

List of Tables ..... **xii**

1. Introduction **1**

1.1. Motivation – main problems 1

1.2. Objectives of the thesis 2

1.3. Methodology 3

1.4. Thesis outline 4

2. State of the Art **6**

2.1. Anatomy and Physiopathology of Atherosclerosis 6

2.1.1. The human Cardiovascular System 6
2.1.2. Atherosclerosis – main protagonists 8
2.1.3. Atherosclerosis – a brief insight 14

2.2. Current Mathematical Models for Atherosclerosis 17

2.2.1. Endothelial Dysfunction and Fatty Streak 18
2.2.2. Fibrofatty Injury and Plaque Maturity 21

2.3. Open questions when modeling atherosclerosis 26

3. Methodology **28**

3.1. Experimental Model 28

3.1.1. Animals 28
3.1.2. Intravital Imaging 28
3.1.3. Blood Quantification 29

3.2. Mathematical Model – A New Approach 29

3.2.1. Simplified Model 31
3.2.2. Modeling atherosclerosis main protagonists inside the intima 31
3.2.3. Plaque Growth inside the intima 38
3.2.4. Governing equations for blood flow inside the lumen 40

3.3. Numerical Methods 41
3.3.1. Mesh Settings 44
3.3.2. Deformed Geometry 45
3.4. Parameters selection 46
3.4.1. Domain Parameters 46
3.4.2. Model Parameters 46
3.5. Sensitivity Analysis 50

4. Results and Discussion 52

4.1. Experimental Results 52
4.2. Numerical Simulations 54
4.2.1. Concentration evolution of species inside the intima 55
4.2.3. More complex geometry 66
4.3. Sensitivity Analysis 71

5. Limitations and Future Work 75

5.1. Limitations of the proposed model 75
5.2. Plans for future work 76

References 79

Appendix A 88

Appendix B 89

Appendix C 91

Appendix D 92

Appendix E 93

List of Figures

Figure 1 - Inside view on the arterial wall. Font: from *https://www.researchgate.net/publication/286948064_SASH1_a_new_potential_link_between_smoking_and_atherosclerosis/figures?lo=1.* 7

Figure 2 – General picture of atherosclerotic plaque growth with the formation of a luminal stenosis. Font: from [79]. 8

Figure 3 - Atherosclerosis schematics showing the main events during plaque genesis and development: LDL and monocytes entrance inside the intima layer, endothelial activation, monocytes differentiation into macrophages, foam cells formation, cytokines production by ECs, macrophages and foam cells and SMCs migration into the intima layer. Font: from [8]. 14

Figure 4 - Diagram of atherosclerosis pathogenesis – stages of plaque development and specific processes during those stages. Font: from [75]. 15

Figure 5 - Three-dimensional geometry of the model. The lumen and the intima were denoted by $\Omega \mathrm{l}$, $\Omega \mathrm{i} \subset \mathrm{R3}$, and their boundaries were defined as $\partial\Omega \mathrm{l} = \Gamma \mathrm{l}, \mathrm{in} \cup \Gamma \mathrm{end} \cup \Gamma \mathrm{l}, \mathrm{out}$ and $\partial\Omega \mathrm{i} = \Gamma \mathrm{i}, \mathrm{in} \cup \Gamma \mathrm{end} \cup \Gamma \mathrm{med} \cup \Gamma \mathrm{i}, \mathrm{out}$, respectively. $\Gamma \mathrm{end}$ stands for the interface between the intima and the lumen, whereas $\Gamma \mathrm{end}$ stands for the interface between the intima and the media. Finally, $\Gamma \mathrm{l}, \mathrm{in}/\Gamma \mathrm{i}, \mathrm{in}$ and $\Gamma \mathrm{l}, \mathrm{out}/\Gamma \mathrm{i}, \mathrm{out}$ are, respectively, the proximal and distal sections of both domains. 22

Figure 6 - Illustration of our simple computational domain, where $\Omega \mathrm{l}$ represents the lumen, $\Omega \mathrm{i}$ the intima, $\Gamma \mathrm{l}, \mathrm{in}$ and $\Gamma \mathrm{l}, \mathrm{out}$ the inlet and outlet luminal boundaries (respectively) and, finally, $\Gamma \mathrm{end}$ and $\Gamma \mathrm{med}$ stand for the endothelial and media boundaries (respectively)..... 31

Figure 8 - Zoom view of the intima spatial discretization, with closer triangles near $\Gamma \mathrm{end}$ (similar for $\Gamma \mathrm{med}$). 45

Figure 7 - Spatial discretization applied to our intima domain ($39\,900$ elements)..... 45

Figure 9 - Illustration of our computational blood vessel, with an intima layer with $0.034\ \mathrm{cm}$ of height and a lumen with a $0.37\ \mathrm{cm}$ diameter..... 46

Figure 10 - Anesthesia procedure: administration of a cocktail of xylazine/ketamine ($0.1\ \mathrm{mL}/10\ \mathrm{g}$ of BW). 52

Figure 11 - Preparation of accurate instruments for the surgical procedure support (left) and the Krebs-Henseleit buffer with $NaHCO_3$ at 37°C bubbled with 95% N_2 and 5% CO_2 (right)..... 52

Figure 12 - Initial cut on the mouse peritoneal cavity (left) to push organs to the side, allowing the abdominal aorta exposure (right). 53

Figure 13 - The mouse is placed on the top of the platina in a multi-photon confocal microscope Leica SP8 MP (Leica, Germany) adapted for intravital fluorescent microscopy. 53

Figure 14 - Abdominal aorta intravital microscopy sequence of images (A – D). White dashed lines indicate the arterial walls and green dots correspond to rolling and some adherent neutrophils. 54

Figure 15 - Concentration evolution of oxLDL inside the intima for times $\mathrm{t} = 0\ \mathrm{s}$, $\mathrm{t} = 79\,000\,000\ \mathrm{s}$ and $\mathrm{t} = 157\,680\,000\ \mathrm{s}$. 56

Figure 16 - Concentration evolution of MCP-1 inside the intima for times $\mathrm{t} = 0\ \mathrm{s}$, $\mathrm{t} = 79\,000\,000\ \mathrm{s}$ and $\mathrm{t} = 157\,680\,000\ \mathrm{s}$. 57

Figure 17 - Influence of MCP-1 on the endothelial permeability to monocytes (a) and LDL (b) for times $t = 6\,000\,000\ s$, $t = 78\,700\,000\ s$ and $t = 100\,000\,000\ s$. 57

Figure 18 - Concentration evolution of macrophages inside the intima for times $t = 0\ s$, $t = 79\,000\,000\ s$ and $t = 157\,680\,000\ s$. 58

Figure 19 - Macrophages chemotactic motion in response to MCP-1 gradient (represented by the arrows) for 59

Figure 20 - Concentration evolution of foam cells inside the intima for times $t = 0\ s$, $t = 79\,000\,000\ s$ and $t = 157\,680\,000\ s$. 60

Figure 21 - Evolution of atherosclerotic plaque growth velocity (represented by the arrows) for times $t = 0\ s$, $t = 82\,800\,000\ s$ and $t = 165\,640\,000\ s$. 61

Figure 22 - Zoom view of intima growth velocity (represented by the arrows) at the endothelial upper left corner (a) and at the endothelial middle (b) for $t = 165\,640\,000\ s$. 62

Figure 23 - Concentration evolution of PDGF inside the intima for times $t = 0\ s$, $t = 150\,000\,000\ s$ and $t = 157\,680\,000\ s$. 63

Figure 24 - Concentration evolution of SMCs inside the intima for times: $t = 79\,000\,000\ s$, where SMCs intima concentration (a) and a zoom at SMCs media influx (b) are represented; $t = 170\,020\,000\ s$ shows the maximum reached SMCs intima concentration; finally, $t = 189\,320\,000\ s$ portrays SMCs singularity, verified at the end of our simulation. 64

Figure 25 - SMCs motion in response to MCP-1 (a) and PDGF (b) gradients for $t = 79\,000\,000\ s$. 64

Figure 26 - Concentration evolution of collagen inside the intima for times $t = 157\,820\,000\ s$, $t = 169\,020\,000\ s$ and $t = 176\,020\,000\ s$. For $t = 189\,320\,000\ s$, the obtained collagen singularity is shown. 66

Figure 27 - Illustration of the LM coronary artery bifurcation into LAD and LCx arteries, where dimensions and angles were taken from[126]. The red arrows stand for blood flow direction; thus, the inlet boundary is placed at LM artery whereas the outlets are located at the end of LCx and LAD branches. 67

Figure 28 - Spatial discretization applied to the subdomains ($20\,271$ elements inside the lumen domain and $61\,896$ elements inside the intima domain). 67

Figure 29 - Representation of the endothelial region (highlighted in red) where WSS magnitude was computed (a) and WSS magnitude evolution along the given endothelial region (b). 68

Figure 30 - Zoom view of WSS magnitude evolution along the given endothelial region. 68

Figure 31 - Blood velocity magnitude inside LM coronary artery bifurcation with its streamlines profile. 69

Figure 32 - Blood pressure inside the LM coronary artery bifurcation. 69

Figure 33 - Influence of WSS on the endothelial permeability to circulating LDL particles (a) and monocytes (b). 70

Figure 34 - LM coronary bifurcation displaying atherosclerosis intima protagonists until Stage II, that is, oxLDL (a), macrophages (b), MCP-1 (c) and foam cells (d) for time $t = 47\,304\,000\ s$. 71

Figure 35 - Scheme of our suggestion for future work on media boundary conditions of Stokes equations. 77

List of Tables

Table 1 - Summary of the state of the art on atherosclerosis modeling and limitations of existing models. Stages are divided in: Endothelial Dysfunction (I), Fatty Streak (II), Fibrofatty Lesion (III), Fibrous and Mature Plaque (IV). 26

Table 2 - Summary of the parameters used in the model. In the “Experimental” column, “A” stands for animal model and “H” for human model. 47

Table 3 - Summary of the obtained results from sensitivity analysis to our model parameters. Average normalized sensitivity values (in percentage) are provided as well as parameters respective origin (experimental, estimated or adapted). Critical parameters (minimum absolute sensitivity value of 50%) are highlighted. 72

Table 4 - Distribution of each parameter origin (experimental, estimated or adapted) between two categories of normalized average sensitivity values: high (≥50%) and low (<50%). 74

1. Introduction

1.1. Motivation – main problems

Despite changes in our lifestyle and the incoming of new pharmacologic solutions, Cardiovascular Diseases (CVDs) remain the leading cause of morbidity and mortality worldwide. In fact, data given by the World Health Organization says that 33% of all global deaths were caused by CVDs in 2016, with a strong tendency to increase over the following years [1], [2], [3]. In Portugal, nowadays, CVDs are responsible for more than 30% of mortality per year [4]. Giving this prevalence numbers, it is not surprising that significant funds are dedicated to the study of this pathophysiology.

Cardiovascular Diseases correspond to chronic disorders of the heart and blood vessels, including peripheral arterial disease, coronary heart disease and rheumatic heart disease. Moreover, those illnesses may, eventually, cause clinical events (such as myocardial infarction or stroke) due to the formation of blood clots inside blood vessels, preventing blood from arriving to the heart or brain, respectively. Blood clots, in turn, are characterized by an acute accumulation of high concentrations of low-density lipoprotein (LDL) cholesterol and cellular debris inside the innermost layer of blood vessel walls, the intima layer [5], [1].

Asymptomatic at the beginning, atherosclerosis is a specific type of arteriosclerosis, which is the general term for the hardening of human arteries. Resulting in the long formation and progression of a lipid plaque inside the intima, it is characterized by a continuous LDL intima accumulation which turns into a chronic inflammation. In a complex set of events, pathological phenomena are starred by different cells and species, such as monocytes, macrophages, foam cells, oxidized LDL (oxLDL), smooth muscle cells (SMCs), and the atheroma plaque, ultimately, starts growing into the arterial lumen, creating the so-called stenosis. In case of instability and, eventually, rupture, plaque debris may trigger the above-mentioned atherothrombotic complications [6], [7], [5].

Giving the prevalence numbers, atherosclerosis has been modeled by several authors (especially during the last decade), focusing on different protagonists and stages of plaque development. Nonetheless, the majority of those is mainly directed towards the earliest stages (inflammatory response) [8], [9], [10], with the exception of [11] and [12] where advanced atherosclerotic plaques were studied.

In addition, to approximate atherosclerosis modeling to human physiological conditions authors claim for the need of more complex geometries (such as arterial bifurcations) where wall shear stress patterns vary [8], [12], [11], [10]. Besides, higher computational times allow for a long-term analysis of atherosclerosis, which is also desirable for a long-term visualization of several species accumulation inside the intima, leading to plaque growth [5], [8].

Furthermore, a remarkable limitation present in previous atherosclerosis mathematical models is the lack of clinical data. In fact, some model parameters are quite difficult to measure *in-vivo* and, besides, animal models always portray some errors when extrapolating to human physiology, resulting in the computation of crudely estimated parameters. Therefore, careful analysis of the model parameters and

respective experimental data are required, providing refinement in future studies [12], [11], [8], [13], [10], [14].

Hence, a thorough understanding of atherosclerotic plaque growth, which can be achieved through mathematical modeling and more realistic numerical simulations with accurate model parameters, provides the development of prevention and earlier detection strategies as well as new and effective therapeutic methods (based on nanoparticles intake) which help in plaque regression [7], [15].

1.2. Objectives of the thesis

Following previous authors procedures on atherosclerosis modeling, a complete work regarding mathematics, computations and experiments, must be performed. In fact, the physiological mechanisms and atherosclerosis functional changes involve such a large set of players required by a complex methodology.

Mathematical Objectives

After a cautious review of some of the existing literature on the topic, we decided to extend the work developed by Silva et al. in [8], which is mainly focused on the early stage of atherosclerosis. Aiming at modeling the atheroma growth inside the intima layer, we couple the above-mentioned model with processes inside advanced lesions. In this thesis, we propose an improved mathematical approach whose main goals are:

- Modeling of endothelial dysfunction and the persistent inflammatory reaction, without requiring LDL and monocytes dynamics. Alternatively, a constant influx is assumed on a lower WSS region at the endothelial surface, where those species transmigrate from the lumen into the intima. In addition, LDL oxidation with the consequent formation of oxidized LDL particles (oxLDL) and monocytes differentiation into macrophages are also modeled;
- Assignment of MCP-1 as the main inflammatory signal, triggering LDL transmigration and monocytes recruitment (thus, the endothelial permeability is an increasing function of MCP-1);
- Description of oxLDL ingestion by macrophages, originating the so-called foam cells which start accumulating, consequently, giving rise to a fatty streak injury;
- Representation of the fibrofatty stage by means of proliferation and migration of SMCs from the media into the intima layer. Migration (or chemotactic motion) occurs due to SMCs response to the continuous chemical gradient activity (starred by monocyte chemoattractant protein-1 and platelet – derived growth factor);
- Modeling of collagen fibres synthesis by migrated SMCs, one of the main relevant processes found in mature atherosclerotic lesions since it provides stability to the plaque;
- Suggestion of a novel plaque growth model that results from the continuous accumulation of massive cells and species (macrophages, foam cells, SMCs and collagen fibres) inside

atherosclerotic injuries, thus, our model assumes that the referred species contribute to intimal volume growth.

Computational Objectives

Besides those theoretical goals, we aim at computing long time simulations so that plaque growth can be visualized and compared with clinical data during a relevant biological lifetime (until five years). Moreover, this work provides a more realistic implementation of the proposed model using a two-dimensional left main coronary artery bifurcation where the intima dynamics is coupled to blood dynamics inside the arterial lumen. This bifurcation, known as a high-risk atherosclerotic region, separates the left coronary artery into the left anterior descending (LAD) artery and the left circumflex (LCx) artery [16].

Experimental Objectives

In addition, we intend to access model parameters origins from literature as well as their values as close as possible to human physiological conditions. Nevertheless, since many of those are only available in animal experiments (no clinical data yet) or there is a lack of experimental data, crudely estimated values are assigned. Therefore, to support the accuracy of our model parameters choices, we performed a sensitivity analysis technique to access the influence of the model parameters on the obtained results.

Finally, as a first phase-approach, an experimental procedure with one healthy mouse, required for accessing atherosclerotic parameters on diseased mice is described.

1.3. Methodology

Mathematical Approach

To achieve our main objectives, mathematical modeling is needed to guide the performance and interpretation of experiments as well as to synthesize the results. Gathering strong assumptions from previous works and after defining two subdomains (intima and lumen) and an interface (endothelial barrier), a complex coupled system of partial differential equations (PDEs) for fluid dynamics is proposed in a novel atherosclerotic lesion growth model.

On the one hand, inside the arterial lumen, blood is considered a Newtonian fluid, and the Navier-Stokes equations are used to model its dynamics. At the endothelium, given concentrations of monocytes and LDLs are assumed as boundary sources (which depend on the endothelial cells' permeability to them), thus, no transport equations are dedicated to those species. On the other hand, intima dynamics is divided within the four atherosclerosis stages: endothelial dysfunction (Stage I), where the evolution of concentrations of oxLDL and MCP-1 is described by reaction-diffusion equations and macrophages are described through a chemotaxis-advection-reaction-diffusion equation; fatty streak (Stage II) which models foam cells concentration though advection-reaction-diffusion equation; fibrofatty injury (Stage III) involves SMCs and PDGF dynamics, where the former resorts to a

chemotaxis-advection-reaction-diffusion equation and the latter uses a reaction-diffusion equation; finally, fibrous and mature plaque (Stage IV) is represented with a collagen advection-reaction equation.

Lastly, to compute plaque growth velocity and intima pressure, Stokes equations are suggested based on creation and continuous accumulation of massive cells (macrophages, foam cells, smooth muscle cells) and species (collagen fibres).

Computational Approach

Numerical simulations are needed to solve boundary and initial value problems that correspond to either experimental or *in vivo* conditions and provide data to be analyzed. Moreover, once non-linearities are intrinsic to biofluid mechanics, computational simulations are powerful tools to visualize meaningful results.

Therefore, we resorted to the longitudinal section of an idealized stenotic coronary artery to observe the result of implementing our system of equations. In fact, fast plaque growth was visualized owing to the increasing accumulation of massive cells (especially SMCs migration in advanced computational times) and the chronic inflammatory signals production (MCP-1 concentration reaching elevated levels). Besides, in response to MCP-1 and PDGF signaling, chemotactic motion of macrophages and SMCs are remarkable events during plaque progression.

A more realistic two-dimensional model was also used to evaluate our model in a high-risk region of atherosclerosis. This bifurcation corresponds to the separation of the left main coronary artery into left anterior descending (LAD) artery and left circumflex (LCx) artery, with the consequent separation of blood flow and wall shear stress pathological patterns which trigger endothelial dysfunction and, eventually, atherogenesis.

Experimental Approach

Experiments are needed to validate mathematical models as well as to allow parameters determination. Thus, we performed an experimental study with a healthy mouse which is the prototype procedure for future work on accessing atherosclerosis parameters using atherosclerotic mice. Resorting to a multi-photon confocal microscope Leica SP8 MP (Leica, Germany) adapted for intravital microscopy and after the exposure of the abdominal aorta, we recorded the luminal leukocytes rolling on the endothelium by means of a fluorescent dye. Leukocytes adherence to the endothelium and the interface between the vessel wall and the aorta lumen were, thus, observed and assessed over time.

1.4. Thesis outline

This thesis is structured into five chapters, divided as follows:

Chapter 1 provides a general introduction concerning our motivation, main objectives and the chosen methodology to reach them.

Chapter 2 presents the biological background associated to atherosclerosis physiopathology, specially focusing on its key protagonists and their respective role during this cardiovascular disease

initiation and progression. Moreover, it also displays current atherosclerosis mathematical models and the most relevant open questions regarding them.

Chapter 3 describes the required experimental approach to access some model parameters on mice models. Moreover, our mathematical approach, divided according to atherosclerosis stages of plaque development, is also addressed. We propose a novel lesion growth model inside the intima, through a complex system of partial differential equations. Besides, we also present the performed numerical methods as well as parameters selection and sensitivity analysis study.

Chapter 4 shows the results obtained from our experimental approach, numerical simulations in a two-dimensional domain and the accomplished sensitivity analysis technique. Finally, this section also reveals the result of computing our system of equations in a more realistic geometry of an idealized two-dimensional arterial bifurcation.

Chapter 5 summarizes the main conclusions and limitations of the proposed model, giving some recommendations for future work on this topic.

2. State of the Art

2.1. Anatomy and Physiopathology of Atherosclerosis

2.1.1. The human Cardiovascular System

Atherosclerosis is mainly considered a cardiovascular disease (CVD) caused by a chronic inflammatory process which affects the entire arterial tree and involves formation, growth and, sometimes, disruption of a lipid plaque [2]. Thus, understanding structure, composition and function of human cardiovascular system (CVS) becomes indispensable.

The human CVS is responsible for the supply of oxygen, nutrients and hormones to biological tissues, thus, enabling substances supply needed for energy production during biological processes and, also, providing metabolic wastes removal throughout the organism (resulting from those processes). It consists of the heart, approximately five liters of blood and an interconnected network of different blood vessels, which allow blood to efficiently flow along the cardiovascular system [17].

Blood, the carrier of the referred substances, is pumped through a closed system of vessels by the heart. From the left ventricle of the heart, it is driven through the arteries and arterioles to the capillaries, which drain through venules into the veins and back to the right atrium of the heart [18]. Apart from several proteins (such as albumin and globulin), which play important roles related to immunity and clotting, blood is also composed by three types of cells (formed in the bone marrow), suspended in an aqueous solution (called plasma) and specialized in distinct functions: red blood cells (or erythrocytes), white blood cells and platelets. The former is responsible for oxygen transport, the second for system immunity and the latter for blood coagulation [19], [18].

Moreover, blood vessels differ in function, size and structure. Hence, they are organized within three major types: arteries, capillaries and veins. Arteries carry highly oxygenated blood away from the heart, thus, their walls are rich in elastic fibers to allow expansion and retreat; capillaries are thinner, their walls only old endothelial cells and a basement membrane (no smooth muscle), so diffusion of gases, water, nutrients and waste products between lumen and tissues is facilitated, according to concentration gradients); and veins, which carry blood from capillaries back to the heart so that cellular waste products are withdrawn and deoxygenated blood can, afterwards, be renewed along the pulmonary circulation, consequently, the venous intima wall is predominantly composed by endothelium with scant connective and elastic tissues, also owing valves to prevent backflow of blood [18], [20].

Furthermore, the arterial tree is composed by distinct vessels with different wall structure and size. Firstly, the aorta is considered our *main artery* seeing that it distributes oxygenated blood to the entire organism and attenuates the pulsatile pressure (resulting from the heart flow). Thus, its wall has many elastic laminas which allow stretching during systole and recoiling during diastole. Secondly, there are other large elastic arteries (such as common iliac, carotids and pulmonary arteries) which are also abundant in elastic fibers. Then, the medium-sized muscular arteries (such as coronary and renal arteries) are abundant in smooth muscle cells that allow the distribution of blood to specific body regions

(thanks to vasoconstriction and vasodilation). The pressure inside those arteries is, though, slightly lower than the previously mentioned arteries because their resistance to flow is smaller. Finally, medium-sized arteries progressively divide into smaller muscle-walled vessels called arterioles and small arteries which, again, control blood flow by contracting or dilating the size of the lumen. In fact, these are the main sites of the peripheral resistance against which the heart pumps, thus, their tunica media layer contains concentric rings of smooth muscle that assure resistance to blood shear stress during heart beats [20], [18].

Atherosclerosis mostly affects the wall of large and medium-sized muscular arteries [2]. Hence, deeper understanding of the arterial wall is essential when it comes to studying atherogenesis. This way, the arterial wall is a vital biological barrier divided into three main layers: tunica intima, tunica media and tunica adventitia, each with specific histology and cell clusters which determine singular functions (see Figure 1) [21].

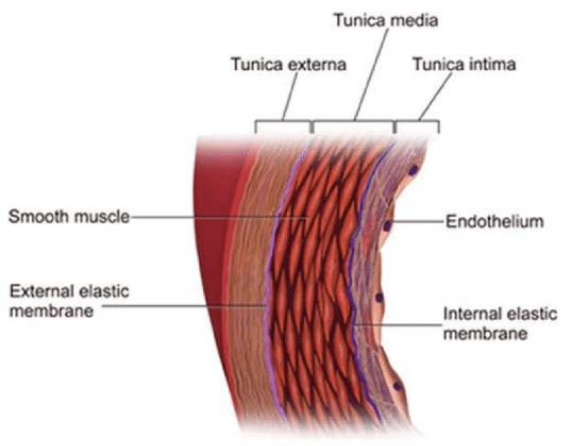

Figure 1 - Inside view on the arterial wall. Font: from *https://www.researchgate.net/publication/286948064_SASH1_a_new_potential_link_between_smoking_and_atherosclerosis/figures?lo=1.*

The tunica intima corresponds to the innermost layer, ensuring direct contact with the arterial blood through a single layer of endothelial cells, a thin basal membrane and a sub-endothelial layer (mainly composed by dispersed smooth muscle cells and collagen fibres for support functions). The endothelium constitutes a large and important organ, controlling flow rate variations, maintaining the vessels wall shear stress within certain levels and responding to circulating substances as well as to inflammatory mediators. Endothelial cells (ECs) are also responsible for secreting growth factors and vasoactive substances, therefore, chemical diffusion between blood and tissues is assured [22] , [18].

At the outer side, the intima is separated from the tunica media thanks to a fenestrated sheet of elastic fibers: the internal elastic lamina [23]. In the media layer, numerous smooth muscle cells are built-in a complex matrix made of collagen and glycoproteins (such as elastin), regulating blood pressure. Separating it from the outermost layer there is an external elastic lamina. Finally, the outer layer of the arterial wall (the so-called tunica adventitia) has about the same size as the tunica media. It is rich in connective tissue and loosely woven collagen fibers which protect blood vessels, merging them in with surrounding tissues. Moreover, the adventitia contains tinny vessels called vasa vasorum to supply vessel walls with blood [24], [18], [25].

Although tunica adventitia is the influx of neo-vessels that sprout into the atherosclerotic plaque (angiogenesis process), intima and media are the most critical layers in atherogenesis seeing that the main events of this CVD occur in those sections of the arterial wall. In particular, as it is explained further on, dissociation of the endothelial cellular network is verified in early atherogenesis (with the consequent increase of intima's permeability), thus, researchers believe that endothelial dysfunction is the starting point of this pathology [6], [26]. Hence, it is relevant to understand physiologies and main functions of intima and media layers, as well as those regarding the atherosclerosis main protagonists.

2.1.2. Atherosclerosis – main protagonists

Atherosclerosis is a specific type of arteriosclerosis, which is the general term for the hardening of human arteries. The word is derived from the Greek words *athero* (which means soft/pasty materials) and *sclerosis* (hardness). Thus, involving a complex sequence of events, it is caused by several factors such as high plasma levels of low-density lipoproteins (LDLs), hyperglycemia (excessive levels of glucose in the blood plasma), hypertension (sustained elevation of the systemic arterial pressure), infectious and smoking agents. Individuals with such diseases are, therefore, more predisposed to atherosclerosis injury and consequent complications [18], [6]. In fact, asymptomatic at the beginning, atherogenesis is caused by cholesterol accumulation at the EC surface which, progressively, leads to an increase of intima's permeability. Hence, a lipid plaque is formed inside the arterial wall, hardening the vessel and, gradually, narrowing its lumen (stenosis), as it is shown in Figure 2 [13].

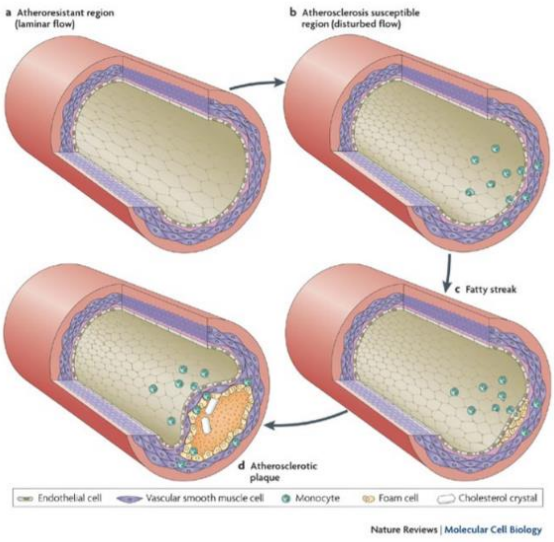

Figure 2 – General picture of atherosclerotic plaque growth with the formation of a luminal stenosis. Font: from [79].

Apart from the lipid content, atherosclerotic lesion is also composed by deposits of calcium, large inflammatory cells called macrophages, migrated smooth muscle cells, among other cells and species. This continuous accumulation triggers plaque growth, which leads to elasticity loss or even a thrombotic occlusion of the vessel [6]. With time, the plaque might, eventually, become fragile and rupture, forming blood clots which can travel through the circulatory system to other parts of the organism (heart, brain

or lower extremity circulations have the most clinical significance). At this point, several cardiovascular events such as myocardial infarction, stroke or peripheral arterial diseases may be caused [27], [28].

Providing this pathogenesis complexity, it is firstly relevant to understand physiology, roles and interactions among atherosclerosis main players. Therefore, in this subchapter, we highlight the most significant atherosclerosis protagonists and respective roles: endothelial cells (ECs) and their interface functions, the impact of the hemodynamics in what LDL accumulation on the ECs surface is concerned, LDL oxidation and its effect during the earliest stages, cytokines influence during the entire process (in particular MCP-1), the role of immune cells (monocytes, macrophages and foam cells), whose differentiation and recruitment lead to the persistent inflammation and, finally, smooth muscle cells (SMCs) that proliferate and migrate from the media into the intima layer, synthetizing collagen fibres.

2.1.2.1. Endothelial Cells

Endothelial cells (ECs) form the so-called endothelium, the interface between blood and tissues along the entire circulatory system, granting it the crucial role of controlling vessel wall and circulatory functions, thus, ECs express surface antigens receptors and lead to specific responses to stimulus [29]. By displaying phenotypic heterogeneity throughout the organism, EC surfaces have specific structures according to vessel size, location and function. In fact, their structure strongly depends on the hemodynamics of vessels. For this reason, ECs of veins and capillaries have a polygonal shape whereas in arteries they are fusiform and elongated in the direction of blood flow [30], [31].

Moreover, ECs are interconnected through dissimilar junctions, which are mainly composed by distinct transmembrane adhesive proteins. These junction structures differ, again, along the vascular system, conditioning the size of molecules and cells which are permitted by the passage [32]. In fact, when a rigorous control of permeability between blood and tissues is required (such as in the brain) junctions are well developed and highly rich in *tight junctions* (TJs) which contain occludins and claudins (transmembrane proteins) [29]. However, when a high rate of proteins and circulating cells exchange is allowed (for example, venous side of a capillary), developed *adherens junctions* (AJs), composed by transmembrane protein E-cadherin, are found [33]. Finally, there is another type of ECs interconnection called *gap junction*, which allows small molecular weight solutes passage between neighboring cells, suggesting that cell-to-cell communication is a crucial factor for vascular homeostasis [32]. Providing the (controlled) diffusion of molecules and cells from blood to tissues, the endothelial transport occurs via two pathways: transcellular (transcytosis) or paracellular [34]. The former, carried out across invaginations in the cell membrane (vesicles called *caveolae*), is responsible for transporting water and macromolecules [29]. The latter occurs between adjacent cells, allowing cellular transport (such as monocytes), initiating and stabilizing cell-cell adhesion[1].

Furthermore, the production of reactive oxygen species (ROS) by ECs is a key mechanism in atherosclerosis pathogenesis, causing an excessive oxidative stress inside the intima, thus, degrading

[1] Adhesion is the binding of a cell to a surface or a substrate which occurs with the intervention of adhesion molecules such as integrins, selectins and others [134].

the available vascular NO (vital free radical[2] for hemostasis) [6]. With time, due to this oxidative stress, cell damage is inevitable as well as the consequent alteration of endothelial junction proteins, increasing vascular permeability (loss of cell-to-cell communication and formation of intercellular gaps that allow the passage of macromolecules without restriction) [35], [21].

Apart from transport functions, the endothelium regulates blood flow within the circulatory system by constricting (endothelins[3] release) or dilating (nitric oxide[4] release) vascular diameters. Hence, ECs control systemic vascular resistance, arterial pressure and blood supply to organs, thus, maintaining the basal vasomotor tone, which is the necessary tension for vascular walls [17]. Once the endothelium is the major regulator of hemostasis[5], under normal physiological conditions it acts to maintain the dynamic balance between platelets, coagulation and fibrinolysis[6], facilitating perfusion[7], healing and vessel structure repair. Therefore, when this balance is disturbed (due to atherosclerosis risk factors), endothelial dysfunctionality may be promoted, triggering several phenomena such as increased endothelial permeability, recruitment, adhesion and transmigration of leukocytes into the subendothelial space (towards the site of infection), production of cytokines as well as proliferation and migration of SMCs into the intima layer [36], [37], [38], [6], [39]. In conclusion, endothelial cells play a fundamental role in atherosclerosis initiation and progression as a selective membrane which regulates the vascular homeostasis to preserve vascular integrity [40].

2.1.2.2. Wall Shear Stress

Mechanical factors which may trigger atherogenesis have been widely explored by many authors, who agree with the fact that hemodynamic conditions lead to the appearance of superficial stresses near the vessel wall, such as shear stress [41]. The latter is defined as the force per unit area exerted by blood on the inner layer of arterial walls, so its vector's direction opposes the blood velocity vector which is closest to the vessel wall.

Under normal physiological conditions, shear stress is crucial to maintain the endothelial homeostasis [42]. In fact, in areas where disturbed blood flow occurs (typically in the aorta or arterial bifurcations with flow recirculation, inner sides of curved arterial segments or even at stagnant blood areas), lower wall shear stress (WSS) amplitude is observed (patterns go from 0.02 to 1.2 *Pa* when compared to non-pathological values between 1.5 and 7 *Pa*) [43].

Lower WSS regions provide higher residence time of blood particles within arterial walls, thus, increasing molecules and cells diffusion through the endothelium (as experimentally concluded by

[2] A free radical is any chemical specie with an odd number of electrons since it contains one (or more) unpaired electron(s), turning it into a highly reactive particle [68].

[3] Endothelins are peptides with 21 amino acids that regulate cellular proliferation and hormone production [135].

[4] inhibits monocytes adhesion to the ECs surface and prevents smooth muscle cells (SMCs) from proliferating and migrating from the media into the intima layer [40].

[5] Hemostasis is the process of forming clots in the wall of damaged blood vessels to prevent blood loss while maintaining the fluid state of blood inside the vascular system [18].

[6] Fibrinolysis is a process in which blood clots are prevented from growing and becoming harmful [136].

[7] Perfusion is the general term for the delivery of nutrients and oxygen to tissues and removal of cellular waste products [137].

Meyer et al. in [44]) as well as ECs mitosis and apoptosis[8], with the consequent formation of leaky junctions. *In vivo* and *in vitro* studies have revealed that flow separation, turbulence and decreased blood velocity are associated with lower WSS levels [45], [30]. Later, Cheng et al. in [46] concluded that the biochemical composition of atherosclerotic lesions depends on their vascular location, thus, on WSS patterns. In conclusion, this pathology affects predisposed locations of the vascular system, evidencing pivotal roles of nanoscale fluid dynamics and macromolecular transport within arterial walls [47], [48].

2.1.2.3. LDL

Lipoproteins are small particles, produced in the liver and gut, essentially composed by glycoproteins and lipids. Through blood stream, they are responsible for lipid delivery to tissues, which is used in cellular mechanisms (such as membrane synthesis, modeling of membrane fluidity and regulation of cell signaling pathways) and for lipid transport out of cells [49]. Lipoproteins are divided into HDL (high density lipoproteins, the so-called *good* cholesterol) and LDL (low density lipoproteins, the so-called *bad* cholesterol). The former transports fat molecules out of cells and back to the liver for breakdown whereas the latter supplies tissues with fat molecules. Although different functions, their structures are similar: a hydrophobic core allows fat molecules transport. HDLs are smaller and denser than LDL particles which, in particular, have antioxidant defenses (vitamin E, for instance) [50], [51].

Despite the importance of lipid transport function, researchers believe that elevated lumen concentrations of LDLs linked to focal WSS pathological patterns induce endothelial dysfunction (ECs mitosis and apoptosis), triggering the creation of gaps between ECs (leaky junctions) and cell-to-cell communication loss [52], [53], [54]. During atherosclerosis initial inflammation, LDL is transported across the arterial wall (paracellular transport) without restriction, thus, accumulating inside the intima [55].

In the intima layer, LDLs are oxidized by free radicals such as reactive oxygen species (ROS), which are produced by ECs and immune cells. Oxidized LDL (oxLDL) particles are considered one of the main critical factors in early atherosclerotic lesions as well as during all stages of this cardiovascular disease [6]. In fact, modified LDL accentuates the creation of gaps between adjacent ECs, leading to endothelial dysfunction, consequently, increasing endothelial permeability to LDL. Moreover, oxLDL promotes ROS and cytokines production, which attract white blood cells and enhance chemotaxis[9]. Proinflammatory response is, thus, induced, with circulating monocytes migration into the intima (ECs express adhesion molecules). Inside the intima layer, after monocytes differentiation into macrophages, the latter ones start engulfing oxLDL particles, triggering more cytokines production and increasing the persistent inflammation [2], [50], [56], [51].

2.1.2.4. Cytokines

Cytokines constitute a large category of small signalling proteins, produced for intercellular communication in order to regulate crucial biological processes such as body growth, lactation and

[8] Cellular death by induced suicide. In atherosclerosis, it happens to ECs, macrophages, foam cells and SMCs due to the accumulation of free cholesterol within the lesions. In fact, it is believed that foam cell apoptosis is the main cause for the lipid core inside the atherosclerotic plaque [100], [68].

[9] Chemotaxis refers to the directed cell migration, that is, cell movement up a chemical gradient.

inflammatory responses. Acting through receptors, they are divided into six classes: interleukins, tumour necrosis factors (TNF), interferons (IFN), colony stimulating factors (CSF), transforming growth factors (TGF) and chemokines [57].

Chemokines (or chemo-attractant cytokines) constitute a family of over 40 different cell signalling molecules which are essential for constitutive trafficking and recruitment of leucocytes in response to inflammatory or infectious mediators. Regarding atherosclerosis, certain chemokines may act as potent mediators of monocyte and SMC migration into the inflammatory sites as well as monocytes differentiation into macrophages, determinative events in plaque progression [58]. Monocyte chemoattractant protein-1 (MCP-1), for instance, is secreted by the endothelium when oxLDL intima concentration is elevated and in hypercholesterolemia conditions. Additionally, macrophages can also express MCP-1, enlarging not only the influx of monocytes into the vascular inflammatory sites but also the accumulation of intima foam cells [6].

Furthermore, circulating platelets adhesion and aggregation to a dysfunctional endothelium lead to PDGF (platelet – derived growth factor) release by ECs, foam cells, macrophages and SMCs. This cytokine has strong mitogenic[10] and chemotactic effects on SMCs. Therefore, SMCs proliferation and migration from the media into the intima is triggered [59], [60].

2.1.2.5. Immune Cells

Atherosclerosis includes several types of immune cells. Monocytes, in particular, are the largest leukocytes[11], representing, approximately, 5% of WBCs, with diameters ranging from 8 to 20 *μm* and. They are produced in the bone marrow and travel through bloodstream [61]. Under inflammatory conditions, apart from monocytes recruitment regulation by chemoattractant molecules (e.g. prominent role of MCP-1), macrophages synthetize a protein called factor increasing monocytopoiesis (FIM) which is transported via the circulatory system towards the bone marrow, where monocytes production is stimulated. Then, monocytes circulation is enhanced, quickly migrating to the inflammation (or infection) sites (8 to 12 hours) and adhering to the vascular EC surface [62], [63].

Providing that WBCs produce free radicals, monocytes diffusion into the intima increases the production of intima ROS. Thus, oxidative stress levels are augmented, consequently, enhancing the oxidation of intima LDL and endothelial dysfunction [64], [65]. Despite the endothelial permeability increase, monocytes extravasation does not occur through leaky junctions. In fact, the size of the largest gaps ranges from 15 to 1330 *nm* (correspondent to mitotic and apoptotic cells) which are not sufficiently large to allow monocytes transmigration, as concluded by *in vivo* studies [66], [67]. Consequently, under the influence of chemoattractant molecules, monocytes undergo morphological changes in the singular sequence: recruitment (capture), rolling, slow rolling (activation), firm adhesion and, finally, transmigration through the endothelial barrier and the subendothelial layer in a process called diapedesis. To attach to inflamed vessels, adhesion molecules such as integrins (vascular cell adhesion

[10] Any substance that induces mitosis (cell division) is called mitogenic [138].

[11] Leukocytes are immune cells commonly called white blood cells (WBCs), ranging from 4500 to 11000 per microliter of blood in adults [61].

molecule-1 or VCAM-1) and selectins (P-selectin and E-selectin) are produced by ECs [6]. All the mentioned steps are reversible, except for diapedesis: once it starts, there is no going back.

In addition, owing to oxLDL presence inside the intima, monocytes differentiate into phagocytic macrophages, the second type of atherosclerosis immune cells. Eventually, macrophages start engulfing oxidized LDL (through the so-called scavenger receptors) in response to local macrophage colony-stimulating factor (MCSF). This reaction transforms macrophages into foam cells[12] [21]. Foam cells, in turn, secrete proinflammatory cytokines (such as MCP-1) that also contribute for endothelial activation, thus, increasing monocytes recruitment as well as SMCs proliferation and migration from the media to the intima layer. These are protective attempts performed by the organism to remove injurious stimuli and initiate the healing process. Once an auto-amplification phenomenon is triggered, atherosclerosis is commonly referred as a chronic inflammatory disease [21]. Ultimately, foam cells die, releasing their lipid content which, together with cellular debris, begins to form the atherosclerotic plaque.

2.1.2.6. Smooth Muscle Cells

Smooth muscle cells (SMCs) are elongated cells which constitute the main components of tunica media of vessel walls. SMCs and extracellular matrix components (such as collagen fibres) form the contractile unit of arteries, assuring vasoconstriction and vasodilation [23]. Moreover, SMCs are considered multifunctional cells since they regulate blood pressure, extracellular matrix components production, vascular ageing and calcification. The ageing phenomenon regulation, in particular, occurs by vascular stiffness increase as well as by SMCs defective autophagy property (which is explained further ahead). Calcification, in turn, arises from the deposition of calcium phosphates inside arterial walls (regulated by SMCs) and from the synthesis of a calcification prone matrix [68], [69].

In normal physiological conditions, ECs inhibit the migration of SMCs from the media into the intima. However, researchers have found that, in diseased vessels (like atherosclerotic ones), SMCs undergo multiple processes (often simultaneously) within different lesion regions and during different stages. Thus, SMCs pathological behaviour is an ongoing research topic, in particular, their ability to retain the property to shift from a contractile (differentiated), inside the media, to a synthetic phenotype (de-differentiated), verified in the intima, in a process called autophagy [70], [69]. Moreover, as already stated, dysfunctional endothelium leads to PDGF release by ECs, foam cells, macrophages and SMCs. This cytokine promotes, thus, SMCs proliferation[13] and chemotactic motion. Additionally, SMCs acquire pro-inflammatory properties, engulfing oxLDL particles (like macrophages), therefore, forming lipid-laden SMCs that also accumulate inside the plaque, ultimately, secreting an extracellular matrix.

A fibrous barrier between the lipid core and the arterial lumen is, progressively, created to protect the plaque from rupture, which explains the benefit of SMCs migration during atherosclerosis [71], [69]. In fact, the fat deposit slowly develops into a fibrofatty injury due to collagen and extracellular matrix synthesis. Nonetheless, with time, exposition to various stimuli (such as oxidative stress, oxidized LDLs

[12] These cells have a *foamy* appearance due to the fact that their cytoplasm is saturated with a lipid content.
[13] Growth or production of cells by multiplication of their parts [21].

and inflammatory cytokines) leads to SMCs apoptosis (cellular death), which weakens the fibrous cap (plaque vulnerability increasing), eventually, causing plaque rupture [72], [69]. The balance between SMCs migration and apoptosis is, therefore, crucial for atherogenesis and intima plaque stability.

2.1.3. Atherosclerosis – a brief insight

Atherosclerosis is an inflammatory disease of large and medium-sized arteries which, due to a progressive auto-amplification phenomenon, results in the formation and growth of a lipid plaque inside the arterial wall [2]. However, it remains unclear whether this inflammation is the cause or the consequence of atherogenesis. During the last decades, many resources have been wasted to deepen the knowledge on this topic [22]. The general picture of atherosclerotic impairment comprises regions of elevated LDL, followed by intimal thickening. Moreover, such zones tend to show abnormal blood shear stress patterns due to turbulent or stagnant flow, inferring that the endothelium is a mechanical sensor, transducing and responding to hemodynamic signals [43].

Many researchers believe that atherosclerosis starting point corresponds to endothelial dysfunction caused by high plasma levels of cholesterol (or hypercholesterolemia), such as low density lipoproteins (LDLs), hyperglycemia, hypertension, obesity, infectious and smoking agents (which constitute atherosclerosis main risk factors). Once vascular permeability is altered, posterior inflammation arises, with the consequent accumulation of lipids and cellular debris inside the innermost layer of the vessel wall – the intima [6], [7]. Despite the controversy, it is known that, due to LDL, hypertension, low shear stress values, smoking toxins or combinations of these and other factors, atherosclerosis is related to a complex chronic inflammatory reaction which plays an important pathogenetic role [24]. Hence, the persistent inflammation is a key contributor during all disease stages, from the initial lesion to the ruptured plaque [73]. Figure 3 shows the general panorama of crucial events during this pathology.

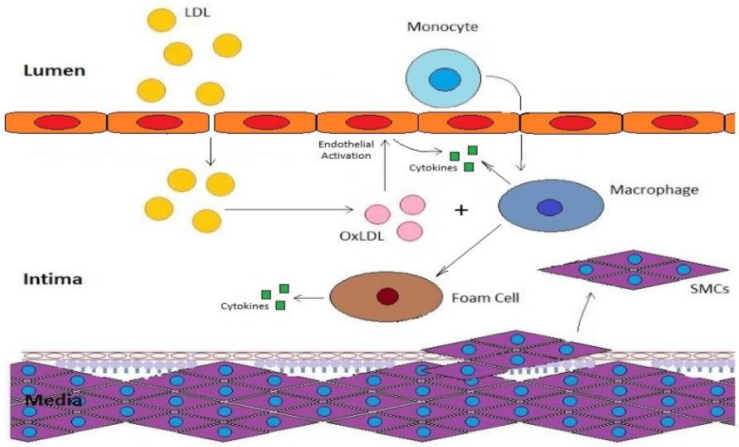

Figure 3 - Atherosclerosis schematics showing the main events during plaque genesis and development: LDL and monocytes entrance inside the intima layer, endothelial activation, monocytes differentiation into macrophages, foam cells formation, cytokines production by ECs, macrophages and foam cells and SMCs migration into the intima layer. Font: from [8].

As it is observable, atherosclerosis risk factors tend to induce endothelial dysfunction, consequently, the intima permeability becomes compromised. In fact, leaky junctions between ECs promote LDL particles entrance and accumulation inside the vessel wall, where they are, eventually, oxidized [74].

Owing to oxLDL formation, different cytokines are synthetized by ECs. Activated ECs enhance circulating monocytes recruitment which, in turn, start proliferating into the site of inflammation in a process called transmigration. Besides, induced by cytokines, SMCs are attracted from the media layer into the intima, tendentially, towards the endothelium to form the fibrous cap (on the top of the plaque). The persistent inflammatory response leads to excessive amounts of a connective tissue matrix production, which constitutes atherosclerosis ultimate point, that is, mature, fibrous and calcified cap [7].

Evidently, complexity is a notorious characteristic of this pathogenesis, so it is common to divide atherosclerosis plaque formation into distinct consecutive stages, each with particular protagonists. Although there is no consensus on the number of stages, experiments have suggested that the progression of atherosclerosis might be divided into four stages, thus, we suggest the same division in this work (see Figure 4) [12], [73]. The earliest phase of atherosclerosis is composed by two stages involving the initial inflammation: Endothelial Dysfunction (Stage I) and the consequent Fatty Streak (Stage II). Hence, this pre-lesioned and (often) reversible phase is a continuous, long and asymptomatic process (preferential time for initial exposure to risk factors), developing silently (that is, without associated symptoms). Finally, the second phase includes the two advanced stages of atherosclerotic lesions: Fibrofatty Injury (Stage III) which progresses to Fibrous and Mature Plaque (Stage IV).

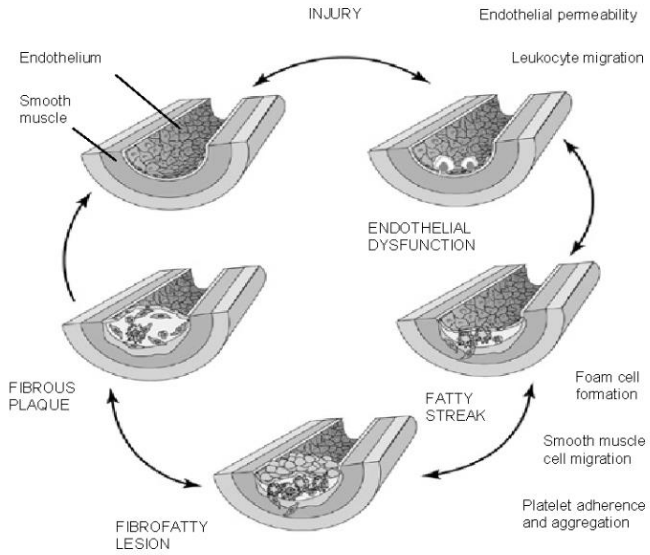

Figure 4 - Diagram of atherosclerosis pathogenesis – stages of plaque development and specific processes during those stages. Font: from [75].

2.1.3.1. Endothelial Dysfunction (Stage I)

Many experimental studies have pointed out that local disturbances of homeostasis are in the pathogenesis of cardiovascular diseases. In fact, hemodynamic alterations are considered the main promoters of endothelial surface charge reduction. Consequently, a non-homogeneous distribution of anionic sites ends up increasing endothelial dysfunction and permeability to luminal LDL and monocytes (overexpression of several chemokines which work as cell adhesion molecules) [43], [76].

Atherosclerosis Stage I stands out for initial abnormal responses of the endothelium to external stimuli, such as disruption of endothelial junctions ECM and formation of gap junctions between

neighboring ECs. Hence, macromolecules like low-density lipoproteins (LDLs) are instigated to enter inside the arterial wall, giving rise to the inflammatory reaction. Unprotected intima environment starts oxidizing LDL due to the presence of free radicals (which react with vitamin E of LDLs). Later, the accumulation of oxLDL enhances endothelial activation, triggering monocytes and platelets recruitment thanks to the expression of proinflammatory cytokines by ECs. This set of reactions is, actually, a protective attempt by the organism to initiate the healing process [77], [68].

Furthermore, in early human atherosclerotic plaques, vasa vasorum (tiny vessels inside the adventitia layer) control the process of neovascularization, that is, thin-walled micro vessels formation inside the plaque itself. Owing to these new leukocytes and erythrocytes, neo-vessels provide the needed oxygen and nutrients for disperse cells within the hypoxic environment, thus, contributing for plaque growth [68].

2.1.3.2. Fatty Streak (Stage II)

As oxidized LDLs are recognized by scavenger receptors of macrophages, endothelial cells, in turn, overexpress adhesion (e.g. E-selectin, P-selectin) and chemoattractant molecules (e.g. MCP-1). These molecules travel through the blood stream and bind to circulating monocytes, thus, coordinating their motion to lesion sites (chemotaxis) and, posteriorly, their transmigration through the endothelial barrier into the intima (diapedesis). Inside the intima layer, leukocytes start differentiating into macrophages through the upregulation of scavenger receptors, as reported in [22]. Still during Stage II, activated macrophages start engulfing oxLDL particles, in a process called phagocytosis. They develop into foam cells, which produce additional cytokines, thus, enhancing the recruitment of new monocytes.

Hence, due to a chronic inflammatory response, the slow accumulation of cholesterol loaded macrophage-derived foam cells sets up the formation of the fatty streak, which marks the end of the earliest atherosclerosis phases [6], [21], [22].

2.1.3.3. Fibrofatty Injury (Stage III)

Foam cells intima accumulation stimulates ECs to segregate cytokines (MCP-1) and growth factors (PDGF). Endothelial cells, therefore, not only contribute for new lumen monocytes recruitment, but also fail to inhibit smooth muscle cells from proliferating and migrating from the media into the intima (see Figure 3) [22], [69]. In this process, macrophages also perform a relevant role by secreting growth factors [68]. In Stage III, with the formation of a fibrous cap over the lipid core by SMCs (surrounding extracellular matrix components), the atherosclerotic plaque evolves into a fibrofatty injury, isolating the lipid deposit from blood stream. Along with the lipid core, the cap creates the so-called atheromatous plaque. Hence, the third stage goes until fibrous cap formation. Providing that the fibrous capsule is in direct contact with the vascular lumen, it helps maintaining plaque's integrity [78], [12], [69].

With time, the atheroma plaque grows and starts invading the lumen. Consequently, the arterial wall thickens and the lumen narrows, so vessel geometry may change, creating the so-called stenosis [68]. Interestingly, plaque growth is anisotropic since it predominantly occurs in the downstream direction (lower shear stress). Of course, plaque progression rate is accelerated by cardiovascular risk factors such as plasma LDL levels, oxidants from smoking, high blood glucose levels, among others [79], [12].

2.1.3.4. Fibrous and Mature Plaque (Stage IV)

Atherosclerotic plaque growth occurs not only due to lipid accumulation but also to other pathological events, such as cellular apoptosis, SMCs migration from the media into the intima or collagen synthesis. Apoptosis is triggered by many agents such as cytokines, oxLDL and low WSS, possibly, leading to necrosis (owing to nutrient starvation) which causes massive cells death. The apoptotic cells (specially ECs, macrophages, foam cells and SMCs) end up releasing their content, which forms the intima necrotic core. The latter accelerates or induces plaque disruption. On top of that, calcification cores can be created, further developing into big calcification centers, an active process largely orchestrated by SMCs (see Figure 2) [72], [69].

The fibrous mature plaque is, finally, formed with an excess of inflammatory cytokines and proteases. Moreover, inside advanced atherosclerotic lesions, activated ECs and migrated SMCs switch to a secretory phenotype, which results in a multilayered basal lamina with an enlarged extracellular matrix, highly rich in collagen bundles and fibres. Cap's integrity depends, thus, on ECM metabolism once the latter is responsible for exerting the vital mechanical strength inside the plaque [80].

Seeing that apoptosis distribution is considerably heterogeneous, atheroma compositions and displayed thicknesses are very different. Although thicker caps (or stable plaques) tend to accentuate the arterial narrowing owing to a robust fibrous cap, their propensity to rupture is lower than thinner caps. Therefore, the latter ones are called vulnerable (or unstable) plaques [72], [81]. Still, continuous progression of advanced lesions induces vasculature geometry changes, eventually, compromising plaque's stability during Stage IV [82], [43].

Finally, some authors also consider a Stage V called Plaque Rupture and Thrombosis [80]. Accordingly, this critical stage happens when vulnerable plaques become fragile due to a decline in SMC density and in collagen synthesis (cap thinning) or a continuous infiltration of macrophages, which digest the stabilizing matrix. Eventually, these factors may trigger plaque rupture, meaning that mechanical forces take over and thrombotic associated symptoms are notorious [82]. A lumen-occluding thrombus (the so-called blood clot) develops thanks to platelets activation and aggregation to the lesion's EC surface. The blood clot might (partially or totally) block luminal flow, compromising blood and oxygen supply to tissues (ischemic areas), leading to irreversible changes [18], [80]. Furthermore, it can travel to another part of the circulatory system, triggering cardiovascular events such as embolism (lung), myocardial infarction (heart) or stroke (brain). Apart from those, chronic pathologies such as coronary heart disease (the most frequent), carotid artery disease, peripheral artery disease or chronic kidney disease, might also be observed, especially in adults [21], [22], [80].

2.2. Current Mathematical Models for Atherosclerosis

Nowadays, several works have been devoted to understanding the mechanisms beyond the atherosclerotic plaque genesis and growth. Nevertheless, the mathematical modeling of atherosclerosis implies a complex system of PDEs describing the main protagonists of this cardiovascular disease (Appendix A clarifies these equation types). In fact, chemical reactions, transport functions, flow

behavior, fluid-structure interactions, movement of cells and dynamics of vessel walls are some of the numerous processes during atherosclerosis [14], [13], [83], [9], [10], [84], [85], [11].

This chapter displays the main contributions on the current mathematical modeling around atherosclerosis plaque formation and progression, existing in the literature since 2009. We divided the known governing equations for atherosclerosis main protagonists according to their respective stages during the disease.

2.2.1. Endothelial Dysfunction and Fatty Streak

The early stages of atherosclerosis encompass initiation, inflammation and lipid accumulation inside the tunica intima. In the last decade, several models have been developed by many authors regarding this stage but focusing different processes, thus, distinct protagonists [84], [9], [10], [13], [14], [11], [8].

Calvez et al. (2009)

Starting with Calvez et al. in [9], apart from describing the initial inflammatory process as it was previously developed by El Khatib et al. (see Appendix B), they also suggested, in relation with hemodynamics, a two-dimensional model for lipid accumulation through a system of reaction-diffusion PDEs, thus, describing the atheromatous plaque growth [9]. Firstly, they considered the intima as a 2D domain of height $h(x,t)$, with $x \in [0,L]$ and $t > 0$, whose lower boundary is fixed. Coordinate y, in turn, corresponds to intima's height, with values from 0 (interface with tunica media) to h (interface with blood).

On the one hand, oxidized LDL concentration (L_{ox}) was modeled by the following equations:

$$\frac{\partial L_{ox}}{\partial t} + \nabla \cdot (\boldsymbol{\nu} L_{ox}) = d_{L_{ox}} \Delta L_{ox} - k_1 L_{ox} \cdot M \quad \text{, in }]0,L[\times]0,h[\tag{2.1.a}$$

$$\frac{\partial L_{ox}}{\partial y} = \tau(x) L_{dl} \quad \text{, if } y = h \text{ for all } x \in]0,L[\tag{2.1.b}$$

$$\frac{\partial L_{ox}}{\partial y} = 0 \quad \text{, if } y = 0 \text{ for all } x \in]0,L[\tag{2.1.c}$$

where $\boldsymbol{\nu}$ stands for the velocity of lesion growth, evidencing that oxLDL particles are transported accordingly to tissue displacement. The first term on the right-hand side, in turn, corresponds to the diffusion term, where $d_{L_{ox}}$ is the diffusion coefficient. Finally, the last right-hand term represents the reaction between oxLDL and macrophages (M) to form foam cells, with k_1 as the constant of proportionality. Then, in Equation (2.1.b), L_{dl} constant represents a given LDL concentration, whereas $\tau(x)$ denotes blood vessel permeability, which is dependent on wall shear stress.

Macrophages concentration (M), on the other hand, was defined as:

$$\frac{\partial M}{\partial t} + \nabla \cdot (\boldsymbol{\nu} M) = d_M \Delta M - k_1 L_{ox} \cdot M \quad \text{, in }]0,L[\times]0,h[\tag{2.2.a}$$

$$\frac{\partial M}{\partial y} = g(S) \quad \text{, if } y = h \text{ for all } x \in]0,L[\tag{2.2.b}$$

$$\frac{\partial M}{\partial y} = 0 \quad \text{, if } y = 0 \text{ for all } x \in]0,L[\tag{2.2.c}$$

where d_M is the diffusion coefficient. This system assumes not only the immediate differentiation of monocytes into macrophages, but also the dependence of monocytes recruitment on a general proinflammatory signal (S), which encompasses chemokines and cytokines, acting through the function $g(S)$. The latter is useful to impose a limit in monocytes recruitment, so it is given by:

$$g(S) = \frac{S}{1+S} \tag{2.2.d}$$

In this model, the general proinflammatory signal was modeled as:

$$\frac{\partial S}{\partial t} = d_S \Delta S - \lambda_S S + k_1 L_{ox} \cdot M \quad \text{, in }]0, L[\times]0, h[\tag{2.3.a}$$

$$\frac{\partial S}{\partial y} = a_{S,L_{ox}}(L_{ox} - L_{ox}^{th}) \quad \text{, if } y = h \text{ for all } x \in]0, L[\tag{2.3.b}$$

$$\frac{\partial S}{\partial y} = 0 \quad \text{, if } y = 0 \text{ for all } x \in]0, L[\tag{2.3.c}$$

As it is observable, the signal may diffuse and d_S represents the diffusion coefficient. The second term on the right-hand side denotes the natural death of the signal, thus, λ_S is the degradation rate. Moreover, the third right hand-side term states that the signal creation is due to oxLDL and macrophages reaction. Lastly, Equation (2.3.b) stablishes a given oxLDL threshold (L_{ox}^{th}) as the starting point for the signal emission, thus, $a_{S,L_{ox}}$ is an activation rate.

Cilla et al. (2013)

A similar study was presented by Cilla et al. (in 2013) in a three-dimensional model [13]. In this work, both fluid and solute dynamics were described for several biological agents/substances, not only inside the lumen and arterial wall (e.g. LDLs, monocytes) but also across the endothelium (solute transport). Furthermore, they inclusively provided understanding of the focal atherosclerosis propensity by modeling the influence of WSS on triggering its initiation. Nevertheless, concerning the earlier stages of atherosclerosis, our interest is mainly focused on the mathematical modeling of oxLDL, macrophages and cytokines. Therefore, we present here the contribution of the authors on these chemicals and cells.

Firstly, cytokines were equally modeled as the proinflammatory signal given in Equations (2.3.a) - (2.3.c), with the difference that diffusion was neglected. In fact, the authors considered that cytokines are retained in the macrophage membrane.

The oxLDL concentration in the intima (L_{ox}), in turn, was defined as:

$$\frac{\partial L_{ox}}{\partial t} + \nabla \cdot \left(\boldsymbol{v}_i L_{ox} - d_{L_{ox}} \nabla L_{ox}\right) = r_{ox} L_{dl} - k_{ox,M} L_{ox} \cdot M \tag{2.4}$$

where $d_{L_{ox}}$ is the diffusion coefficient of oxLDL and $\nabla \cdot (\boldsymbol{v}_i L_{ox})$ is the advection term. The first term on the right-hand side corresponds to the oxidation of LDL particles (L_{dl}), with r_{ox} as the oxidation rate (or degradation rate of LDL). The last term on the right-hand side corresponds to the oxLDL uptake by macrophages (M) per second, so $k_{ox,M}$ is the rate of oxLDL uptake by one macrophage.

The evolution of macrophages concentration (M) was modeled by:

$$\frac{\partial M}{\partial t} + \nabla \cdot (-d_M \Delta M) = m_{dif} m - \frac{M_{r1}}{M_{r2}} k_{ox,M} L_{ox} \cdot M \tag{2.5}$$

where d_M is the diffusive coefficient of macrophages and advection term was neglected. The first term on the right-hand side corresponds to the monocytes (m) that differentiated into macrophages, thus, m_{dif} is the rate of differentiation. Finally, the second term on the right-hand side refers to foam cell formation, which depends on the oxLDL uptake by macrophages ($k_{ox,M}L_{ox} \cdot M$) and was multiplied by M_{r1} and divided by M_{r2} constants, which stand for the oxidized LDL concentration that one macrophage should ingest to convert into a foam cell (per second) and the rate of foam cell formation (per second), respectively.

Hao and Friedman (2014)

In 2014, Hao and Friedman presented another mathematical model using reaction-diffusion equations (e.g. LDL particles, free radicals, MCP-1 or PDGF) and advection-reaction-diffusion equations (for cells such as macrophages or foam cells) [14]. As the innovative approach, the authors purpose was to prove that HDL helps preventing atherosclerosis, not only by reacting with free radicals that, otherwise, would be available for LDL, but also by removing cholesterol from FCs. Thus, they modeled plaque evolution for any pair of values for HDL and LDL concentrations. Again, we only display the substances and cells which are relevant for our study, that is, oxLDL particles, macrophages and cytokines (e.g. MCP-1).

Firstly, oxidized LDL concentration evolution was equally modeled as in Equation (2.4), with two differences: the oxidation term was also multiplied by free radical's concentration (r) and the advection term was neglected.

$$\frac{\partial L_{ox}}{\partial t} + \nabla \cdot \left(-d_{L_{ox}} \nabla L_{ox}\right) = r \cdot r_{ox} L_{dl} - k_{ox,M} L_{ox} \cdot M \tag{2.6}$$

Secondly, the authors modeled the macrophage concentration evolution as:

$$\frac{\partial M}{\partial t} + \nabla \cdot (\boldsymbol{v} M) - d_M \Delta M = -\nabla \cdot \left(M \chi_C \nabla M_{cp}\right) + a_{M,I_\gamma} \frac{I_\gamma}{I_\gamma + K_{I_\gamma}} M - M_{ap} M \tag{2.7}$$

where the first term on the right-hand side corresponds to the macrophage recruitment by MCP-1 (M_{cp}) and χ_C is the chemotactic sensitivity parameter. The second hand-right side term, in turn, accounts for the activation of macrophages by IFN-γ (whose dynamics is not pertinent for our work, so it is not shown here) with an activation rate (a_{M,I_γ}). The last term corresponds, again, to macrophages natural death.

In the same work, they suggested an evolution for MCP-1 concentration, written as:

$$\frac{\partial M_{cp}}{\partial t} - d_{M_{cp}} \Delta M_{cp} = r_{M_{cp}} \frac{L_{ox}}{L_{ox} + K_{L_{ox}}} - \lambda_{M_{cp}} M_{cp} \tag{2.8}$$

where the first right-hand side term is the production term, due to endothelial cells (whose density is assumed to be constant), under the influence of oxLDL concentration (upper limit represented by $K_{L_{ox}}$). The last term stands for MCP-1 degradation, with rate $\lambda_{M_{cp}}$.

Silva et al. (2016)

Finally, Silva et al. proposed in [8] a novel approach specially focused on the initiation and inflammation processes of atherosclerosis disease. Apart from describing LDL and monocytes transport inside the arterial lumen and through the endothelium, they also simulated LDL accumulation in the region of low WSS. Therefore, the endothelial permeability was defined as decreasing function of WSS and increasing function of MCP-1 (shown further ahead on this work) [8]. Moreover, as already stated, giving our interest in certain intima key variables during early atherosclerosis we present the most relevant contributions of this work, specially concerning oxLDL and macrophages.

Firstly, oxLDL concentration inside the intima (L_{ox}) was modeled by:

$$\frac{\partial L_{ox}}{\partial t} + \nabla \cdot \left(\boldsymbol{v}_i L_{ox} - d_{L_{ox}} \nabla L_{ox}\right) = r_{ox} L_{dl} - k_{ox,M} \frac{L_{ox}}{L_{ox}+K_{L_{ox}}} M \tag{2.9}$$

where is $d_{L_{ox}}$ the diffusion coefficient and r_{ox} is the oxidation rate of LDL particles inside the intima. The last right-hand side term accounts for the ingestion of oxLDL by macrophages, with rate $k_{ox,M}$. Moreover, this term considers an upper limit for the oxLDL ingestion rate by one macrophage, thus, $K_{L_{ox}}$ stands for this rate.

In their model, the concentration of macrophages was described by:

$$\frac{\partial M}{\partial t} + \nabla \cdot \left(-d_M \Delta M + M \chi_C \nabla M_{cp}\right) = m_{dif} m^i + M_{pro} M - k_{F_c} \frac{L_{ox}}{L_{ox}+K_{L_{ox}}} M \tag{2.10}$$

where d_M is the diffusive coefficient of macrophages and $\nabla \cdot (M \chi_C \nabla M_{cp})$ stands for their chemotactic motion in response to MCP-1 gradient (∇M_{cp}). Constants m_{dif} and M_{pro} are, respectively, the monocytes rate of differentiation into macrophages and the macrophages rate of proliferation. Hence, Silva et al. assumed that macrophages accumulation inside the intima layer depends on their local proliferation and on monocytes recruitment (which then differentiate into macrophages). The last term on the right-hand side represents the degradation of macrophages due to their transformation into foam cells (after oxLDL ingestion). Coefficient k_{F_c} is the rate of foam cells formation.

2.2.2. Fibrofatty Injury and Plaque Maturity

Although little is known regarding the mathematical modeling of atherosclerosis advanced stages (plaque progression and fibrous maturity), we present here the main contributions on this subject existing in the literature. The main protagonists of this phase are foam cells, smooth muscle cells, collagen, MCP-1 and PDGF.

Calvez et al. (2009)

Regarding the advanced stages of atherosclerosis, fatty streak due to foam cells creation and plaque growth was also portrayed by Calvez et al. in [9], as it is displayed in this subset.

The authors assumed that activated macrophages (when phagocyting oxLDL inside the intima) immediately differentiate into foam cells. Thus, foam cells concentration (F_C) was described as:

$$\frac{\partial F_C}{\partial t} + \nabla \cdot (\boldsymbol{\nu} F_C) = k_1 L_{ox} \cdot M \quad \text{, in }]0, L[\times]0, h[\tag{2.11.a}$$

$$\frac{\partial F_C}{\partial y} = 0 \quad \text{, if } y = 0, h \text{ for all } x \in]0, L[\tag{2.11.b}$$

Furthermore, local incompressibility was also assumed, that is, foam cells creation (given by the right-hand term) locally increases the intima volume (growth modeled through the second left hand-side term, with velocity $\boldsymbol{\nu}$).

Besides, Calvez and coauthors assumed that oxLDL particle dimensions and macrophage size (before ingesting oxidized LDL) were small in comparison with the size of foam cells. Thus, in this work, only the creation and accumulation of the latter contributed for plaque growth. Hence, they defined the biomass (Z) as the rest of the intimal medium such as extracellular matrix (ECM), SMCs and others which do not contribute to the inflammatory process, given by:

$$\frac{\partial Z}{\partial t} + \nabla \cdot (\boldsymbol{\nu} Z) = 0 \quad \text{, for all } x \in \Omega_i \tag{2.12.a}$$

Furthermore, a constant E was defined as the intima average density to allow the local matter incompressibility assumption, stated as:

$$Z(x, y, t) + F_C(x, y, t) = E \quad \text{, for all } x \in [0, L],\ y \in [0, h] \text{ and } t > 0 \tag{2.12.b}$$

They also assumed that $\boldsymbol{\nu}(0) = 0$ and the uniform lesion growth exclusively occurring in the y direction, that is:

$$\frac{\partial \boldsymbol{\nu}}{\partial x} = 0 \quad \text{, for all } x \in [0, L],\ y \in [0, h] \text{ and } t > 0 \tag{2.12.c}$$

Hence, through a system of reaction-diffusion PDEs, they reached the following one-dimensional model for the atherosclerosis plaque growth:

$$\boldsymbol{\nu}(h) = \frac{dh}{dt} = \frac{k_1}{E} \int_0^h L_{ox} \cdot M dy \tag{2.12.d}$$

Calvez et al. (2010)

The same authors reached a more complex 3D model one year later, where they coupled the previous lesion growth model with blood flow dynamics and mass transfer (see Figure 5) [10]. For that, the authors considered a fluid-wall model where the intima was represented by a single layer which allowed the LDLs transport from the lumen into the intima (transfer equation through the endothelium).

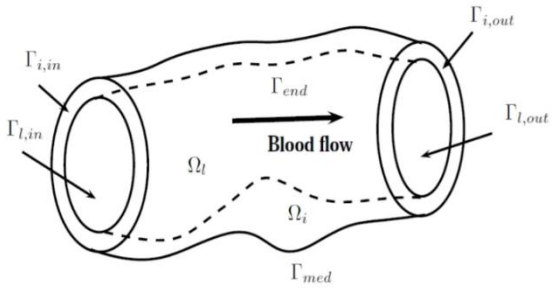

Figure 5 - Three-dimensional geometry of the model. The lumen and the intima were denoted by $\Omega_l, \Omega_i \subset \mathbb{R}^3$, and their boundaries were defined as $\partial\Omega_l = \Gamma_{l,in} \cup \Gamma_{end} \cup \Gamma_{l,out}$ and $\partial\Omega_i = \Gamma_{i,in} \cup \Gamma_{end} \cup \Gamma_{med} \cup \Gamma_{i,out}$, respectively. Γ_{end} stands for the interface between the intima and the lumen, whereas Γ_{end} stands for the interface between the intima and the media. Finally, $\Gamma_{l,in}/\Gamma_{i,in}$ and $\Gamma_{l,out}/\Gamma_{i,out}$ are, respectively, the proximal and distal sections of both domains.

In this model, under the (already stated) local matter incompressibility assumption and after adding Equations (2.11.a), (2.12.a) and (2.12.b), atherosclerotic plaque growth was described by the system:

$$-\nabla \cdot \boldsymbol{D}(\boldsymbol{v}) + \nabla q = 0 \qquad \text{, for all } x \in \Omega_i \tag{2.13.a}$$

$$\nabla \cdot \boldsymbol{v} = \frac{k_1}{E} L_{ox} \cdot M \qquad \text{, for all } x \in \Omega_i \tag{2.13.b}$$

$$\boldsymbol{D}(\boldsymbol{v})\boldsymbol{n}_i - q\boldsymbol{n}_i = 0 \qquad \text{, for all } x \text{ on } \Gamma_{end} \tag{2.13.c}$$

$$\boldsymbol{v} = 0 \qquad \text{, for all } x \text{ on } \partial\Omega_i \setminus \Gamma_{end} \tag{2.13.d}$$

which was inspired by Stokes equations, allowing plaque growth velocity determination.

Cilla et al. (2013)

Later, Cilla et al. in [13], continued to model plaque development, aiming at foam cells creation, smooth muscle cells (dividing them into contractile and synthetic) migration and collagen synthesizes.

The authors modeled foam cells concentration (F_C) by:

$$\frac{\partial F_C}{\partial t} = \frac{M_{r1}}{M_{r2}} k_{ox,M} L_{ox} \cdot M \tag{2.14}$$

where all constants were already introduced in Equations (2.4) and (2.5). Hence, the authors neglected diffusion and advection terms due to foam cells dimensions. The reaction term corresponds to macrophages apoptosis.

They assumed that SMCs express a contractile phenotype (S_{mcc}) which, owing to the presence of cytokines, differentiates into a synthetic phenotype (S_{mcs}). Thus, both types were modeled by:

$$\frac{\partial S_{mcc}}{\partial t} = -S_{mcc}\left[1 + \exp\left(\frac{-S_{mcc}^{diff} C}{C^{th}}\right)\right] \tag{2.15.a}$$

$$\frac{\partial S_{mcs}}{\partial t} = S_{mcc}\left[1 + \exp\left(\frac{-S_{mcc}^{diff} C}{C^{th}}\right)\right] + S_{mcs}\frac{S}{C^{th}} m_{S_{mcs}} \tag{2.15.b}$$

with S_{mcc}^{diff} as the differentiation rate and C^{th} the maximum concentration of cytokines, at which the differentiation is maximized. Contractile SMCs formation (mitosis) and death tend to be in equilibrium, so these terms were not included in the equation. Finally, in Equation (2.15.b), $m_{S_{mcs}}$ is the migration rate of synthetic SMCs from the media into the intima by chemoattractant molecules. Moreover, advection and diffusion terms were neglected in both species due to SMCs size and quiescence[14] property, respectively.

As a novelty, the authors considered collagen's significant role during the atheroma plaque development, describing its concentration (C_{ol}) by:

$$\frac{\partial C_{ol}}{\partial t} = r_{C_{ol}} S_{mcs} - \lambda_{C_{ol}} C_{ol} \tag{2.16}$$

where $r_{C_{ol}}$ and $\lambda_{C_{ol}}$ are the secretion and degradation rates, respectively. As it is visible through the first right-hand side term, it was considered that collagen synthesis was mainly due to synthetic SMCs.

[14] Quiescent cells are spread by migration, so no diffusion is considered [13].

Finally, they assumed that the volume increase of the atheroma was mainly dependent on FCs, SMCs and collagen concentrations, so the contribution of the other species was neglected [13]. Therefore, the isotropic[15] atheroma plaque growth was written as:

$$\nabla \cdot \boldsymbol{\nu} = \frac{\partial F_C}{\partial t} Vol_{FC} + \frac{\partial \delta S_{mc}}{\partial t} Vol_{SMC} + \frac{\partial C_{ol}}{\partial t} \frac{1}{\rho_{C_{ol}}} \quad (2.17)$$

where δS_{mc} is the variation of contractile and synthetic SMCs with respect to the initial concentration of both species (before the atheroma initiation), Vol_{FC} and Vol_{SMC} are, respectively, the volume of one foam cell and one SMC (estimated through their radius), and $\rho_{C_{ol}}$ is the collagen density.

Hao and Friedman (2014)

Hao and Friedman, in [14], defined atheroma plaque development through Darcy's equation[16]. Key variables such as foam cells, smooth muscle cells and cytokine PDGF were modeled.

With a production term due to the ingestion of a large amount of oxLDL by macrophages (as written on the given first right-hand side term), the authors modeled foam cells by:

$$\frac{\partial F_C}{\partial t} + \nabla \cdot (\boldsymbol{\nu} F_C) - d_{F_C} \Delta F_C = r_{F_C,M} \frac{L_{ox}}{L_{ox} + K_{L_{ox}}} M - F_{C_{ap}} F_C \quad (2.18)$$

with the degradation rate $F_{C_{ap}}$. It is relevant to enhance the saturation term, under the influence of oxLDL concentration, which is evidenced through $K_{L_{ox}}$(the oxLDL ingestion saturation rate by one macrophage).

Furthermore, Hao and Friedman assumed a new model for SMCs concentration, bearing in mind chemotaxis and haptotaxis processes, that is:

$$\frac{\partial S_{mc}}{\partial t} + \nabla \cdot (\boldsymbol{\nu} S_{mc}) - d_{S_{mc}} \Delta S_{mc} = -\nabla \cdot \left(S_{mc} \chi_C \nabla M_{cp}\right) - \nabla \cdot (S_{mc} \chi_C \nabla G) - \nabla \cdot (S_{mc} \chi_H \nabla \rho) \quad (2.19)$$

where the first two terms on the right-hand side account for chemotaxis by MCP-1 (M_{cp}) and PDGF (G), whereas the last term represents haptotaxis by ECM (whose modeling was also performed but it is no concern for our study). Thus, χ_C stands for the chemotaxis parameter and χ_H the haptotaxis parameter.

Among other chemokines, PDGF (P_{gf}) was also modeled by:

$$\frac{\partial P_{gf}}{\partial t} - d_{P_{gf}} \Delta P_{gf} = r_{P_{gf},M} M + r_{P_{gf},F_C} F_C + r_{P_{gf},S_{mc}} S_{mc} - \lambda_{P_{gf}} P_{gf} \quad (2.20)$$

where its production is performed by macrophages, foam cells and SMCs, with rates $r_{P_{gf},M}$, r_{P_{gf},F_C}, and $r_{P_{gf},S_{mc}}$ respectively. The last hand-right side term stands for PDGF degradation, with $\lambda_{P_{gf}}$ as the degradation rate.

[15] Isotropic growth of plaques means that the plaque is growing equally in all directions [11].

[16] Darcy's equation allows the computation of plaque growth velocity along all directions. This assumption is not feasible according to Stokes assumption, where the velocity vector is unidirectional [14].

Yang al. (2015)

Later, a remarkable approach was suggested by Yang et al. in [11], where a two-dimensional model described how plaques are formed and developed. Based on the assumption that monocytes penetration into the intima and consequent foam cells accumulation lead to plaque growth and considering the interaction between blood flow and the vessel wall, the authors considered the changing of mechanical properties of the vessel wall. For that, elastic structure equations were used to define vessel deformation, as it is shown below.

In fact, they considered that isotropic plaque growth not only contributes for intima mass increasing but also for geometry changes on the vessel wall. Hence, a new variable, called the metric of growth (g_s), was introduced to define the deformation induced by mechanics, given by:

$$\frac{\partial g_s}{\partial t} = \frac{k f_M^r}{\rho_s} g_s \tag{2.21}$$

where ρ_s is the constant density of the arterial wall and k a positive constant coefficient which depends on the dimension of the space that is being modeled. f_M^r stands for the reaction term of foam cells.

Silva et al. (2016)

Lastly, in their model, Silva et al. also suggested a particular description for MCP-1 and foam cells concentrations, which are provided below [8].

The authors assumed that foam cell resulted from macrophages ingestion of large amounts of oxLDL particles. In addition, advection and diffusion of these cells were neglected (due to their size). Thus, the evolution of foam cells concentration (F_C) was described by:

$$\frac{\partial F_C}{\partial t} = k_{F_C} \frac{L_{ox}}{L_{ox}+K_{L_{ox}}} M - F_{C_{ap}} F_C \tag{2.22}$$

where r_{F_C} is the foam cells rate of formation and $F_{C_{ap}}$ is the apoptotic rate of foam cells. The first hand-right term is a production term, which considers an upper limit for the oxLDL consumption rate by one macrophage ($K_{L_{ox}}$).

Moreover, Silva et al. considered that the production of cytokines was dependent on the concentration of oxLDL, macrophages (M), and foam cells (F_C). In fact, the presence of oxidized LDL induces the expression of MCP-1 (M_{cp}) by endothelial cells which triggers the recruitment and transmigration of monocytes into the intima. Besides, they also assumed, in a more advanced atherosclerotic stage, that foam cells also contribute to the MCP-1 expression and, consequently, the continued influx of monocytes into the lesion site. Therefore, this chemokine concentration was given by:

$$\frac{\partial M_{cp}}{\partial t} + \nabla \cdot \left(\boldsymbol{v} M_{cp}\right) - d_{M_{cp}} \Delta M_{cp} = k_{M_{cp},M} M + k_{M_{cp},F_C} F_C - \lambda_{M_{cp}} M_{cp} \tag{2.23}$$

where $d_{M_{cp}}$ and $\lambda_{M_{cp}}$ are, respectively, MCP-1 diffusive coefficient and degradation rate. Advection term is represented by $\nabla \cdot \left(\boldsymbol{v} M_{cp}\right)$.

2.3. Open questions when modeling atherosclerosis

To conclude this chapter, Table 1 summarizes our cautious review of literature on current mathematical models for atherosclerosis understanding. We enhance their specific atherosclerotic stages, novelties and main limitations (some pointed out by the authors themselves).

Table 1 - Summary of the state of the art on atherosclerosis modeling and limitations of existing models. Stages are divided in: Endothelial Dysfunction (I), Fatty Streak (II), Fibrofatty Lesion (III), Fibrous and Mature Plaque (IV).

	Atherosclerosis Stages	**Novelties**	**Main Limitations**
Calvez et al. (2009)	I, II (1D)	Atheroprone region with respect to hemodynamics; intimal volume growth due to foam cells intima accumulation.	One-dimensional R-D equations for intima species; the biomass does not contribute to the inflammatory process.
Calvez et al. (2010)	I, II (2D)	Fluid wall model (fluid dynamics for blood, transport equations for LDLs and transfer equations for the endothelium); endothelial permeability to LDL as decreasing function of WSS.	Slow plaque formation; endothelial response to WSS and its mechanical behavior need improvement; lack of physiological parameters; the biomass does not contribute to the inflammatory process.
Cilla et al. (2013)	I, II, III (3D)	Plaque growth in a region with higher propensity for atherosclerosis; WSS as the main trigger of atherosclerosis initiation.	Parameters from a wide variety of experiments; sensitivity analysis needed; low complexity in terms of modelled species (e.g. cytokines) and processes.
Hao and Friedman (2014)	I, II, III (2D)	Atheromatous plaque evolution simulated for any pair of two circulating particles: LDL and HDL.	Crudely estimated parameters (clinical data needed); circulating oxLDL, triglycerides and influence of risk factors not included in the model.
Yang et al. (2015)	II, III (2D)	Plaque growth considering vessel wall mechanical changes; fluid structure interaction (NS equations for blood and elastic structure equation for endothelium).	Oscillatory blood flow not considered; crudely estimated parameters (clinical data needed).
Silva et al. (2016)	I, II (2D)	Early atherosclerosis, specially focusing circulating LDL and monocytes dynamics; endothelial permeability as a decreasing function of WSS and an increasing function of MCP-1.	Low simulation time; simple geometry; crudely estimated parameters (clinical data needed); no comparison to experimental data; no plaque growth coupled.

We conclude that our motivation comes from the shared mathematical focus on the first two stages of atherosclerosis, the short simulations time and the lack of clinical data (inaccurately estimated

parameters). Therefore, extending the work developed by Silva et al. in [8], in chapter 3 we propose a more complete mathematical model with the major concern at stages III and IV, thus, coupling the above-mentioned model with atheroma growth.

Foam cells creation and accumulation to form the fibrofatty lesion, SMCs proliferation and migration from the media into the intima, the continuous chemical gradient activity (starred by PDGF and MCP-1) and collagen synthesis by migrated SMCs (assuring stability to the mature plaque) are some of the critical biological processes and agents that arise in advanced lesions and, consequently, in our model. Although it gathers some strong assumptions from referred authors, our main novelty regards the assumption that species which contribute for intimal volume growth are massive cells (such as foam cells, macrophages and SMCs) and collagen fibres.

As a first phase-approach, an experimental procedure with one healthy mouse, required for accessing atherosclerotic parameters on diseased mice is described. Additionally, we intend to access model parameters origins in literature as well as their values as close as possible to human physiological conditions. Hence, a table summarizing parameters origins (whether they are estimated or come from animal/human experiments) and assumed values is provided. Once many correspond to crudely estimated parameters, a sensitivity analysis was performed to access the influence of model parameters on the obtained results. This technique is explained in the next chapter.

Finally, model features, computational settings and numerical methods are also provided in chapter 3 to elucidate the reader about the software and geometry used for computational simulations.

3. Methodology

3.1. Experimental Model

3.1.1. Animals

One Lys-EGFP-ki mouse with 18 weeks old was used in this work (EGFP indicates enhanced green fluorescent protein) [86]. The animal was kept in an animal facility with a 12 h light/dark cycle and housed in cages in a temperature-controlled room. It was kept on a diet standard mouse food and water ad libitum. The animal received human care in accordance with the Directive of the European Community 2010/63/EU, that mentions the protection of animals used for economic and other scientific ends, also according to the Portuguese Legislation Law 113/2013.

3.1.2. Intravital Imaging

For the surgical procedures and microcirculatory measurements, the mouse was anesthetized intraperitoneally (i.p.) with a cocktail of xylazine/ketamine ($0.1\ mL/10\ g$ of BW). Body temperature was maintained between 35 and 37 °C with auto-regulated heating platform.

The surgical procedures for intravital microscopy were made in an appropriate support as described and used by Silva and coauthors in [87]. In our experiments, the abdominal aorta was exposed by opening the peritoneal cavity and gently pushing organs to the side. After this surgical preparation the support with the animal was placed in a multi-photon confocal microscope Leica SP8 MP (Leica, Germany) adapted for intravital microscopy, equipped with a 20×water objective and a 10×ocular. The exposed tissue was superfused with Krebs–Henseleit buffer with $NaHCO_3$ at 37°C bubbled with 95% N_2 and 5% CO_2 and the excess of liquid was removed with a vacuum system. All the images were recorded using the LAX software for offline analysis.

Different parts of the aorta were recorded to verify the presence or not of areas with atherosclerotic plaques. From the recorded images the interactions between leukocytes and endothelial cells were also quantified by the parameters already established: number of rolling leukocytes and their rolling speed, number of adherent leukocytes and vessel diameter [88]. The leukocytes were assumed to be rolling on the endothelium if they were moving at a slower speed than the erythrocytes in the same vessel over 1 min duration. A leukocyte was considered adherent to the endothelium if it remained stationary for more than 30 s in a 100 μm length [87].

In Appendix C, we describe the ideal procedure for studying atherosclerosis disease points towards the usage of mouse apolipoprotein E deficient ($ApoE^{-/-}$). In order to achieve stages III or IV of atherosclerosis (which correspond to the interest of our study), and according to a review published by Whitman (2004), the mice need to have the accurate age and fat diet [89]. However, during the time we had to perform this work, mice with those characteristics were not available and the necessary

procedures to promote their atheroma plaque growth would imply even more time and resources (for more details see Appendix C).

3.1.3. Blood Quantification

After performing the described procedure, a sample of $100\ \mu L$ of abdominal arterial blood was removed to undergo a spectrophotometry method for the quantification of blood LDL levels. At the end of the experiment, the animal was euthanized with a pentobarbital injection $100\ mg/kg$ of BW.

3.2. Mathematical Model – A New Approach

Currently, mathematical modeling and numerical simulations are vastly used by researchers to replicate biological processes through simple geometries and physics, allowing their computational manipulation, thus, providing a better understanding of those processes as well as their modification according to the interest of study. Therefore, those are useful tools for the development of more effective treatment and prevention strategies. Since partial differential equations (PDEs) have shown to be a suitable approach to model biological events ([90], [91]), we apply the same methodology.

As mentioned above, the model suggested by Silva et al. in [8] lacks atherosclerosis advanced stages modeling. Thus, we aim to extend their model by coupling the earliest stages of atherosclerosis (e.g. endothelial dysfunction, accumulation and oxidation of intima LDLs and the consequent inflammatory signaling) with the prolonged process of subendothelial plaque growth which, eventually, occludes the arterial lumen. Based on the biological background reported in chapter 2, our focus stays in modeling stages III and IV, with special attention to mechanisms behind foam cells creation and accumulation inside the intima, SMCs proliferation and migration from the media into the intima, collagen synthesis followed by fibrous and mature plaque development and, finally, the action of chemical gradients (starred by PDGF and MCP-1) which trigger each of those phenomena.

In order to describe the behavior of the main atherosclerosis players inside the intima layer, we assume the following transport equations in the model: reaction-diffusion (R-D) equations for oxLDL, MCP-1 and PDGF, a advection-reaction-diffusion (A-R-D) equation for foam cells inside the intima, a simple advection-reaction (A-R) equation for collagen and, finally, a chemotaxis-advection-reaction-diffusion (χ-A-R-D) equation for macrophages and SMCs (for more details on these groups of equations see Appendix A). Moreover, Navier-Stokes (NS) equations are used to model blood flow inside the lumen and basic principles of continuum mechanics are used to describe matter dynamics inside the intima.

This subchapter describes this new mathematical approach, detailed for each stage of atherosclerosis. For simplicity, our model congregates not only some assumptions already reported from works on this field, which are present in literature (see chapter 2), but also novel ones. Our assumptions are, then, listed below:

1. Owing to the small sizes of blood suspended particles when compared to large and medium artery diameters, blood is considered a homogeneous, isothermal, incompressible and Newtonian fluid;

2. Deformation of the arterial wall under the blood flow action can be neglected;

3. Although diffusion and degradation coefficients usually depend on specific factors (such as substances concentration), in this work they are considered constant known parameters;

4. On the EC surface, a given elevated LDL influx is taken as the starting point for its oxidation, giving rise to oxLDL formation. Hence, the continuous intima accumulation of oxLDL leads to the inflammatory response initiation, thus, no modeling is specifically dedicated to LDL dynamics inside the lumen and the intima. Likewise, a certain monocytes influx at the endothelium and a rate of monocytes differentiation into macrophages are also assumed, so our model does not describe monocytes dynamics inside the lumen and the intima;

5. LDL entrance through the EC surface occurs for lower WSS penetration regions and higher MCP-1 production areas, thus, endothelial permeability to LDLs is decreasing function of WSS and increasing function of MCP-1;

6. Inflammatory signal is starred by monocytes chemoattractant protein-1 (MCP-1) once the intima oxLDL level reaches a given threshold;

7. The recruitment of monocytes is controlled and limited by MCP-1 intima concentration;

8. In response to MCP-1 signaling, macrophages transmigrate into the intima layer moved by the chemotactic gradient. Moreover, induced by oxLDLs, macrophages evolution is also dependent on their local proliferation;

9. Inside the intima, macrophages engulf oxLDLs, originating the so-called foam cells. There is, though, an imposed upper limit to oxLDL ingestion rate by one macrophage;

10. The rate of oxLDL uptake by macrophages is different from the rate of foam cells creation because the consumption of oxLDL does not transform macrophages immediately into foam cells;

11. Macrophages and foam cells contribute to the production of MCP-1 and PDGF, thus, they are triggers of the chronic inflammatory reaction. Besides, we assume that PDGF is also synthetized by SMCs;

12. We consider a constant influx of SMCs at the media boundary, and these cells dynamics depends on their chemotaxis by MCP-1 and PDGF signals, which stimulate their migration from the media into the intima. Besides, SMCs apoptosis inside the intima layer is also assumed;

13. For simplicity, collagen production by SMCs is assumed as the key variable for fibrous cap stability and plaque maturity in advanced atherosclerotic stages;

14. The average density inside the intima is constant in time and space;

15. Fluid dynamics inside the intima results from the formation, migration and accumulation of foam cells, macrophages, collagen, and smooth muscle cells, so these are the relevant protagonists for intima volume growth and all the rest of intima medium (the biomass) does not contribute for the inflammation. Thus, transport term is considered in these species' dynamics, with the velocity corresponding to intima volume growth velocity, whereas this term is negligible in the other atherosclerosis protagonists (oxLDL, MCP-1 and PDGF);

16. The intima volume dynamics is associated to a continuum medium by linear momentum and mass balance equations, under a local matter incompressibility assumption. Due to species migration, creation and accumulation intima volume is locally increasing (at a certain velocity). Furthermore, all species are assumed to have zero velocity on every boundary except for the endothelial barrier, which deforms into the lumen with plaque growth velocity.

3.2.1. Simplified Model

An idealized rectangular geometry is used to represent our computational domain, which consists of two compartments representing the lumen and the tunica intima, that is, $\Omega = \Omega_l \cup \Omega_i$. Figure 6 shows the longitudinal section of our idealized stenotic coronary artery (note that the deformed interface stands for intima plaque growth into the arterial lumen).

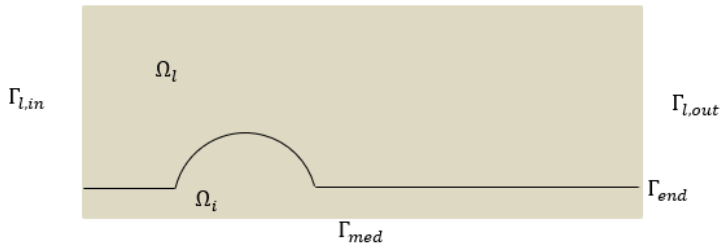

Figure 6 - Illustration of our simple computational domain, where $\boldsymbol{\Omega_l}$ represents the lumen, $\boldsymbol{\Omega_i}$ the intima, $\boldsymbol{\Gamma_{l,in}}$ and $\boldsymbol{\Gamma_{l,out}}$ the inlet and outlet luminal boundaries (respectively) and, finally, $\boldsymbol{\Gamma_{end}}$ and $\boldsymbol{\Gamma_{med}}$ stand for the endothelial and media boundaries (respectively).

As it is observable, Γ_{end} stands for the interface between the intima and the lumen (the so-called endothelium) while Γ_{med} is the interface between intima and media layers. The adventitia layer is not modeled because it does not play a relevant role in atherosclerosis disease.

In the lumen domain, the unknowns of blood flow are approximated by P2-P1 Taylor Hood finite elements, that is, piecewise polynomials of second-order (for velocity $\boldsymbol{u}_l$) and first order (for pressure p_l). Similarly, intima variables are spatially discretized through quadratic Lagrange elements (order 2), except for the intima pressure (p), which is discretized by means of linear Lagrange elements.

3.2.2. Modeling atherosclerosis main protagonists inside the intima

For simplicity, our mathematical approach is divided in concordance with atherosclerosis stages of evolution, presented in chapter 2. Accordingly, Endothelial Dysfunction (Stage I) involves oxLDL,

macrophages and MCP-1 dynamics, that is, the initial protagonists of inflammation. Then, Fatty Streak (Stage II) also comprises an equation for foam cells (owing to oxLDL and macrophages reaction) and, afterwards, Fibrofatty Injury (Stage III) complements it by adding PDGF and SMCs dynamics, which are responsible for critical events in plaque growth. Finally, Fibrous and Mature Plaque (Stage IV) also portrays collagen dynamics, the key variable for plaque stability in advanced atherosclerosis plaques.

Resorting to previous works (present in the literature) on atherosclerosis protagonists modeling, we performed some (justified) changes whenever needed to assure framework with our assumptions.

3.2.2.1. Endothelial Dysfunction (Stage I)

In the first stage of the disease, the main players in our model are oxLDL, macrophages and MCP-1. Following up the work proposed by Silva et al. in [8] regarding this period, we assume that the endothelial permeability to LDLs and monocytes is a decreasing function of WSS and an increasing function of MCP-1. Therefore, LDLs and monocytes can enter from the lumen into the intima through a penetration region, consequently, triggering atherosclerosis initiation. However, our model does not describe the dynamics of the mentioned species, as explained further on. According to our assumptions, endothelial boundary conditions are defined based on another work from those authors (in the same year) [91].

Oxidized LDL

Firstly, as one of the main triggers of the inflammatory reaction, oxidized LDL particles modeling is crucial for the initial stage of the disease. Hence, looking back at Equation (2.9), one observes that Silva and coauthors included LDL dynamics in the oxLDL equation, nonetheless, intima LDLs are not modeled in the present work. Instead, we consider an initial concentration of LDL (at a lower WSS region on the endothelial boundary) as the starting point for its oxidation, thus, transforming them into oxLDL particles and, consequently, triggering the inflammatory process.

In Equation (3.1.a), $d_{L_{ox}}$ represents the oxLDL diffusion coefficient and the last right-hand side term accounts for the ingestion of oxLDL by macrophages, at the constant rate $k_{ox,M}$, thus, its degradation is linear in macrophages concentration (M) and saturating in oxLDL concentration (as experimental findings in [92] have concluded), therefore, $K_{L_{ox}}$ stands for the upper limit to oxLDL ingestion rate by one macrophage.

Besides, the authors considered a transport term for oxLDLs. However, under our assumptions, once oxLDL mass is irrelevant for intima volume, the advection term can be neglected. Therefore, let us introduce the evolution of intima oxLDL concentration (L_{ox}) through the following R-D equation:

$$\frac{\partial L_{ox}}{\partial t} + \underbrace{\nabla \cdot \left(-d_{L_{ox}} \nabla L_{ox}\right)}_{\text{Diffusion}} = \underbrace{- k_{ox,M} \frac{L_{ox}}{L_{ox}+K_{L_{ox}}} M}_{\text{Ingestion by macrophages}} \qquad (3.1.a)$$

subject to Neumann (flux) boundary conditions, homogeneous everywhere, except for Γ_{end}. According to our assumptions, at the EC surface a given elevated LDL influx (C_{LDL}) is taken as the starting point

for its oxidation, promoted by intima free radicals. Therefore, LDL entrance into the intima layer occurs through this biological barrier, thus, oxLDL boundary condition depends on the endothelial permeability (P_{LDL}), defined further in Equation (3.4), and oxidation rate (r_{ox}).

$$\left(-d_{L_{ox}}\nabla L_{ox}\right)\cdot \boldsymbol{n}_i = P_{LDL}\, r_{ox}\, C_{LDL}\,, \qquad \text{on } \Gamma_{end} \tag{3.1.b}$$

However, at the other intima subdomain boundaries, no flux condition is imposed, which yields:

$$\left(-d_{L_{ox}}\nabla L_{ox}\right)\cdot \boldsymbol{n}_i = 0\,, \qquad \text{on } \partial\Omega\backslash\Gamma_{end} \tag{3.1.c}$$

Macrophages

Giving the fundamental role of macrophages in atherosclerosis initiation, the intima dynamics of these immune cells is also based on the work developed by Silva et al. Two differences, though, stand out from that model when compared to ours.

As it is visible in Equation (2.10), monocytes dynamics was modeled by those authors, similarly to LDLs in the previous case. Likewise, for simplicity, intima monocytes are not described by our model. Instead, we propose an endothelial concentration of monocytes and a constant differentiation rate of monocytes into macrophages.

Furthermore, owing to macrophages size, a transport term is required. In fact, contrarily to the referred model, we assume that macrophages contribute to the inflammatory process, thus, a advection term is considered in macrophages dynamics. Consequently, the evolution of these immune cells' concentration (M) is described by the χ-A-R-D equation:

$$\frac{\partial M}{\partial t} + \underbrace{\nabla\cdot(\boldsymbol{v}M)}_{\text{Advection}} + \underbrace{\nabla\cdot\left(-d_M\nabla M + \chi_M M\nabla M_{cp}\right)}_{\substack{\text{Diffusion}\\ \text{Chemotactic motion in response to MCP-1 signal}}} = \underbrace{M_{pro}M}_{\text{Proliferation}} - \underbrace{k_F\frac{L_{ox}}{L_{ox}+K_{L_{ox}}}M}_{\substack{\text{Degradation due}\\ \text{to foam cells}}} \tag{3.2.a}$$

subject to Neumann (flux) boundary conditions homogeneous everywhere, except for Γ_{end}:

$$\begin{cases} \left(-d_M\nabla \mathrm{M} + \chi_M M\nabla M_{cp} + \boldsymbol{v}M\right)\cdot\boldsymbol{n}_i = P_m\; r_{diff}\; C_m, & \text{on } \Gamma_{end} \\ \left(-d_M\nabla \mathrm{M} + \chi_M M\nabla M_{cp} + \boldsymbol{v}M\right)\cdot\boldsymbol{n}_i = 0\,, & \text{on } \partial\Omega\backslash\Gamma_{end} \end{cases} \tag{3.2.b}$$

Starting with Equation (3.2.a), it is possible to conclude that several terms affect macrophages concentration inside the intima. In the left-hand side, it is relevant to enhance the transport and the diffusion terms. The former includes plaque growth velocity ($\boldsymbol{v}$) whereas the latter contains d_M, macrophages diffusion coefficient. The last left-hand side term, in turn, represents macrophages chemotactic motion (with chemotaxis sensitivity parameter given by χ_M) in response to MCP-1 gradient (∇M_{cp}).

Moving now to the right-hand side, macrophages local proliferation is considered inside the intima layer. Induced by oxLDLs, it corresponds to a natural movement of these immune cells (at a constant proliferation rate M_{pro}) while acting within an inflamed environment. Additionally, the last term represents

macrophages degradation due to their transformation into the so-called foam cells, after ingestion of large amounts of oxLDLs. Thus, the coefficient k_{F_c} corresponds to the rate of foam cells creation, which is different from macrophages rate of oxLDL ingestion ($k_{ox,M}$), present in Equation (3.1.a). In fact, oxLDL consumption does not, generally, transform macrophages immediately into foam cells [8]. Once more, this term is linear in macrophages concentration (M) and saturating in oxLDL concentration, so $K_{L_{ox}}$ stands for the upper limit of oxLDL ingestion rate by one macrophage.

Finally, in Equation (3.2.b), the imposed boundary condition at the endothelium includes three key members. Firstly, P_m stands for the endothelial permeability to monocytes (defined in Equation (3.4)) and the constant r_{diff} represents monocytes rate of differentiation into macrophages. At last, a given monocytes concentration (C_m) is assumed as the endothelial influx of monocytes.

MCP-1

In our model, the inflammatory signal is starred by monocytes chemoattractant protein-1 (MCP-1), which is segregated by endothelial cells (whose density is assumed constant) once the intima oxLDL level reaches a given threshold, consequently, triggering the recruitment and posterior transmigration of monocytes from the lumen into the intima. Moreover, like Silva and coauthors proposed, we consider that both macrophages and foam cells contribute for MCP-1 production, giving rise to atherosclerosis chronic inflammation.

By observing Equation (2.23), the main difference rises from the transport term. As an alternative to the stated assumption, we neglect this term in our model due to MCP-1 irrelevant mass for intima volume growth, as already explained. Therefore, the evolution of MCP-1 intima concentration (M_{cp}) is given by the following R-D equation:

$$\frac{\partial M_{cp}}{\partial t} + \underbrace{\nabla \cdot \left(-d_{M_{cp}} \nabla M_{cp}\right)}_{\text{Diffusion}} = \underbrace{k_{M_{cp},M} M}_{\substack{\text{Synthesis by} \\ \text{macrophages}}} + \underbrace{k_{M_{cp},F_c} F_c}_{\substack{\text{Synthesis by} \\ \text{foam cells}}} - \underbrace{\lambda_{M_{cp}} M_{cp}}_{\text{Degradation}} \tag{3.3.a}$$

subject to Neumann (flux) boundary conditions homogeneous everywhere, except for Γ_{end}:

$$\begin{cases} (-d_{M_{cp}} \nabla M_{cp}) \cdot \boldsymbol{n}_i = a_{M_{cp},L_{ox}} (L_{ox} - L_{ox}^{th}) & , \text{on } \Gamma_{end} \\ \left(-d_{M_{cp}} \nabla M_{cp}\right) \cdot \boldsymbol{n}_i = 0 & , \text{on } \partial\Omega \backslash \Gamma_{end} \end{cases} \tag{3.3.b}$$

In Equation (3.3.a), constants $d_{M_{cp}}$ and $\lambda_{M_{cp}}$ are, respectively, the diffusion coefficient and the degradation rate of MCP-1. On the right-hand side, it is possible to confirm the expected MCP-1 production by macrophages and foam cells concentrations (M and F_c, respectively), thus, those cells have specific MCP-1 production rates, which are represented by $k_{M_{cp},M}$ and k_{M_{cp},F_C}, respectively.

The boundary condition described in Equation (3.3.b) accounts for EC activation, that is, the MCP-1 segregation by endothelial cells (at the rate $a_{M_{cp},L_{ox}}$). Therefore, a given high threshold oxLDL concentration (L_{ox}^{th}) is considered the starting point for the inflammatory reaction. In other words, the inflammatory process activation only occurs when oxLDL concentration (L_{ox}) is greater than L_{ox}^{th}.

Endothelial Permeability to LDL and monocytes

A crucial factor, not only regarding the earlier stages of atherosclerosis but also during plaque development, is the endothelial permeability (EP) to LDL particles and monocytes. In fact, in pathological conditions, due to cytokines influence, permeability to arterial plasma is changing along the artery with time, owing to cellular apoptosis (in particular, endothelial cells) and inflammation itself [34]. Therefore, influenced by WSS patterns and MCP-1 expression by ECs, our model assumes that EP ends up affecting the intima dynamics of oxLDL and macrophages.

Hence, according to our assumptions and following [8], EP is defined as decreasing function of WSS and increasing function of MCP-1. Thus, Equations (3.1.b) and (3.2.b) resort to the expression for endothelial permeability to LDL (P_{LDL}) and to monocytes (P_m), respectively:

$$P_{LDL/m}(WSS, M_{cp}) = P_{LDL/m}^{st} + \frac{\epsilon_{LDL/m}^{max}}{2}\left(\frac{WSS_0}{WSS_0+WSS} + \frac{M_{cp}}{K_{M_{cp}}+M_{cp}}\right) \quad (3.4)$$

where $K_{M_{cp}}$ refers to MCP-1 natural saturation rate due to ingestion by macrophages, WSS_0 stands for the standard value of wall shear stress and, finally, $\epsilon_{LDL/m}^{max}$ is given by $(P_{LDL/m}^{max} - P_{LDL/m}^{st})$, that is, the difference between the maximum EP (to LDL or to monocytes) and its standard value. Moreover, WSS stands for this vector's magnitude (defined further on this chapter).

In conclusion, the EP function is:

- Equal to zero if $P_{LDL/m} - P_{LDL/m}^{st} \leq \frac{\epsilon_{LDL/m}^{max}}{4}$, that is, $WSS \geq WSS_0$ and $M_{cp} = 0$;
- Equal to $P_{LDL/m}$ if $P_{LDL/m} - P_{LDL/m}^{st} > \frac{\epsilon_{LDL/m}^{max}}{4}$.

3.2.2.2. Fatty Streak (Stage II)

Concerning the second stage of atherosclerosis, the most relevant event relies on the creation and continuous accumulation of foam cells due to oxLDL ingestion by macrophages, consequently, generating the so-called fatty streak. Therefore, we model these cells dynamics based on the work developed by Hao and Friedman in [14] since they also consider a saturation rate on the ingestion of oxLDL by one macrophage.

Foam Cells

Generally, after ingesting large amounts of oxLDL, macrophages transform into lipid laden cells, called foam cells. Looking again at Equation (2.18), one concludes that Hao and Friedman defined a constant k_F, which stands for the rate of foam cells formation. According to these authors, it differs from oxLDL uptake rate by macrophages, as settled by our assumptions.

Furthermore, a transport term for foam cells was also proposed (owing to these cells size), which is in concordance with our assumptions. Thus, the following A-R-D equation is used to describe foam cells evolution (F_c) in our model:

$$\underbrace{\frac{\partial F_c}{\partial t}}_{} + \underbrace{\nabla \cdot (\boldsymbol{v} F_c)}_{\text{Advection}} + \underbrace{\nabla \cdot (-d_F \nabla F_c)}_{\text{Diffusion}} = \underbrace{k_F \frac{L_{ox}}{L_{ox}+K_{L_{ox}}} M}_{\text{Formation}} - \underbrace{\lambda_F F_c}_{\text{Degradation}} \tag{3.5.a}$$

subject to Neumann (flux) boundary conditions homogeneous everywhere:

$$(-d_F \nabla F_c + \boldsymbol{v} F_c) \cdot \boldsymbol{n}_i = 0 \qquad , \text{on } \partial\Omega \tag{3.5.b}$$

The left-hand side of Equation (3.5.a) contains a advection and a diffusion term. The former stands for the contribution of foam cells for intima volume (consequently, for the inflammatory process), thus, it carries plaque growth velocity ($\boldsymbol{v}$), whereas the latter comprises foam cells diffusion coefficient inside the intima layer (d_F).

Then, the right-hand side of Equation (3.5.a) is composed by two reaction terms. The first refers to foam cells formation, whose saturation term is pertinent to highlight. In fact, just like macrophages PDE, foam cells concentration remains under the influence of oxLDL concentration, evidenced through $K_{L_{ox}}$ (the upper limit to oxLDL ingestion by one macrophage). The second term stands for the degradation of these lipid-laden cells, with degradation rate λ_F. Finally, when it comes to the domain boundaries, zero flux is assumed for foam cells.

3.2.2.3. Fibrofatty Injury (Stage III)

The third stage of atherosclerosis stands out for the critical proliferation and migration of smooth muscle cells (SMCs) from the media into the intima, as well as for the synthesis of other cytokines, such as PDGF. Therefore, this stage is also based on the work developed by Hao and Friedman in [14] who considered SMCs chemotactic motion and PDGF production, which has strong mitogenic and chemotactic effects on SMCs, thus, emphasizing the inflammatory reaction, which is in concordance with our assumptions and with the above-mentioned authors.

SMCs

In advanced atherosclerotic disease, SMCs, eventually, proliferate and migrate from the media into the intima layer, moved by chemotaxis processes. Analyzing Equation (2.19), the authors defined this process by means of MCP-1 and PDGF gradients whereas another motion (haptotaxis) was described through extracellular matrix (ECM) gradient. The latter, for simplicity, is no concern for our study, since the ECM is not considered a relevant protagonist in atherosclerosis, only the main component of the biomass.

In addition, an influx influx of SMCs is, similarly, assumed at the media boundary, as well as a transport term owing to SMCs relevant mass for intima volume growth. Finally, SMCs degradation term (proposed in [13]) is disregarded in this work because our simulations do not arrive at those too advanced instability plaque conditions. Therefore, SMCs concentration inside the intima is written through the following χ-A-R-D equation:

$$\frac{\partial S}{\partial t} + \underbrace{\nabla \cdot (\boldsymbol{v}S)}_{\text{Advection}} + \underbrace{\nabla \cdot (-d_S \nabla S)}_{\text{Diffusion}} = \underbrace{-\nabla \cdot \left(S\chi_C \nabla M_{cp}\right)}_{\substack{\text{Chemotactic} \\ \text{motion by} \\ \text{MCP-1}}} \underbrace{- \nabla \cdot (S\chi_C \nabla G)}_{\substack{\text{Chemotactic} \\ \text{motion by} \\ \text{PDGF}}} \quad (3.6.a)$$

subject to Neumann (flux) boundary conditions homogeneous everywhere, except for Γ_{med}:

$$\begin{cases} (-d_S \nabla S + \boldsymbol{v}S) \cdot \boldsymbol{n}_i = \alpha_S \, (S_0 - S) & , \text{on } \Gamma_{med} \\ (-d_S \nabla S + \boldsymbol{v}S) \cdot \boldsymbol{n}_i = 0 & , \text{on } \partial\Omega \backslash \Gamma_{med} \end{cases} \quad (3.6.b)$$

where $\alpha_S = \tilde{\alpha}_S \frac{M_{cp}+G}{P_0+G_0}$, with $\tilde{\alpha}_S$ standing for the influx rate of SMCs into the intima, P_0 and G_0 refer to given MCP-1 and PDGF concentrations (respectively) and S_0 represents SMCs influx at the media boundary. SMCs flux over the other boundaries is, therefore, considered absent.

The left-hand side of Equation (3.6.a) comprises a advection term, since SMCs contribute for the inflammatory process so, again, it carries plaque growth velocity ($\boldsymbol{v}$). Furthermore, a diffusion term is also present, thus, d_S corresponds to SMCs diffusion coefficient inside the intima. In the right-hand side, both terms account for SMCs chemotactic motion in response to MCP-1 and PDGF gradients (∇M_{cp} and ∇G, respectively), thus, χ_C stands for SMCs chemotaxis parameter.

PDGF

Progressive dysfunctional endothelium leads to platelet adhesion and aggregation, consequently, releasing platelets-derived growth factor (PDGF), which has strong mitogenic and chemotactic effects on SMCs within the site of the lesion. Moreover, our model assumes that PDGF is synthetized by macrophages, foam cells and SMCs, similarly to Hao and Friedman in [14]. Giving the relevance of its attractant role in atherosclerosis, the mentioned authors proposed Equation (2.20) to model PDGF concentration inside the intima. Following similar assumptions, we describe this cytokine intima dynamics (G) through the R-D equation:

$$\frac{\partial G}{\partial t} + \underbrace{\nabla \cdot (-d_G \nabla G)}_{\text{Diffusion}} = \underbrace{k_{G,M} M}_{\substack{\text{Production by} \\ \text{macrophages}}} + \underbrace{k_{G,F} F_c}_{\substack{\text{Production} \\ \text{by foam} \\ \text{cells}}} + \underbrace{k_{G,S} S}_{\substack{\text{Production} \\ \text{by SMCs}}} - \underbrace{\lambda_G G}_{\text{Degradation}} \quad (3.7.a)$$

subject to Neumann (flux) boundary conditions homogeneous everywhere:

$$(-d_G \nabla G) \cdot \boldsymbol{n}_i = 0 \qquad , \text{on } \partial\Omega \quad (3.7.b)$$

In Equation (3.7.a), it is observable that PDGF production is performed by macrophages, foam cells and SMCs, with rates $k_{G,M}$, $k_{G,F}$, and $k_{G,S}$, respectively. The diffusion of this cytokine is also assumed, thus, d_G stands for PDGF diffusion coefficient inside the intima. The last right-hand side term accounts for its natural degradation, thus, λ_G represents PDGF degradation rate. Lastly, boundary conditions determine no PDGF flux through any boundary of our domain, as portrayed by Equation (3.7.b).

3.2.2.4. Fibrous Plaque (Stage IV)

The last stage of atherosclerosis plaque development is remarkably distinguished by ECM metabolism and the consequent plaque maturation and cap's integrity. Once collagen fibres are assumed the main ECM component in our model, it is possible to say that fibrous plaques depend on a key variable which is starred by collagen dynamics. In fact, the latter is responsible for exerting the vital mechanical strength inside the plaque, as verified in literature [72].

Moreover, although intima foam cells might produce it, collagen is mostly produced by migrated SMCs. Since we describe the advanced stage by adding collagen PDE, we resorted to the work developed by Cilla et al. in [13].

Collagen

To complete our intima model, fibrous plaque synthesis and maturation are assured by means of collagen dynamics. Analyzing Equation (2.16), Cilla and coauthors modeled collagen degradation and production phenomena. However, similarly to SMCs dynamics, collagen degradation consists on a phenomenon which, typically, occurs during advanced instability atherosclerosis conditions (which is not our goal). Thus, collagen dynamics only assumes a transport term for these fibres since their mass is considered significant for intima volume growth, according to our assumptions. Therefore, we address the intima collagen concentration evolution (C_{ol}) through the simple C-R equation:

$$\frac{\partial C_{ol}}{\partial t} + \underbrace{\nabla \cdot (\boldsymbol{v} C_{ol})}_{\text{Advection}} = \underbrace{k_{C_{ol}} S}_{\substack{\text{Production} \\ \text{by SMCs}}} \tag{3.8.a}$$

subject to Neumann (flux) boundary conditions homogeneous everywhere:

$$(\boldsymbol{v} C_{ol}) \cdot \boldsymbol{n}_i = 0 \qquad , \text{on } \partial\Omega \tag{3.8.b}$$

In Equation (3.8.a), $k_{C_{ol}}$ stands for collagen synthesis rate. As expected, the production term guarantees that collagen synthesis is performed by SMCs.

There is, though, a particularity with this atherosclerosis protagonist, since no diffusion term is considered in its intima dynamics. In fact, once collagen fibres are not cells but contribute for the inflammatory process, their transport term (divergent operator) is only given by the advection due to intima volume growth, which is the reason why the latter carries plaque growth velocity ($\boldsymbol{v}$). To finish, no collagen flux is considered through our domain boundaries, as shown in Equation (3.8.b).

3.2.3. Plaque Growth inside the intima

In our simulations, each of the four stages of plaque development is accompanied by the velocity of intima plaque growth. In fact, due to continuous creation and accumulation of cells and species, the fluid pressure inside the intima layer and the resultant plaque growth in the y-direction are crucial factors in what atherosclerosis advanced plaques are concerned. This leads us to the main novelty of this work.

As far as we know, previous authors have restricted the modeling of plaque growth to foam cells creation and accumulation [9], [10], [8]. Instead, we are assuming that all the referred species which have considerable mass (macrophages, foam cells, smooth muscle cells and collagen) contribute to intima volume growth into the arterial lumen.

Under the local matter incompressibility assumption (when species are created the intima volume is locally increasing), there is a constant A which stands for the average intima density, such that:

$$A = M(x,y,t) + F_c(x,y,t) + S(x,y,t) + C_{ol}(x,y,t) + Z(x,y,t) \tag{3.9}$$

where all variables have already been introduced, except for Z. The latter stands for the biomass, that is, the rest of the intima medium (including the extracellular matrix and other) which does not contribute to the inflammatory response. Therefore, the biomass is defined with the simple advection equation:

$$\frac{\partial Z}{\partial t} + \nabla \cdot (\boldsymbol{v} Z) = 0 \tag{3.10}$$

Moreover, let us assume, for $i = 1$ to $i = 5$, that each of the referred cells (C_i) verifies

$$\frac{\partial C_i}{\partial t} + \nabla \cdot (\boldsymbol{v} C_i) - \nabla \cdot (d_i \nabla C_i) = R_i(C_i) \tag{3.11}$$

where the advection terms have velocity $\boldsymbol{v}$, owing the fact that cells undergo a passive transport inside the intima. On the other hand, diffusion terms depend on each diffusion coefficient and, finally, reaction terms include production and degradation terms.

Assuming that A is constant in time, one obtains:

$$\frac{\partial A}{\partial t} = 0 \tag{3.12}$$

Thus, by adding Equations (3.9) and (3.11), and considering the assumption in Equation (3.12), the system yields:

$$\nabla \cdot \boldsymbol{v} = \frac{1}{A} \sum_{i=1}^{5} \nabla \cdot (d_i \nabla C_i) + R_i(C_i) \tag{3.13}$$

To determine $\boldsymbol{v}$ (a model unknown), we resort to $\boldsymbol{D}(\boldsymbol{v})$, the rate of deformation tensor or strain rate tensor. The latter stands for the symmetric part of the velocity gradient and it is defined as:

$$\boldsymbol{D}(\boldsymbol{v}) = \frac{1}{2}[\nabla \boldsymbol{v} + (\nabla \boldsymbol{v})^T] \tag{3.14}$$

Once the mass growth of our continuum domain is due to different species accumulation, the system is closed by defining a kind of Stokes system, such as the one proposed by Calvez et al. in [10]:

$$\begin{cases} -\nabla \cdot \boldsymbol{D}(\boldsymbol{v}) + \nabla p = 0, & x \in \Omega_i, \ \ t \in [0,T] \\ \nabla \cdot \boldsymbol{v} = \frac{1}{A} \sum_{i=1}^{4} \nabla \cdot (d_i \nabla C_i) + R_i(C_i), & x \in \Omega_i, \ \ t \in [0,T] \\ \boldsymbol{D}(\boldsymbol{v}) \boldsymbol{n}_i - p \boldsymbol{n}_i = 0, & x \text{ on } \Gamma_{end}, \ \ t \in [0,T] \\ \boldsymbol{v} = 0, & x \text{ on } \partial\Omega_i \backslash \Gamma_{end}, \ \ t \in [0,T] \end{cases} \tag{3.15}$$

where p represents the intima pressure, which is also a model unknown.

Furthermore, all species are assumed to have zero velocity on every boundary except for the endothelial barrier, which deforms into the arterial lumen with velocity $\boldsymbol{v}$, allowing plaque growth into the arterial lumen.

3.2.4. Governing equations for blood flow inside the lumen

Seeing that blood is characterized as a suspension of numerous particles (e.g. erythrocytes, leukocytes, platelets) in a fluid called plasma, one may conclude that it is a very complex fluid with peculiar mechanical properties. In fact, thanks to erythrocytes property of changing their microstructure, blood resistance to deformation by shear rates (the so-called viscosity) is not constant over the circulatory system, decreasing when the rate of deformation increases. Thus, blood is, actually, a non-Newtonian fluid [93].

However, many authors have considered blood flow as a Newtonian (constant viscosity), laminar, isothermal and incompressible fluid ([91], [10], [13], [85], [11], [8]) and so, as a first approach (and because we are dealing with simplified domains), we apply the same methodology in this thesis. The shear deformation applied to the arterial walls by blood flow is, thus, neglected.

Then, to accurately represent blood behavior inside the lumen subdomain (see Figure 3.1). Thus, the Navier-Stokes (NS) equations were exploited to perform a simple description of blood motion inside the lumen:

$$\rho_l\left[\frac{\partial \boldsymbol{u}_l}{\partial t} + (\boldsymbol{u}_l \cdot \nabla)\boldsymbol{u}_l\right] - \nabla \cdot \boldsymbol{T}_l(\boldsymbol{u}_l, p_l) = 0 \ , \ \ x \in \Omega_l \ , \ t \in [0, T] \tag{3.16}$$

$$\nabla \cdot \boldsymbol{u}_l = 0 \ , \ \ x \in \Omega_l \ , \ t \in [0, T] \tag{3.17}$$

where $\boldsymbol{u}_l$ represents the blood velocity field, ρ_l is blood density and p_l is blood pressure. Equation (3.16) guarantees the conservation of linear momentum, stating that forces acting on the fluid must be in equilibrium (reason why the right-hand side is equal to zero). Function $\boldsymbol{T}_l$, in turn, represents the Cauchy stress tensor, defined as:

$$\boldsymbol{T}_l(\boldsymbol{u}_l, p_l) = -p_l \boldsymbol{I} + 2\mu_l \boldsymbol{D}(\boldsymbol{u}_l) \tag{3.18}$$

with μ_l representing the dynamic viscosity[17] and $\boldsymbol{D}(\boldsymbol{u}_l)$ the strain rate tensor. Multiplied by blood pressure, $\boldsymbol{I}$ stands for the unit matrix. Finally, Equation (3.17) corresponds to the continuity equation and represents the conservation of mass for an incompressible fluid.

Furthermore, our interest of study is the atheromatous plaque formation, however, there is an elevated time "gap" between lumen and intima dynamics: lesion growth needs decades to occur whereas time scale of blood is seconds. Thus, pulsatile (o periodic) characteristic of blood flow might be neglected and steady-state condition assumed for blood flow, that is. For simplicity, stationary incompressible Navier-Stokes equations are rewritten as:

$$\begin{cases} (\boldsymbol{u}_l \cdot \nabla)\boldsymbol{u}_l - \nu_l \Delta \boldsymbol{u}_l + \nabla p_l = 0 \\ \nabla \cdot \boldsymbol{u}_l = 0 \end{cases} \tag{3.19}$$

where $\nu_l = \frac{\mu_l}{\rho_l}$ stands for the kinematic viscosity and the unknowns correspond to blood velocity ($\boldsymbol{u}_l$) and blood pressure (p_l). This is a nonlinear system that needs to be closed with appropriate boundary

[17] Contrarily to our simplified approach, realistic models consider blood as a non-Newtonian fluid, therefore, the dynamic viscosity is not constant in those models. Nonetheless, for simplicity, we take it as a known constant [139].

conditions. At all luminal wall (Γ_{end}), we assume the zero velocity for blood ($u = 0$), meaning a homogeneous Dirichlet boundary condition. At the luminal inlet ($\Gamma_{l,in}$), in turn, entering velocities are given by Poiseuille velocity profile:

$$\boldsymbol{U} = \left(u_{max}\left(1 - \left(\frac{y - r_l}{r_l}\right)^2\right), 0\right) \tag{3.20}$$

where u_{max} stands for the spatial mean velocity and r_l for the luminal arterial radius. Finally, at the outlet boundary ($\Gamma_{l,out}$), we consider a constant pressure, $p_l = p_{out}$.

Wall Shear Stress

In atherosclerosis pathological conditions, hemodynamic shear stresses distribution is highly nonuniform. Therefore, when coupling lumen and intima fluid dynamics, it is relevant to estimate the real value of the shear deformation applied to a region of the arterial wall by blood flow. We report, thus, an accurate strategy which comes from blood dynamics inside the lumen, that is, from NS solutions.

Considering that the preservation of *in vivo* vascular endothelial cells is influenced by a surface stress generated by blood flow, we implemented a commonly used approach to model this variable [8]. By decomposing the surface stress into normal and tangential components, one obtains the normal stress and the apical frictional force (which is the so-called shear stress, which deforms cells in the flow direction), respectively.

Furthermore, once WSS plays a significant role in the local distribution of atherosclerosis lesions (see chapter 2), we adopt the same procedure of the mentioned authors to define it as the tangential component of the normal fluid stress at the endothelium, which yields:

$$\boldsymbol{WSS} = \boldsymbol{T}_l^n - (\boldsymbol{T}_l^n \cdot \boldsymbol{n}_l)\boldsymbol{n}_l \tag{3.21}$$

where $\boldsymbol{T}_l^n = \boldsymbol{T}_l \cdot \boldsymbol{n}_l$.

As previously stated in Equation (3.4), WSS value is needed when accessing the endothelial permeability to circulating LDLs and monocytes.

3.3. Numerical Methods

Numerical simulations are useful tools to illustrate complex mathematical models as well as to improve the understanding of biological system behaviors. Hence, they are currently considered by many authors a valuable tool to model atherosclerosis [13], [14], [10], [85]. Some methods, though, are previously required before moving to the implementation of our scheme of equations.

For spatial discretization of our PDEs, we resort to the finite element method[18] (FEM), a strong tool to approximate the solution of numerical model equations to the real solution of PDEs. This approximation is computed using linear combinations of basis functions. If u is a dependent variable in

[18] FEM portrays remarkable advantages such as a good theoretical foundation, well-conditioned linear systems, easily handled boundary conditions and the complete cover of any region by the elements.

a PDE, it can be approximated by a function u_h (that is, $u \approx u_h$) using linear combinations of basis functions (ψ_i), according to:

$$u_h = \sum_i u_i \psi_i \tag{3.22}$$

where u_i denotes the coefficients of the functions that approximate u with u_h.

FEM discretization is based on their variational (or weak) formulation. To illustrate this formulation, let us consider Poisson Equation, which is used to model several important phenomena within a certain domain (Ω) subjected to a generic function $f(x, y)$. Accordingly, we are looking for the solution to the following problem:

Find real-valued u defined on Ω such that

$$\begin{cases} -\Delta u(x,y) = f(x,y), & \forall (x,y) \in \Omega \\ u = 0, & \text{on } \partial\Omega_D \\ \nabla u \cdot \boldsymbol{n} = h, & \text{on } \partial\Omega_N \end{cases} \tag{3.23}$$

where $\Delta \equiv \frac{\partial^2}{\partial x^2} + \frac{\partial^2}{\partial y^2}$ stands for the Laplacian operator, $\nabla \equiv (\frac{\partial}{\partial x}, \frac{\partial}{\partial y})$ represents the Gradient operator and the Dirichlet condition on $\partial\Omega_D$ fixes the domain at that boundary. This is the classical formulation of the boundary value problem [94]. When analyzing Poisson Equation pertinent questions arise, specially concerning the existence, uniqueness and regularity of the solution (which involves its *a priori* estimation), the dependence (or sensitivity) of the solution on the input data and the methods of resolution to arrive at a suitable solution (analytic or by approximation). Answering these questions requires dealing with the weak formulation, which can be derived as follows: differential equations are multiplied by a test function and integrated by parts in the domain, utilizing their respective boundary conditions [91], [94]. Firstly, the weak formulation considers the solution u as a particular element to be found in a function space V. Then, if v denotes a generic element of space V (vanishing on $\partial\Omega_D$), the differential equation is multiplied by v and integrated in the domain, which yields:

$$\int_\Omega -\Delta u \, v \, dx = \int_\Omega f \, v \, dx \, , \forall \, v \in V \tag{3.24}$$

After using Green's formula (Divergence Theorem), and considering that all v elements satisfy the above-mentioned boundary conditions, one obtains the weak formulation for the PDE:

$$\int_\Omega \nabla u \cdot \nabla v \, dx - \int_{\partial\Omega} \nabla u \cdot \boldsymbol{n} \, v \, dS = \int_\Omega f \, v \, dx \, , \forall \, v \in V \tag{3.25}$$

where $\boldsymbol{n}$ is the outward unit normal vector to boundary surface. Considering the applied boundary conditions, the second left-hand term is reduced to the Neumann part, that is, $\int_{\partial\Omega_N} \mathrm{h} \, v \, dS$. Thus, by substituting the test function with basis functions (ψ_j), which were introduced in Equation (3.22), and approximating u with u_h, we obtain the same linear system written in the discretized form, that is:

$$\sum_i^n u_i \int_\Omega \nabla\psi_i \cdot \nabla\psi_j dx = \int_\Omega f \, \psi_j dx + \int_{\partial\Omega_N} h \, \psi_j \, dS \tag{3.26}$$

where n is the dimension of the basis space. For $j = 1, \ldots, n$, it yields the matrix system $AU = F$, where A is the $n \times n$ system matrix with entrances $A_{ij} = \int_\Omega \nabla\psi_i \cdot \nabla\psi_j dx$, vector U contains coefficients

u_i (used in Equation (3.22)) and, finally, F is the $n \times 1$ vector with components $F_j = \int_\Omega f\, \psi_j\, dx + \int_{\partial\Omega_N} h\, \psi_j\, dS$.

Although the solution may contain less smoothness than the continuous form (suitable mathematical tools are further required to solve raised questions), the variational formulation requires lower continuity on the solution and provides flexibility to the system of equations. Moreover, the FEM order represents the approximation function order. It affects the number of degrees of freedom (DOFs)[19] as well as the accuracy of the obtained solution [94], [95], [96].

Applying that methodology to our system of PDEs (see from Equation (3.1.a) to (3.8.b)), taking $R(C)$ as the reaction/chemotactic term of a generic concentration C, d as its diffusion coefficient and h as its non-homogeneous Neumann (flux) boundary condition, we obtained the following weak formulations in COMSOL Multiphysics:

$$\int_\Omega d\, \nabla C \cdot \nabla \psi\, dx - \int_\Omega R(C)\, \psi\, dx - \int_{\partial\Omega_N} h\, \psi\, dS = 0 \tag{3.27}$$

for a generic A-R-D equation with a non-homogeneous Neumann boundary condition.

Furthermore, representing intima growth velocity vector by $\boldsymbol{u}$ and intima pressure by p, Stokes system (see from Equation (3.9) to (3.15)) was implemented through:

$$\begin{cases} \int_\Omega \mathbf{D}(\boldsymbol{u}) : \nabla \psi\, dx - \int_\Omega p\, \nabla \psi\, dx = 0 \\ \int_\Omega (\nabla \cdot \boldsymbol{u})\, \psi\, dx - \int_\Omega \frac{1}{A} \sum_{i=1}^{4} \nabla \cdot (d_i \nabla C_i) + R_i(C_i)\ \psi\, dx = 0 \end{cases} \tag{3.28}$$

where we assumed that macrophages, foam cells, SMCs and collagen are the only protagonists that contribute for the inflammation, and homogeneous Neumann conditions for all boundaries except for the endothelium (which was assigned homogeneous Dirichlet condition).

Finally, considering that $\boldsymbol{u}_l$ represents blood velocity, p_l blood pressure and ν_l kinematic viscosity, Navier-Stokes equations (see Equation (3.19)) were rewritten as:

$$\begin{cases} \int_\Omega (\boldsymbol{u}_l \cdot \nabla)\boldsymbol{u}_l\, \psi\, dx - \int_\Omega\ \ \nu_l \mathbf{D}(\boldsymbol{u}_l) : \nabla \psi\, dx + \int_\Omega p_l\, \nabla \psi\, dx = 0 \\ \int_\Omega (\nabla \cdot \boldsymbol{u}_l)\, \psi\, dx = 0 \end{cases} \tag{3.29}$$

Regarding temporal discretization, we used backward differentiation formulas (BDFs) which refer to implicit, stable and linear multistep methods based on numerical differentiation for solutions to ordinary differential equations [95], [97], [94]. BDFs approximate the derivative of a function using information from already computed times. In our case, providing their enough robustness to our model, BDFs of order 2[20] were computed. If a generic time-dependent concentration C is described by a simple reaction-diffusion equation, that is:

$$\frac{\partial C}{\partial t} - \Delta C = R(C) \tag{3.30}$$

Then, the general formula for a BDF at $t = n + 2$ with step size h is written as:

[19] DOFs are the number of independent parameters that can be described by an approximate function.

[20] A BDF method of order *n* computes the solution using an n^{th} - grade polynomial in terms of backward differences, determining the order of accuracy of the discretization [95].

$$C_{n+2} = \frac{4}{3}C_{n+1} + \frac{1}{3}C_n - \frac{2}{3}hf(t_{n+2}, C_{n+2}) \quad (3.31)$$

Since in Equation (3.27) f can be given by $f(t, C) = \frac{\partial C}{\partial t} = \Delta C + R(C)$, we obtain:

$$C_{n+2} = \frac{4}{3}C_{n+1} + \frac{1}{3}C_n - \frac{2}{3}h(\Delta C_{n+2} + R(C_{n+2})) \quad (3.32)$$

Owing to temporal and spatial discretization as well as to Navier-Stokes implementation, a nonlinear problem arises. In this work, nonlinear system is linearized with Newton's method, an iterative method to estimate possible solutions [94]. Additionally, the iterative method MUMPS (multifrontal massively parallel sparse direct solver) was used to approach the solution gradually, benefiting from shared memory parallelism when compared to direct solvers [94].

Finally, numerical instabilities[21] are also originated by chemotaxis-advection-reaction-diffusion (χ-A-R-D) equations which describe macrophages and SMCs. Those are overcome with stabilization techniques that add artificial diffusion to PDEs, allowing not only robust and faster computational performances but also physical solutions achievement (see [94] for more details).

3.3.1. Mesh Settings

Our FEM uses finite dimensional subspace to approximate the solution in both subdomains (intima and lumen). For that, the rectangular computational domain is approximated by triangular elements, as presented in Figure 7. Additionally, once the interface between our two subdomains undergoes a deformation process, the elements along the endothelial boundary (Γ_{end}) are smaller triangles, as shown in a closer view (Figure 8). Besides, this smaller discretization is also computed for Γ_{med} owing to SMCs migration from the media surface into the intima domain.

[21] In a general A-R-D equation, the Peclet number (Pe) is given by $Pe = \frac{||\beta||h}{2c}$, where $||\beta||$ is the norm of the advective velocity, h the mesh element size and c stands for the specie's diffusion coefficient. For each spatial element, when Pe is higher than 1 spurious oscillations occur, giving rise to numerical instabilities [93], [94].

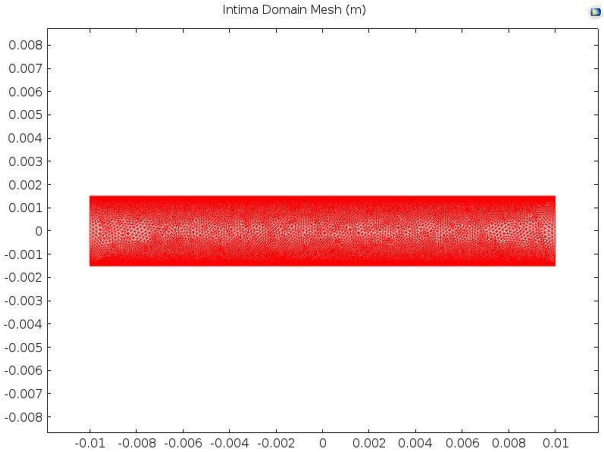

Figure 8 - Spatial discretization applied to our intima domain (**39 900** elements).

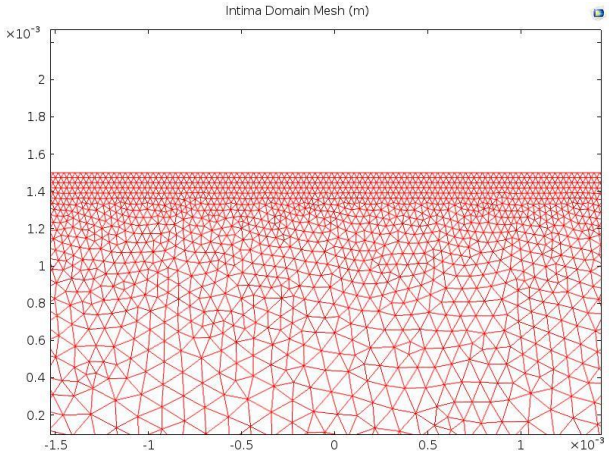

Figure 7 - Zoom view of the intima spatial discretization, with closer triangles near Γ_{end} (similar for Γ_{med}).

3.3.2. Deformed Geometry

The Arbitrary Lagrangian-Eulerian (ALE) formulation is used to couple the deformation with Navier-Stokes (NS) equations. Eulerian equations (such as NS) are written with respect to a mesh, which can be moving in relation to both Eulerian frame[22] and Lagrangian frame[23] [94]. Therefore, the ALE method joints the best features of both Eulerian and Lagrangian approaches, allowing moving boundaries with no need for the mesh movement to follow the material.

Considering our domain subdivision and the lack of expected rotations, *Deformed Geometry* interface (available in COMSOL Multiphysics 5.0) was used to run the simulation for the coupled system (from Equation (3.1.a) to (3.15)). Giving the fact that the original geometry is growing due to mass addition, through *Deformed Geometry* interface the total domain volume change is allowed (for more details see [94]).

Once endothelial boundary elements are assigned free displacement, the chosen mesh should be smoothly deformed, according to the given boundary conditions. We chose Laplace mesh smoothing

[22] Eulerian frame relates with spatial coordinate system (fixed in space).
[23] Lagrangian frame is linked to material coordinate system (fixed to the material).

type, the cheapest option that allows enough numerical simulations accuracy since it consists on a linear method that uses one equation for each coordinate direction (which are not coupled to each other) [94].

3.4. Parameters selection

Before starting the computational implementation, both domain and model parameters were selected from the available literature on atherosclerosis experiments. Nonetheless, once some parameters lack on experimental data, we used previously suggested values by above-mentioned authors or adapted those to our simulation conditions. Owing to these estimations, the present work provides a sensitivity analysis study (explained at the end of this section) to access model parameters influence on the obtained results.

3.4.1. Domain Parameters

In a first approach, we implemented our model in an idealized two-dimensional rectangular geometry of a coronary artery. Then, in a second approach, we resorted to a more complex 2D geometry representing left coronary artery bifurcation (introduced in chapter 4).

In our two-dimensional idealized rectangular geometry, specific features are implemented according to the clinical study present in [98] and [99] regarding the physiological dimensions of human coronary artery (left anterior descending or LAD). Intima and lumen dimensions are, thus, shown in Figure 9. Since we are assuming blood as a laminar and Newtonian flow, the length of both subdomains is taken as $10\ cm$ to obtain a completely developed flow.

Figure 9 - Illustration of our computational blood vessel, with an intima layer with $0.034\ cm$ of height and a lumen with a $0.37\ cm$ diameter.

3.4.2. Model Parameters

As far as possible, we aim at approximating our model parameters to their human physiological values, with the starting point that, for physically reasonable solutions, all of them must be real and non-negative. Therefore, we conducted an extensive research through a wide variety of experimental studies (available in the literature) regarding atherosclerosis pathology. Some parameters, however, had to be adapted to our simulations conditions to allow biologically reasonable results during the computational time, as reported in this section. Table 2 provides a summary of parameters physiological meaning, origin (animal/human experiment or estimated order of magnitude), reference of the work where they were obtained and used value for numerical simulations.

In lumen dynamics, blood mean velocity ($\mathrm{U_{max}}$) is taken as $24\ cm/s$ since it corresponds to the average of diastolic and systolic velocities measured inside the left anterior descending coronary (LAD) artery [100]. Furthermore, endothelial permeability requires wall shear stress standard value ($\mathrm{WSS_0}$), assumed as $11\ g/(cms^2)$, that is, $1.1\ Pa$, which comes from experimental studies performed in cat coronary artery in [101]. Contrarily to human LAD physiological conditions, for simplification reasons, blood pressure at the outlet ($\mathrm{p_{out}}$) is taken as zero, and not $70\ mmHg$ (as reported in literature).

Moreover, we assume that LDL endothelial influx (C_{LDL}) corresponds to LDL concentration at the luminal inlet ($1.9\ g/cm^3$), experimentally measured in rabbit models in [102]. Likewise, monocytes influx at the EC surface (C_m) is taken as ($5.0 \times 10^{-5}\ g/cm^3$) according to monocytes luminal inlet concentration, also considered by Hao and Friedman, and clinically obtained in [103]. Moreover, considering early atherosclerosis estimated parameters of some mentioned authors, we also assume that standard permeability to monocytes (P_m^{st}) is 10 times lower than the standard permeability to LDL, as previously proposed in [10] and [8]. The oxLDL threshold concentration (L_{ox}^{th}), the minimum concentration that activates atherosclerosis inflammatory reaction, was clinically obtained in [104] assuming value $8 \times 10^{-6}\ g/cm^3$.

Additionally, some needed parameters were estimated by previous authors for different models, consequently, we had to adapt them to ours. For instance, macrophages proliferation rate ($\mathrm{M_{pro}}$) and MCP-1 activation rate ($\mathrm{a_{M_{cp},L_{ox}}}$) were reduced from their value measured in [68] and [10] (respectively), to obtain non-negative values of concentrations (see Table 2). Also, clinical values of macrophages and SMCs chemotaxis sensitivity parameters (χ_{M} and χ_{c}, respectively) were changed (final values are shown in Table 2). Consequently, sensitivity analysis is highly pertinent to access the influence of used parameters in our model, with a special concern at estimated and adapted parameters.

Table 2 - Summary of the parameters used in the model. In the "Experimental" column, "A" stands for animal model and "H" for human model.

Parameter Notation	Physiological Meaning	Value (Units)	Reference	Experimental (A or H)	Estimated
Blood Parameters					
WSS_0	Standard WSS in human coronary artery	*1.1 (Pa)*	[101]	Yes (A)	--
U_{mean}	Mean artery inlet velocity	*24.0 (cm/s)*	[100]	Yes (A)	--
μ_l	Blood viscosity	*3.5x10^{-2} (gcm^{-1}s^{-1})*	[105]	Yes (H)	--
ρ_l	Blood density	*1.05 (g/cm^3)*	[105]	Yes (H)	--

Diffusion Coefficients					
$d_{L_{ox}}$	oxLDL diffusion coefficient	*8.0x10^{-9} (cm^2/s)*	[106]	Yes (H)	--
d_M	Macrophages diffusion coefficient	*1.0x10^{-11} (cm^2/s)*	[107]	Yes (H)	--
$d_{M_{cp}}$	MCP-1 diffusion coefficient	*2.0x10^{-6} (cm^2/s)*	[108]	Yes (H)	--
d_{F_c}	Foam cells diffusion coefficient	*1.0x10^{-11} (cm^2/s)*	[109]	Yes (H)	--
d_S	SMCs diffusion coefficient	*1.0x10^{-11} (cm^2/s)*	[109]	Yes (H)	--
d_G	PDGF diffusion coefficient	*1.0x10^{-6} (cm^2/s)*	[110]	Yes (H)	--
Rates					
$k_{M_{cp},M}$	MCP-1 production rate by macrophages	*1.0x10^{-10} (s^{-1})*	[111]	Yes (H)	--
k_{M_{cp},F_c}	MCP-1 production rate by foam cells	*3.0x10^{-10} (s^{-1})*	[111]	Yes (H)	--
$k_{G,M}$	PDGF production rate by macrophages	*1.16x10^{-6} (s^{-1})*	[59]	Yes (H)	--
k_{G,F_c}	PDGF production rate by foam cells	*3.82x10^{-7} (s^{-1})*	[59]	Yes (H)	--
$k_{G,S}$	PDGF production rate by SMCs	*5.79x10^{-6} (s^{-1})*	[59]	Yes (H)	--
k_{F_c}	Foam cells formation rate	*1.39x10^{-6} (s^{-1})*	[112]	Yes (A)	--
k_{col}	Collagen synthesis rate by SMCs	*2.16x10^{-11} (gcell^{-1}s^{-1})*	[113]	Yes (H)	--
$\lambda_{M_{cp}}$	MCP-1 degradation rate	*2.31x10^{-5} (s^{-1})*	[114]	Yes (H)	--
λ_{F_c}	Foam cells degradation rate	*3.47x10^{-7} (s^{-1})*	[115]	Yes (A)	--
λ_G	PDGF degradation rate	*4.44x10^{-5} (s^{-1})*	[110]	Yes (H)	--
r_{diff}	Monocytes differentiation rate into macrophages	*1.15x10^{-6} (s^{-1})*	[115]	Yes (A)	--

r_{ox}	LDL oxidation rate	*3.0x10^{-4} (s^{-1})*	[116]	Yes (H)	--
M_{pro}	Macrophages proliferation rate	*1.0x10^{-9} (s^{-1})*	[68]	Adapted	Yes
$k_{L_{ox}}$	Saturation rate of oxLDL uptake by one macrophage	*0.5 (g/cm^3)*	[92]	Yes (A)	--
$k_{M_{cp}}$	Saturation rate of MCP-1 due to ingestion by macrophages	*2.5x10^{-5} (g/cm^3)*	[103]	Yes (H)	--
$k_{L_{ox},M}$	Rate of oxLDL uptake by macrophages	*1.0x10^{-4} (s^{-1})*	[68]	--	Yes
$a_{M_{cp},L_{ox}}$	Rate of MCP-1 activation due to high oxLDL concentration	*1.0x10^{-10} (s^{-1})*	[10]	Adapted	Yes
$\tilde{a}_S$	Influx rate of SMCs into the intima	*0.2 (cm^{-1})*	[14]	--	Yes
Concentrations					
C_{LDL}	LDL endothelial source	*1.9 (g/cm^3)*	[102]	Adapted	--
C_m	Monocytes endothelial source	*5.0x10^{-5} (g/cm^3)*	[103]	Yes (H)	--
L_{ox}^{th}	Threshold oxLDL concentration	*8.0x10^{-6} (g/cm^3)*	[104]	Yes (H)	--
A	Plaque average density	*1.22 (g/cm^3)*	[117]	Yes (H)	--
S_0	SMCs influx at the media boundary	*6.0x10^{-3} (g/cm^3)*	[118]	Yes (H)	--
P_0	MCP-1 influx concentration	*3.0x10^{-10} (g/cm^3)*	[119]	Yes (H)	--
G_0	PDGF influx concentration	*1.5x10^{-8} (g/cm^3)*	[60]	Yes (H)	--
Others					
χ_C	SMCs chemotaxis sensitivity parameter	*1.16x10^{-4} (cm^{5}g^{-1}s^{-1})*	[120]	Adapted	--
χ_M	Macrophages chemotaxis sensitivity parameter	*8.64x10^{-6} (cm^{5}g^{-1}s^{-1})*	[121]	Adapted	--
P_{LDL}^{st}	Standard endothelial permeability to LDL	*1.07x10^{-11} (cm/s)*	[10]	--	Yes

P_{LDL}^{max}	Maximum endothelial permeability to LDL	*2.09x10^{-8} (cm/s)*	[100]	Yes (H)	--
P_{m}^{st}	Standard endothelial permeability to monocytes	*1.07x10^{-12} (cm/s)*	[8]	--	Yes
P_{m}^{max}	Maximum endothelial permeability to monocytes	*5.0x10^{-6} (cm/s)*	[122]	Yes (H)	--

It is relevant to mention that, among the parameters that were experimentally obtained from animal models, the majority corresponds to rabbit models, except for r_{diff}, k_{F_c} and λ_{F_c} (which were measured in mice models), $k_{L_{ox}}$ (bovine models) and, finally, WSS_0 (cat models).

Besides, from the last column of Table 2 it is observable that we used crude estimations for several parameters (previously suggested by other authors). Owing to lack of experimental data, those are the less likely to match with their human physiological values. Once certain values had to be adapted to our computational conditions, we performed a sensitivity analysis technique to each parameter of all implemented PDEs, detailed in the following section.

3.5. Sensitivity Analysis

Methods for sensitivity analysis, when ran on crudely estimated parameters which appear in partial differential equations and in boundary conditions, are valuable tools to support mathematical models and assure robustness to simulation results. The theory behind it regards the evaluation of derivatives of all solution variables with respect to a small number of control variables, thus, it requires one extra linear system solution for each control variable.

There are several sensitivity models, depending on the interest of study. In this work, we performed a sensitivity analysis technique displayed in COMSOL Multiphysics 5.0 by means of the *Sensitivity Interface*. When added to a multiphysics model, it does not introduce new equations nor set of solution variables. Instead, an auxiliary linear problem must be solved [123], [94]. Once our parameters correspond to independent variables whose values are not affected by the solution process and considering our additional need for sensitivity of the entire solution field, the suitable explicit method is the *Forward Sensitivity*. The latter allows to specify a set of control variables (which might be scalars, vectors or elements in some infinite-dimensional function space) and calculate derivatives of all solution variables with respect to variations in certain parameters included in the model. With this method, solution time increases with the number of parameters (see [94] for more details).

To help understanding this method, we provide the general theory applied in steady studies. Taking $Q(\xi)$ as a scalar-valued objective function with the control variable ξ at a specific point ξ_0, one may rewrite the sensitivity problem of Q with respect to ξ as calculating the derivative $\partial Q/\partial \xi$ at $\xi = \xi_0$. However, since we are in the context of a multiphysics model, Q is also function of solution variables u which, in turn, are implicitly functions of ξ, that is, $Q(u(\xi), \xi)$. After discretization, the PDE problem is

represented by the system of equations $L(u(\xi),\xi)=0$. If the latter has a unique solution $u=L^{-1}(\xi)$, the sensitivity problem can be rephrased using the chain rule:

$$\frac{d}{d\xi}Q(u(\xi),\xi)=\frac{\partial Q}{\partial \xi}+\frac{\partial Q}{\partial u}\cdot\frac{\partial u}{\partial L}\cdot\frac{\partial L}{\partial \xi} \tag{3.33}$$

where the first term is an explicit partial derivative of the objective function with respect to the control variables and the second term is composed by different sized matrices. The middle factor of the second term can be computed as $\partial u/\partial L=(\partial L/\partial u)^{-1}$, where $\partial L/\partial u$ is the PDE Jacobian at the solution point, thus, one obtains:

$$\frac{d}{d\xi}Q(u(\xi),\xi)=\frac{\partial Q}{\partial \xi}+\frac{\partial Q}{\partial u}\cdot\left(\frac{\partial L}{\partial u}\right)^{-1}\cdot\frac{\partial L}{\partial \xi} \tag{3.34}$$

However, seeing that the inverse matrix is too expensive, an auxiliary linear problem is introduced, as already referred. Considering that the PDE solution has N degrees of freedom and n control variables ξ_i, the forward sensitivity method introduces the N-by- n matrix of solution sensitivities:

$$\frac{\partial u}{\partial \xi}=\left(\frac{\partial L}{\partial u}\right)^{-1}\cdot\frac{\partial L}{\partial \xi} \tag{3.35}$$

which means that n linear systems of equations must be solved, using the same Jacobian $\partial L/\partial u$ evaluated at $u(\xi_0)$:

$$\frac{\partial L}{\partial u}\cdot\frac{\partial u}{\partial \xi_i}=\frac{\partial L}{\partial \xi_i} \tag{3.36}$$

lastly, allowing the desired sensitivities computation through the equation:

$$\frac{d}{d\xi}Q(u(\xi),\xi)=\frac{\partial Q}{\partial \xi}+\frac{\partial Q}{\partial u}\cdot\frac{\partial u}{\partial \xi} \tag{3.37}$$

As an example of "*Forward Sensitivity*" method applied to our mathematical model, we display the sensitivity analysis of the proposed model with respect to standard endothelial permeability to monocytes (P_m^{st}). In fact, from Equation (3.2.b), one concludes that macrophages intima concentration (M) is function of endothelial permeability to monocytes (P_m) which, in turn, is function of P_m^{st} . Similarly, M might be represented by Q (the scalar-valued objective function); P_m represents the solution variable u; finally, P_m^{st} corresponds to the control variable ξ.

In a sensitivity analysis interpretation, this means that $M(P_m(P_m^{st}),P_m^{st})$. Thus, in the context of our multiphysics system, the sensitivity problem of M with respect to P_m^{st} is rewritten in the form $\partial M/\partial P_m^{st}$ and it can be performed at a specific point of the control variable ($P_{m\,0}^{st}$) through the computation:

$$\frac{d}{dP_m^{st}}[M(P_m(P_m^{st}),P_m^{st})]=\frac{\partial M}{\partial P_m^{st}}+\frac{\partial M}{\partial P_m}\cdot\frac{\partial P_m}{\partial P_m^{st}} \tag{3.38}$$

This analysis is, thus, readily extendable to any model parameter. Results of the accomplished sensitivity analysis technique are provided in chapter 4.

4. Results and Discussion

4.1. Experimental Results

According to the already described experimental procedure, we had to measure the body weight (BW) of the Lys-EGFP-ki mouse to calculate the administered dose of i.p. anesthesia. Once the obtained value for the BW was, approximately, $26.30 \pm 2.3\ g$, it determines an anesthesia dose of about $270\ \mu L$ (the administration is observable in Figure 4.1). During the preparation phase, the followed main steps are shown in Figures 10, 11 and 12.

Figure 10 - Anesthesia procedure: administration of a cocktail of xylazine/ketamine ($\mathbf{0.1\ mL/10\ g}$ of BW).

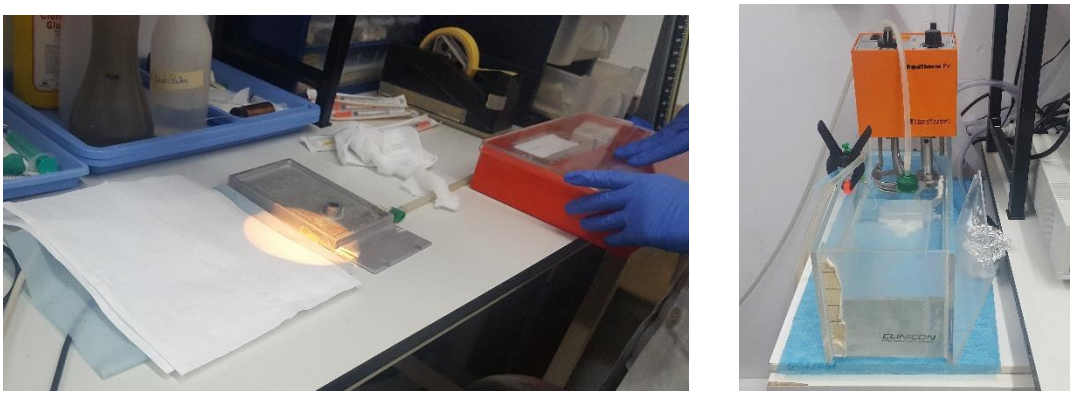

Figure 11 - Preparation of accurate instruments for the surgical procedure support (left) and the Krebs-Henseleit buffer with $NaHCO_3$ at 37°C bubbled with 95% N_2 and 5% CO_2 (right).

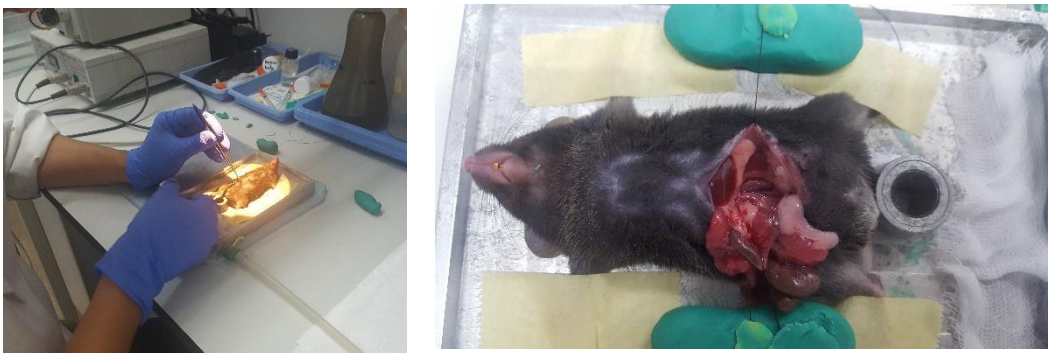

Figure 12 - Initial cut on the mouse peritoneal cavity (left) to push organs to the side, allowing the abdominal aorta exposure (right).

Figure 13 - The mouse is placed on the top of the platina in a multi-photon confocal microscope Leica SP8 MP (Leica, Germany) adapted for intravital fluorescent microscopy.

Finally, resorting to LAX software and after recorded frames analysis, we obtained *in vivo* images of mouse leukocytes movement within the abdominal aorta (see Figure 13). The Lys-EGFP-ki mouse strain that was used in this work has fluorescent neutrophils due to the presence of a GFP protein in the lysozyme gene. In Figure 14 it is possible to see a sequence of the intravital microscopy images obtained from the abdominal aorta. In those images we identify the presence of rolling, and also some adherent, neutrophils. The dashed white lines were draw in order to facilitate the identification of the arterial wall, where no atherosclerotic plaques or accumulation of neutrophils is observed.

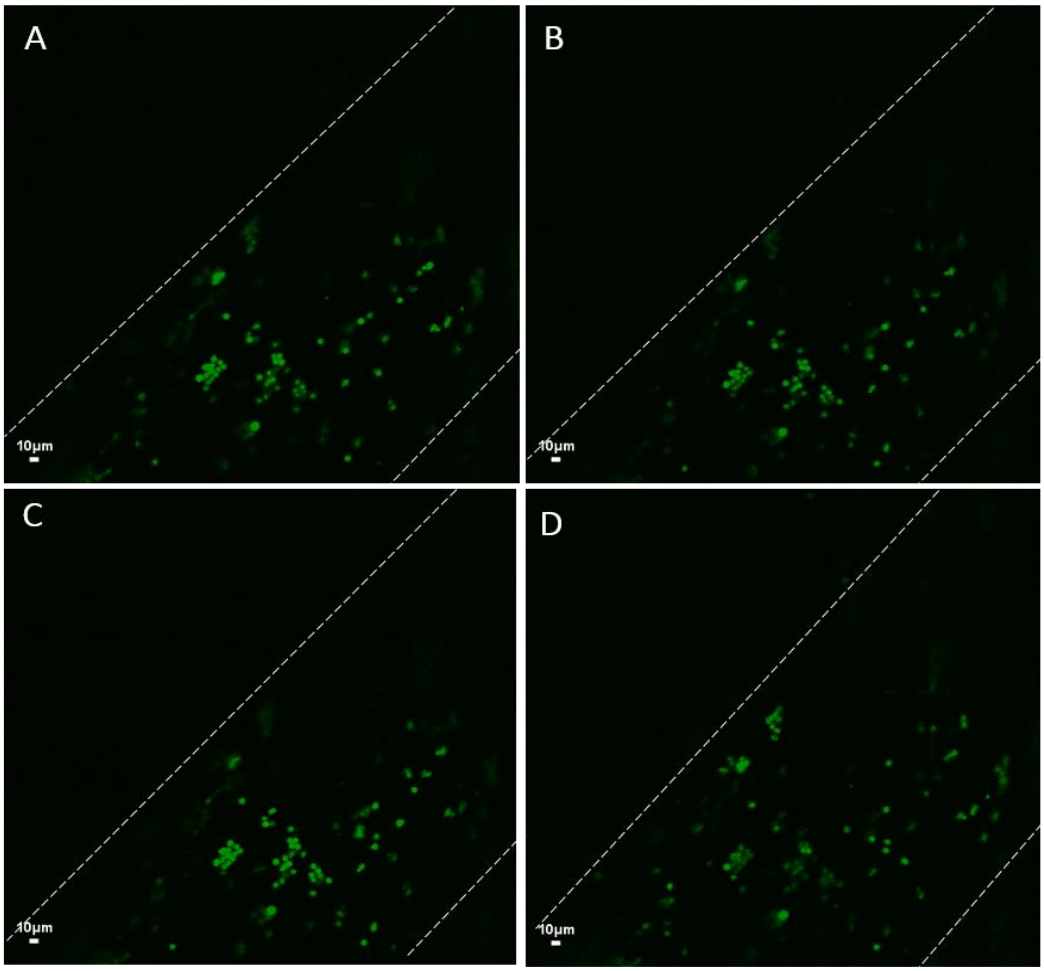

Figure 14 - Abdominal aorta intravital microscopy sequence of images (A – D). White dashed lines indicate the arterial walls and green dots correspond to rolling and some adherent neutrophils.

At the end of the trial, we removed blood from the mouse abdominal aorta to determine LDL circulating levels through a spectrophotometry method and the obtained value was $1.0\ mmol/L$.

As already mentioned, by overcoming logistic and financial difficulties, future work should perform this surgical procedure using ApoE$^{-/-}$ mice models, so that parameters which are needed for the model are as close as possible to their real values in mice atherosclerotic plaques (which can be the starting point for extrapolation for human physiological conditions). From the obtained images, we believe that, by using a more adequate mice model with the suitable age and diet, we could visualize neutrophils adherence to the aortic endothelium, transmigration and posterior accumulation inside the intima layer.

4.2. Numerical Simulations

Atheromatous plaque growth consists of a complex and long process involving a high number of species and processes relating them. Once numerical simulations are useful tools for better understanding of biological mechanisms, the weak form (see Equations (3.27) until (3.30)) of the suggested system was implemented in COMSOL Multiphysics version 5.0, a commercial finite element

solver and simulation software for the solution of partial differential equations (see [94] for more details). In this section, we provide the obtained results and, simultaneously, a discussion of those after comparison with previous works present in literature.

In the simplified rectangular model, since we are interested in visualizing the long process of plaque development, the total simulation time corresponds to five years, that is, $T = 157\,680\,000\,s$. We present, also, for each atherosclerosis protagonist, the intima concentration for times $t = 0\,s$ and $t = 79\,000\,000\,s$, the initial and the middle time (two and a half years), respectively. Besides, to estimate the coupling of the simplified model with lumen domain, WSS magnitude (needed to compute EP) was taken as 50% of its normal value, accordingly to [124].

Due to the complexity of the coupled system, a progressive implementation was performed leading to a workflow (detailed in Appendix D). After verifying the full model is well coupled, we expected to obtain the following main results:

- Increasing oxLDL levels at the penetration region, where WSS is lower;
- Quite fast activation of the inflammatory signal (starred by MCP-1) owing to the elevated endothelial influx of LDL, with a stronger MCP-1 concentration near the penetration region;
- Intensified MCP-1 signaling increases the endothelial permeability to LDL and to monocytes, which start accumulating at the endothelium;
- At the penetration region, monocytes differentiation into macrophages and LDL oxidation are increasingly triggered, thus, forcing them to diffuse inside the intima layer;
- Macrophages proliferation intensifies their diffusion inside the intima, as well as their chemotactic motion in response to MCP-1 signal;
- After reaction of macrophages with oxLDL, foam cells are continuously originated, and cytokines production is intensified (both MCP-1 and PDGF start spreading over the intima layer);
- SMCs chemotactic motion in response to both MCP-1 and PDGF signals, simultaneously, synthetizing collagen;
- The progressive accumulation of populations of massive cells (macrophages foam cells and SMCs) and collagen gradually leads to intima volume growth, that is, EC surface deformation with the intima layer invading the arterial lumen.

4.2.1. Concentration evolution of species inside the intima

4.2.1.1. Stage I

In the simplified rectangular geometry for the intima layer, $730\,863$ degrees of freedom are considered. To implement atherosclerosis Stage I (see Equation (3.1.a) until Equation (3.4)) we chose a high endothelial influx of LDL particles at the penetration region ($1.9\,g/cm^3$), to speed up the inflammatory initiation, thus, enabling less time-consuming computations. According to literature, it is

considerably higher than human pathological levels of circulating LDL (superior to $1.6\,mg/cm^3$, as reported in [125]).

As foreseen by literature (see chapter 2), increasing inflammatory signal and lower WSS values contribute for LDL diffusion from the arterial lumen into the wall gap junctions and accumulation at the endothelial surface [8], [11], [13], [9]. Once LDL particles undergo the oxidation process, they gradually lead to oxLDL formation and diffusion inside the intima domain, which is portrayed by Figure 15. Providing the elevated LDL endothelial source, intima oxLDL concentration reaches value $5.6 \times 10^{-4}\ g/cm^3$. Nonetheless, the computed inflammation period (five years) allows enough time for significant oxLDL ingestion by macrophages, thus, despite its increasing penetration at the endothelial boundary, oxLDL particles do not reach significantly further from the entrance region, which is in accordance with our assumptions.

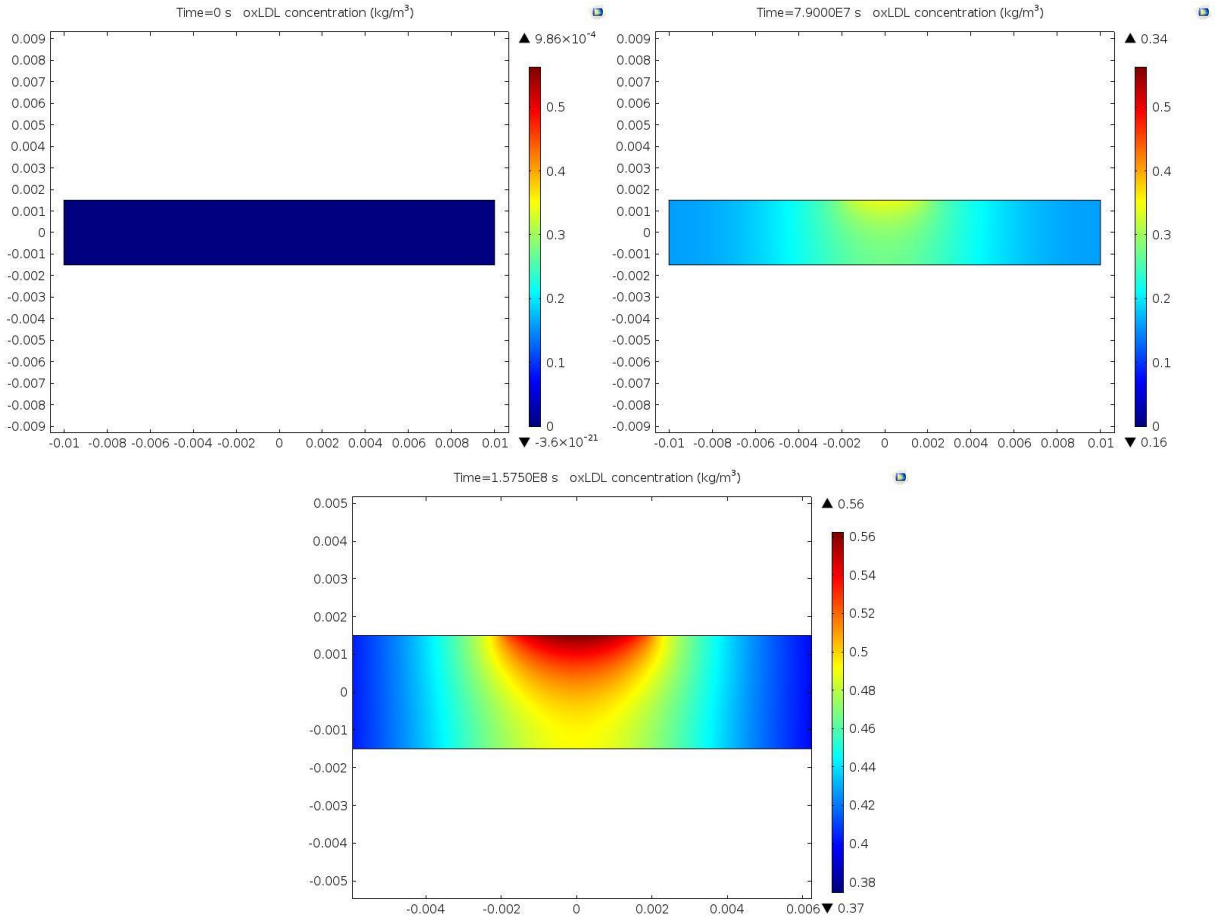

Figure 15 - Concentration evolution of oxLDL inside the intima for times $\boldsymbol{t = 0\ s}$, $\boldsymbol{t = 79\,000\,000\ s}$ and $\boldsymbol{t = 157\,680\,000\ s}$.

As already explained, at the beginning of the simulation oxLDL intima levels rapidly equal the threshold concentration, which is taken as the starting point for the inflammatory reaction ($8 \times 10^{-6}\ g/cm^3$). Consequently, MCP-1 is expressed by activated ECs, especially those within the penetration region, where the LDL influx is located (see Figure 16, where the chemokine reaches value $9.56 \times 10^{-7}\ g/cm^3$). In fact, in a protective attempt by the organism to remove the inflammatory stimuli, increasing MCP-1 sets up the recruitment of circulating monocytes, as expected by literature.

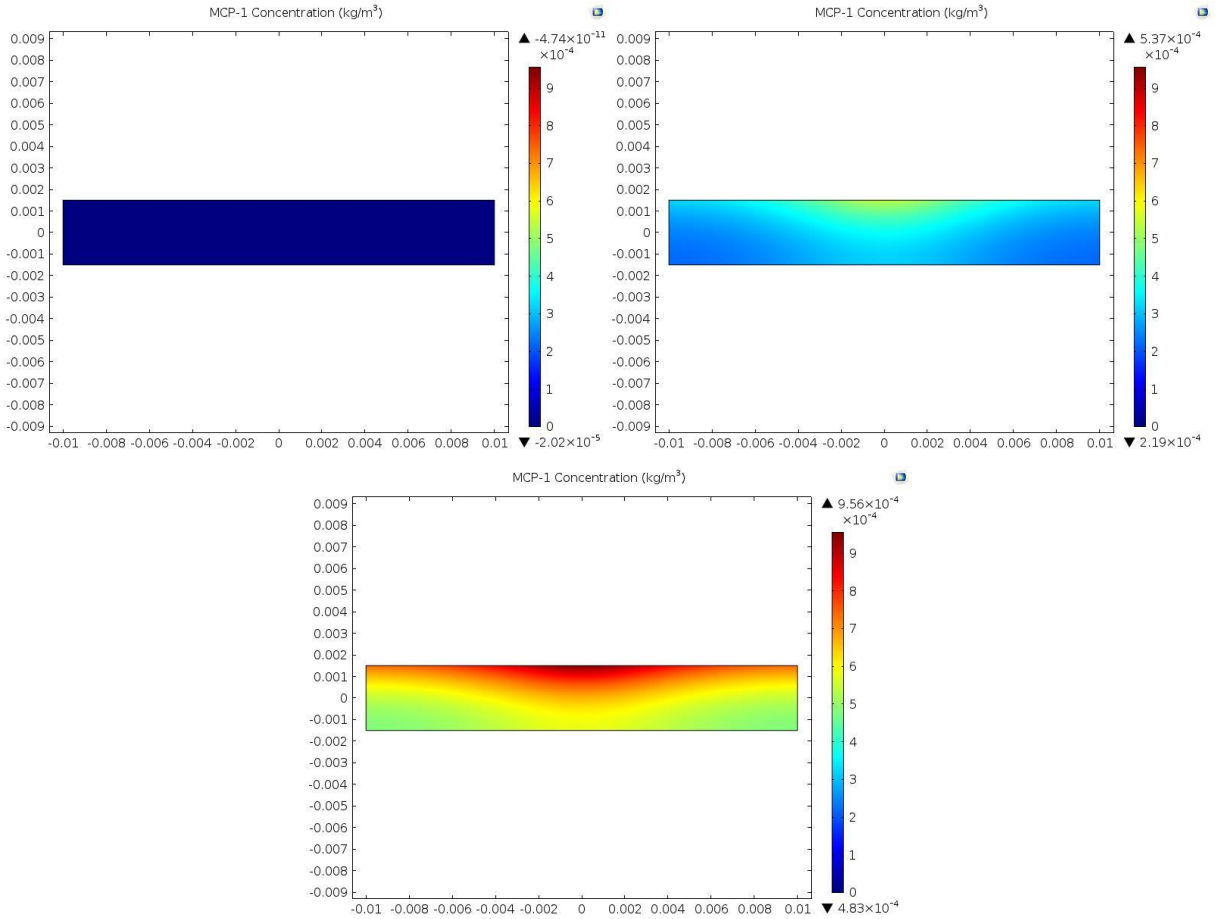

Figure 16 - Concentration evolution of MCP-1 inside the intima for times $\boldsymbol{t = 0\ s}$, $\boldsymbol{t = 79\,000\,000\ s}$ and $\boldsymbol{t = 157\,680\,000\ s}$.

Furthermore, increasing levels of MCP-1 over time intensify the endothelial permeability to circulating monocytes at the penetration region, as portrayed in Figure 17 (a). Likewise, Figure 17 (b) shows that LDL entrance is also augmented with MCP-1 increase, as already verified by other authors [8], [13]. Monocytes, eventually, differentiate into macrophages, accentuating the inflammatory signal and leading to new monocytes recruitment. The concentration evolution of this cytokine illustrates, therefore, the chronic inflammatory origin of atherosclerosis disease, as already described in chapter 2.

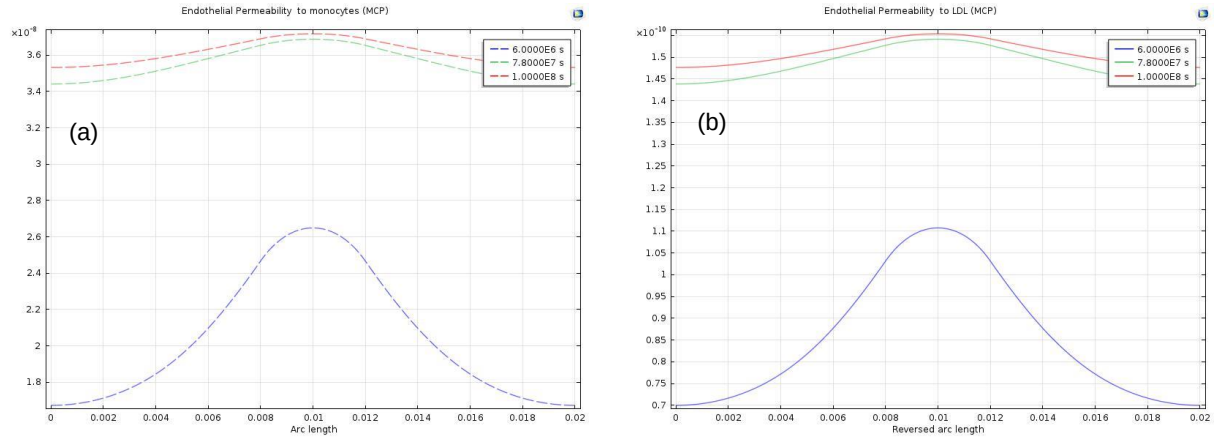

Figure 17 - Influence of MCP-1 on the endothelial permeability to monocytes (a) and LDL (b) for times $\boldsymbol{t = 6\,000\,000\ s}$, $\boldsymbol{t = 78\,700\,000\ s}$ and $\boldsymbol{t = 100\,000\,000\ s}$.

Similarly to LDL accumulation at the lower WSS region, monocytes distribution along the artery wall is also not uniform, which is in accordance with our model assumptions. Moreover, owing to monocytes differentiation into macrophages over time, intima concentration of the latter ones is intensified at the penetration region (see Figure 18), reaching value $6.52 \times 10^{-8}\ g/cm^3$. Nevertheless, the evident effect of their proliferation from the EC surface into the intima domain enforces its time evolution to be remarkably different from oxLDL. In fact, we verify that macrophages proliferation rate is a crucial model parameter once we decreased its experimental value from $1 \times 10^{-2}\ s^{-1}$ to $1 \times 10^{-9}\ s^{-1}$ (as reported in chapter 3) and, still, proliferation is quite significant.

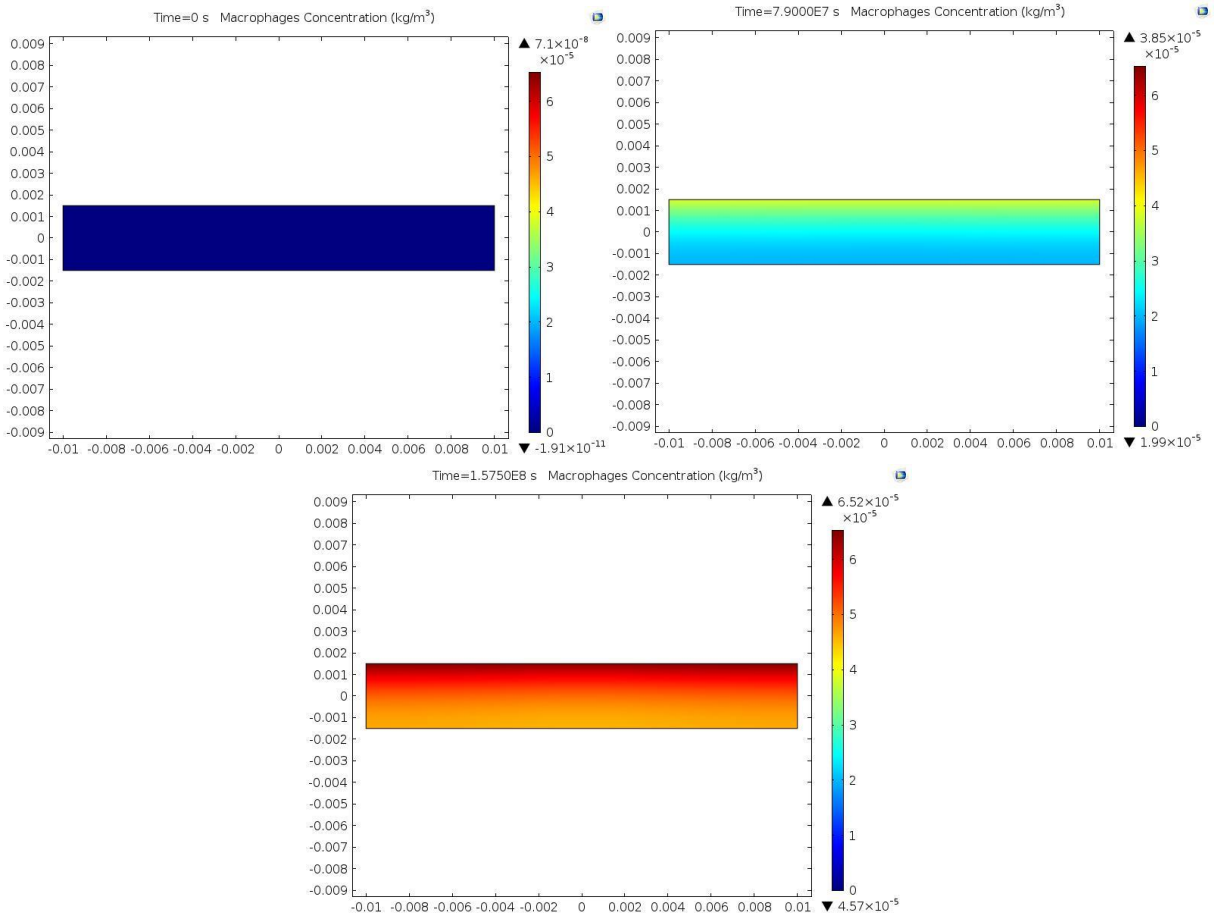

Figure 18 - Concentration evolution of macrophages inside the intima for times $\boldsymbol{t = 0\ s}$, $\boldsymbol{t = 79\,000\,000\ s}$ and $\boldsymbol{t = 157\,680\,000\ s}$.

In addition, macrophages diffusion is even influenced by their chemotactic motion in response to MCP-1 signaling. To illustrate the mentioned phenomenon, Figure 19 shows macrophages distribution at the end of the simulation and, overlaid, the MCP-1 gradient (which is represented by the arrows). Gradients, by definition, point from lower concentration regions towards higher concentration regions. Species with affinity to that chemokine (such as immune cells) tend to follow that gradient direction. Accordingly, macrophages intima evolution strongly depends on MCP-1 concentration seeing that it is significantly higher where MCP-1 signaling is stronger (which is nearby the penetration region), as expected by our model assumptions and previously reported in [8]. As previously said, the chemotactic

sensitivity parameter was reduced from its experimental value ($8.64 \times 10^{-1} cm^5/(g\ s)$) and taken as $8.64 \times 10^{-6} cm^5/(g\ s)$.

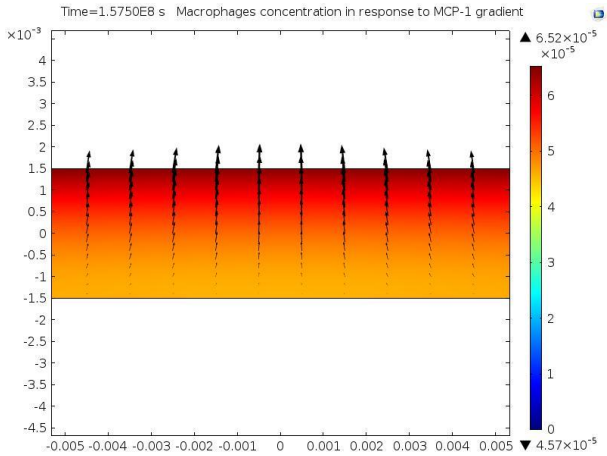

Figure 19 - Macrophages chemotactic motion in response to MCP-1 gradient (represented by the arrows) for $\boldsymbol{t = 157\ 680\ 000\ s}$.

Another satisfactory confirmation relies in the upper limit that was suggested for oxLDL ingestion by one macrophage. The latter would lead to a considerable freely diffusing amount of oxLDL particles inside the intima domain, with a stronger tendency near the endothelial barrier. In fact, the maximum oxLDL intima concentration that is found at the end of the simulation ($5.6 \times 10^{-4}\ g/cm^3$) is significantly higher than macrophages (reached value was $6.52 \times 10^{-8}\ g/cm^3$), a result that is in accordance with previous works like [8] and [14] as well as with our initial assumptions.

4.2.1.2. Stage II

Stage II includes Equations (3.1.a) until (3.5.b) and starts when macrophages engulf large amounts of oxLDL particles, originating the so-called foam cells. The concentration evolution of the latter ones is displayed in Figure 20, showing a reached concentration of $2.78 \times 10^{-10}\ g/cm^3$.

As expected from our assumptions, once these lipid-laden cells result from the reaction of oxLDL with macrophages, they are mainly located in areas where these species concentrations are higher (near the endothelial penetration region). However, considering our assumption that foam cells production rate is lower than the rate of oxLDL uptake by macrophages, it suggests that not all phagocytic macrophages develop into foam cells. Therefore, as predicted, at the end of the simulation foam cells concentration is lower when compared to macrophages ($2.78 \times 10^{-10}\ g/cm^3$ and $6.52 \times 10^{-8}\ g/cm^3$, respectively), a conclusion which was also reached by other authors, such as [8], [14] and [11].

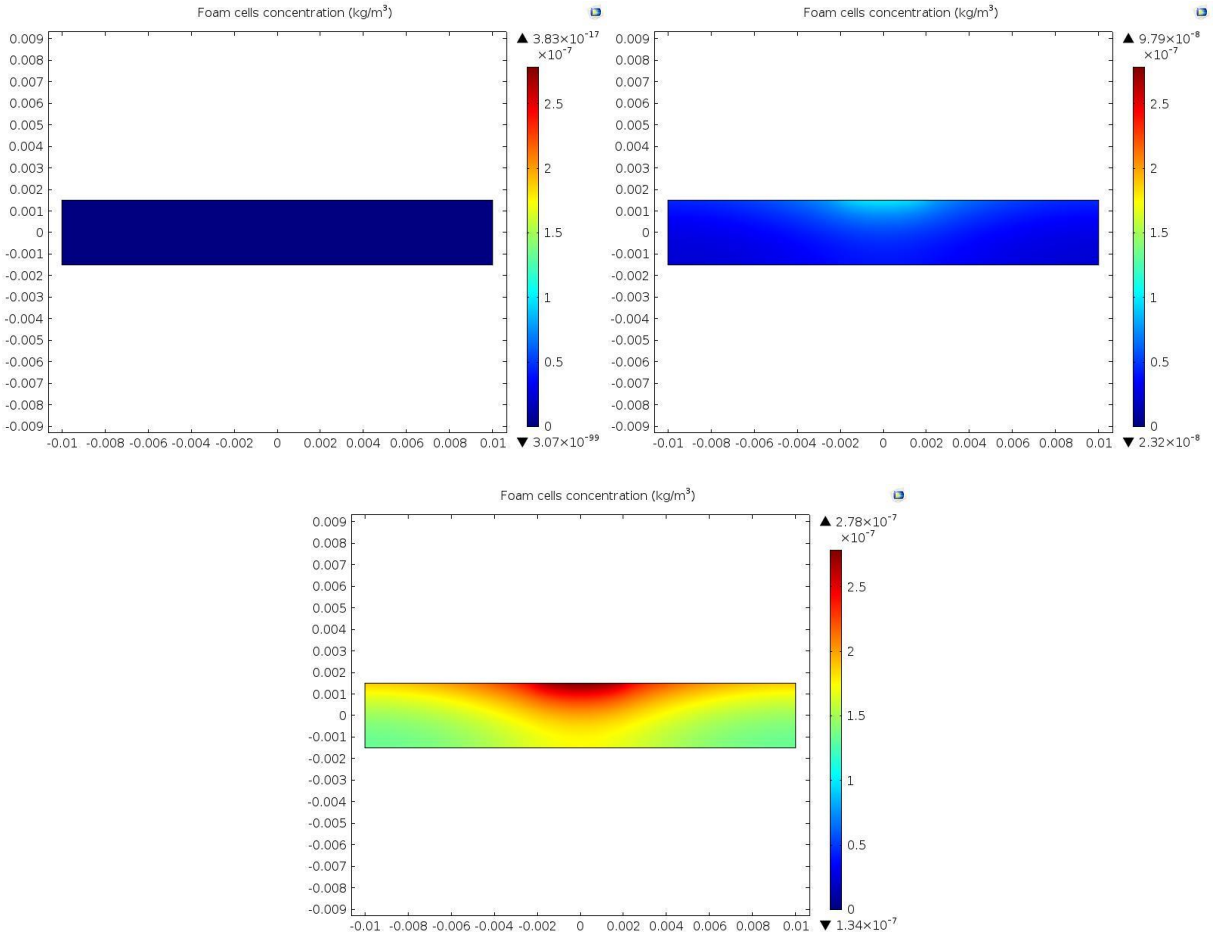

Figure 20 - Concentration evolution of foam cells inside the intima for times $\boldsymbol{t = 0\ s}$, $\boldsymbol{t = 79\,000\,000\ s}$ and $\boldsymbol{t = 157\,680\,000\ s}$.

Furthermore, from our results we conclude that foam cells significantly trigger the persistent inflammatory signal production (in our model, starred by MCP-1 and PDGF), thus, also triggering the recruitment of new monocytes, as anticipated by literature [8], [13], [14], [11], [10], [9].

Plaque growth

With the progressive creation and accumulation of massive cells and collagen fibres, atherosclerotic plaque growth into the arterial lumen is eminent. Following the suggested model (from Equation (3.9) to Equation (3.15)), intima volume progression is represented in Figure 21, for little more than five years of simulation ($t = 165\,640\,000\ s$).

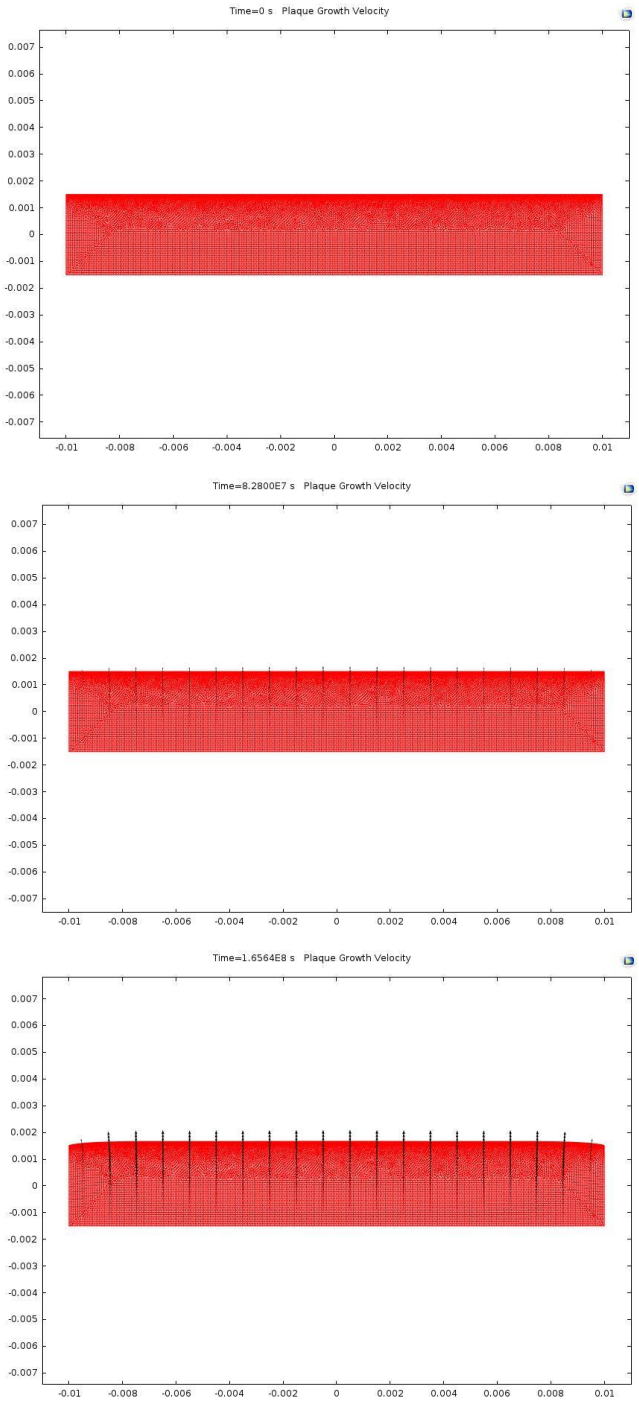

Figure 21 - Evolution of atherosclerotic plaque growth velocity (represented by the arrows) for times $\boldsymbol{t = 0\ s}$, $\boldsymbol{t = 82\,800\,000\ s}$ and $\boldsymbol{t = 165\,640\,000\ s}$.

As it is observable, better in Figures 22 (a) and 22 (b), the endothelial barrier freely deforms with the lesion growth velocity vectors, which are stronger at the penetration region, where the accumulation of cell populations is more significant. This result is in good agreement with literature once it explains the arterial lumen invasion by the atherosclerotic plaque.

Moreover, as already detailed, the concentration evolution of macrophages (Stage I) and foam cells (Stage II) is significantly higher at larger deformation regions, thus, demonstrating consistency with our assumptions. Therefore, our system of PDEs allows the visualization of atheroma plaque growth for 5

years owing to the accumulation of macrophages and foam cells. Then, it can be considered a step forward towards studying atherosclerotic plaque progression.

Nonetheless, future work should complete this model by considering the contribution of massive cells (such as SMCs in Stage III) and collagen fibres (Stage IV) for intima volume growth.

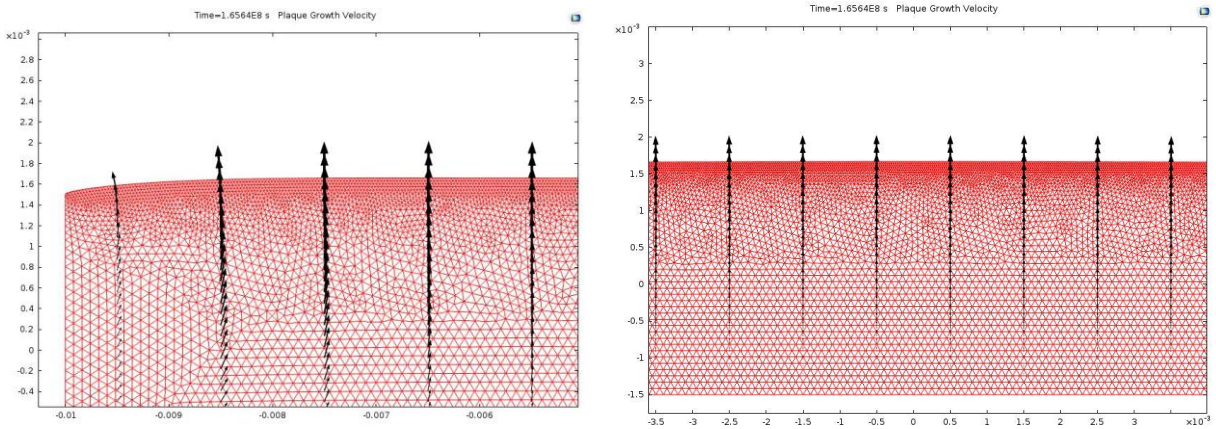

(a) (b)

Figure 22 - Zoom view of intima growth velocity (represented by the arrows) at the endothelial upper left corner (a) and at the endothelial middle (b) for $\boldsymbol{t = 165\,640\,000\ s}$.

4.2.1.3. Stage III

Stage III stands out for PDGF synthesis and SMCs proliferation and migration into the intima (see Equations (3.1.a) until (3.7.b)). Firstly, as our model's second cytokine, PDGF results from endothelial dysfunction which, eventually, causes circulating platelets adhesion to ECs. Due to the endothelial activation, intima macrophages and foam cells start producing PDGF. Although PDGF synthesis by SMCs (see Equation 3.7.a) was initially considered, we verified that this factor was neglectable during simulations, specially when compared to macrophages and foam cells production terms. This result is, in fact, in accordance with [2] so we disregarded that term.

As it is visible in Figure 23, PDGF rapidly spreads out inside the intima domain, widely contributing for the inflammatory signal amplification (reached value of $7.8 \times 10^{-4} g/cm^3$). Its intima concentration is progressively increasing and mainly focusing near the endothelial entrance region but also arriving at the media boundary, which is in good agreement with literature [14]. Note that the middle simulation time is higher than the previous ones ($150\,000\,000\ s$) to display its concentration evolution, thus, allowing the visualization of different PDGF intima distribution sets.

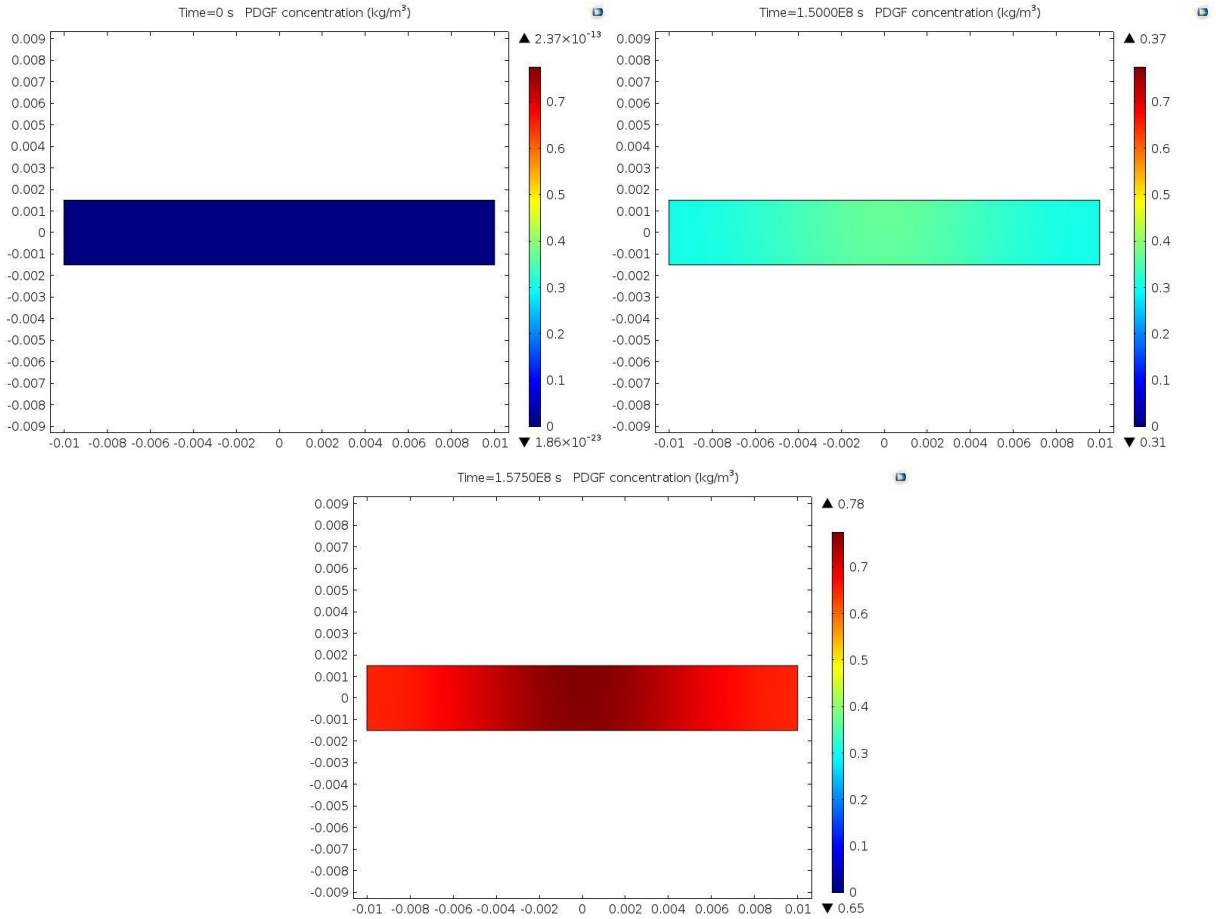

Figure 23 - Concentration evolution of PDGF inside the intima for times $\boldsymbol{t = 0\ s}$, $\boldsymbol{t = 150\ 000\ 000\ s}$ and $\boldsymbol{t = 157\ 680\ 000\ s}$.

Moreover, providing cytokines rapid diffusion inside the intima (see the last illustrations of Figures 16 and 23), the media boundary is, eventually, reached and SMCs activation is triggered. Providing the persistency of the inflammation, endothelial cells fail to prevent SMCs from migrating into the intima layer [13], [14], [11]. Nonetheless, once this phenomenon is verified inside advanced atherosclerotic lesions, the computed time was augmented to five and a half years ($t = 170\ 020\ 000\ s$).

For that time, a significant SMCs chemotactic motion is verified, with SMCs invading the intima layer towards the endothelium, highly directed by MCP-1 and PDGF gradients. Figures 24 (a) and 24 (c) provide SMCs intima concentration evolution from $t = 79\ 000\ 000\ s$ until $t = 170\ 020\ 000\ s$, where the maximum reached concentration was $8.69 \times 10^{-3} g/cm^3$. For higher times than those, we faced a hard-numerical instability that we could not overcome in the available time, as revealed by the singularity present in Figure 24 (d). Further work should, thus, improve the PDEs system implemented for Stage III.

Besides, note the uniformly distributed SMCs influx, visible and zoomed at the media boundary (see Figure 24 (b)), as expected from our model assumptions.

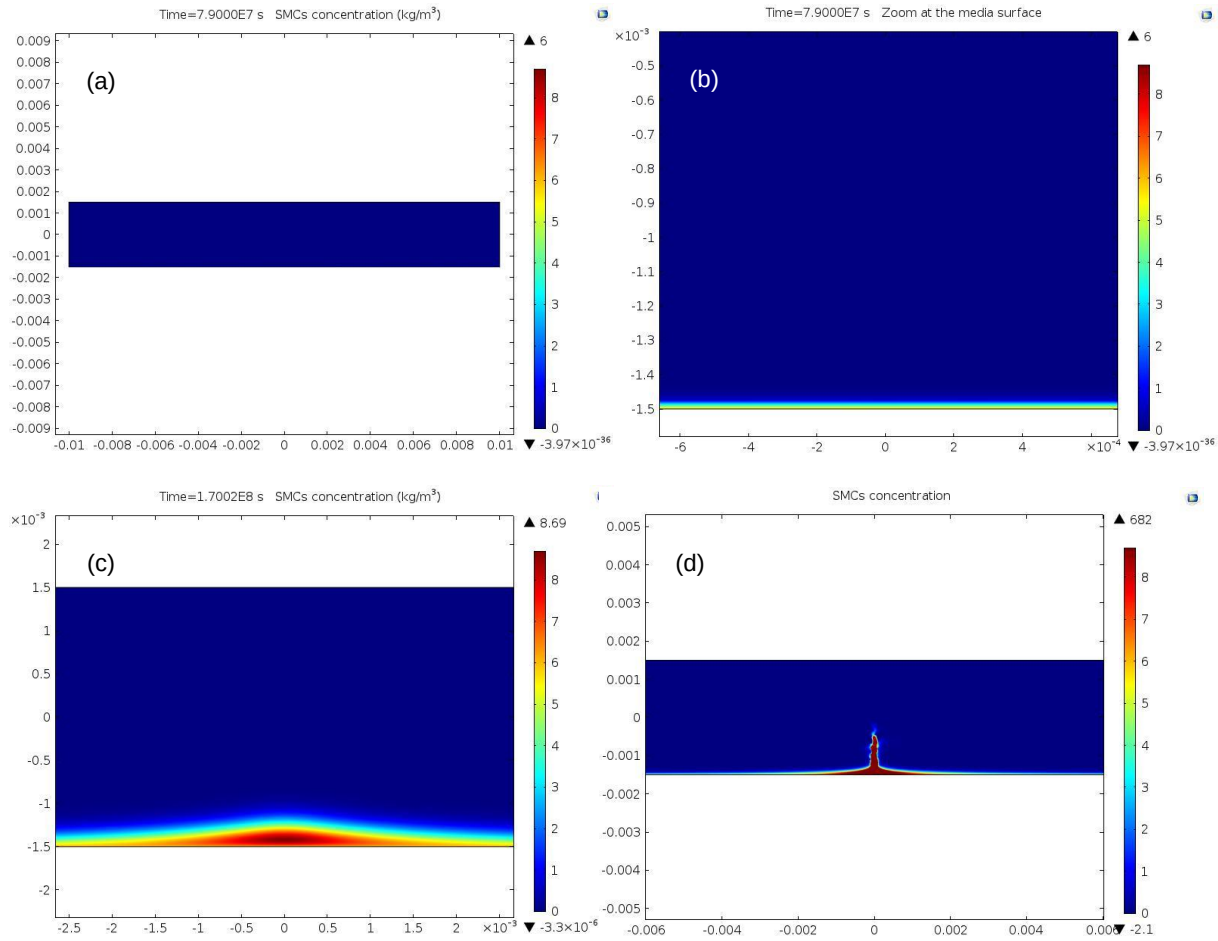

Figure 24 - Concentration evolution of SMCs inside the intima for times: $\boldsymbol{t = 79\,000\,000\ s}$, where SMCs intima concentration (a) and a zoom at SMCs media influx (b) are represented; $\boldsymbol{t = 170\,020\,000\ s}$ shows the maximum reached SMCs intima concentration; finally, $\boldsymbol{t = 189\,320\,000\ s}$ portrays SMCs singularity, verified at the end of our simulation.

In addition, to access the chemotactic effects of MCP-1 and PDGF gradients on SMCs motion, we present the obtained results in Figures 25 (a) and 25 (b), respectively. Note that the arrows correspond to the respective cytokine gradient for time $t = 79\,000\,000\ s$.

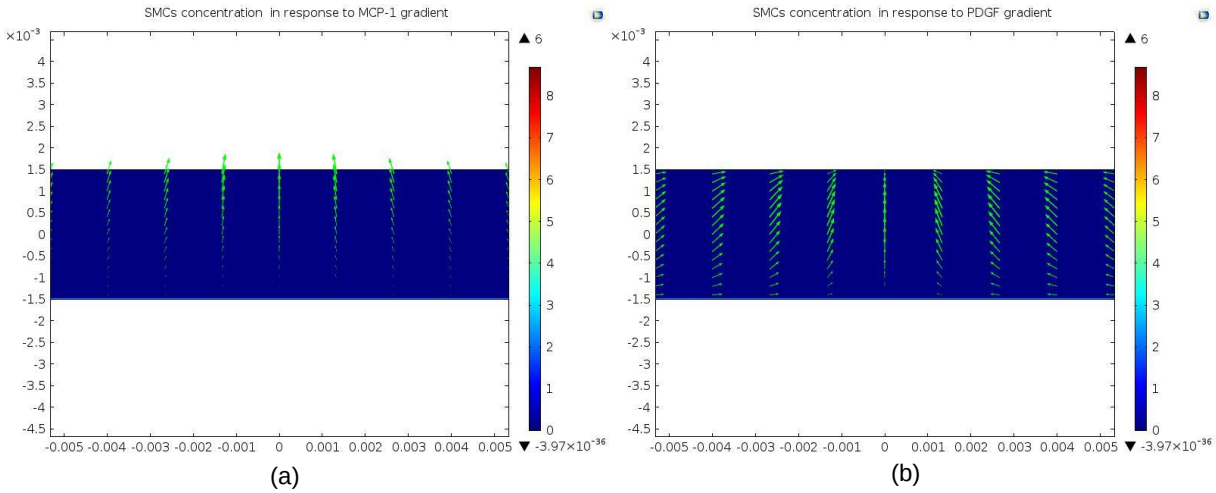

(a) (b)

Figure 25 - SMCs motion in response to MCP-1 (a) and PDGF (b) gradients for $t = 79\,000\,000\ s$.

According to literature, SMCs migrate towards the endothelium, creating the fibrous cap on the top of the fatty plaque, thus, fibrofatty lesion progresses and plaque stability is assured [23]. Looking at our results, although SMCs are correctly distributed along the media boundary (where their influx is located), the chemotactic motion towards EC surface is moderately visible (see Figure 4.13 (c)). In other words, the obtained results are inconclusive regarding this topic.

One relevant limitation of SMCs modeling relies on the short-computed time for plaque growth. In five years, SMCs are not allowed to significantly proliferate and migrate. Cilla et al., for example, simulated the atheroma plaque growth for 10 years in [13], so SMCs motion inside the intima domain was successfully observed. Also, we modified some model parameters to accelerate the inflammatory initiation which, at a certain point, might have affected the obtained results, especially regarding SMCs chemotactic motion. For further progress on chemotaxis effects visualization, accessing physiological parameters needed for SMCs motion, such as their influx rate into the intima ($\tilde{a}_S$), is extremely required.

Our results for plaque growth regard Stage II (Fatty Streak) only. Owing to the reported non-solved numerical instabilities from SMCs, coupling it with the ALE deformation was not accomplished, so this should also be the subject of future work.

4.2.1.4. Stage IV

As suggested by Cilla et al. in [13], our model assumes that SMCs segregate collagen fibres, giving rise to atherosclerosis Stage IV, encompassing Equations (3.1.a) until (3.8.b). Once collagen evolution over time is controlled by SMCs motion, it also displays a uniform distribution tendency within the media boundary layer which, gradually, spreads inside the intima domain according to SMCs chemotaxis towards the EC surface (see Figure 26 (c)), which is in accordance with our assumptions and literature [25], [72], [69].

Total simulation time corresponds to five and a half years ($t = 170\,020\,000\,s$) too. Like in the previous case, collagen concentration portrays a numerical instability for higher times (see Figure 26 (d)), which was not possible to overcome in this work. Collagen concentration reaches value $3.14 \times 10^{-6} g/cm^3$. On the other hand, simulations of ten years like those performed by Cilla and coauthors in [13] allow stabilized values for collagen concentration around $1.9 \times 10^{-4} g/cm^3$.

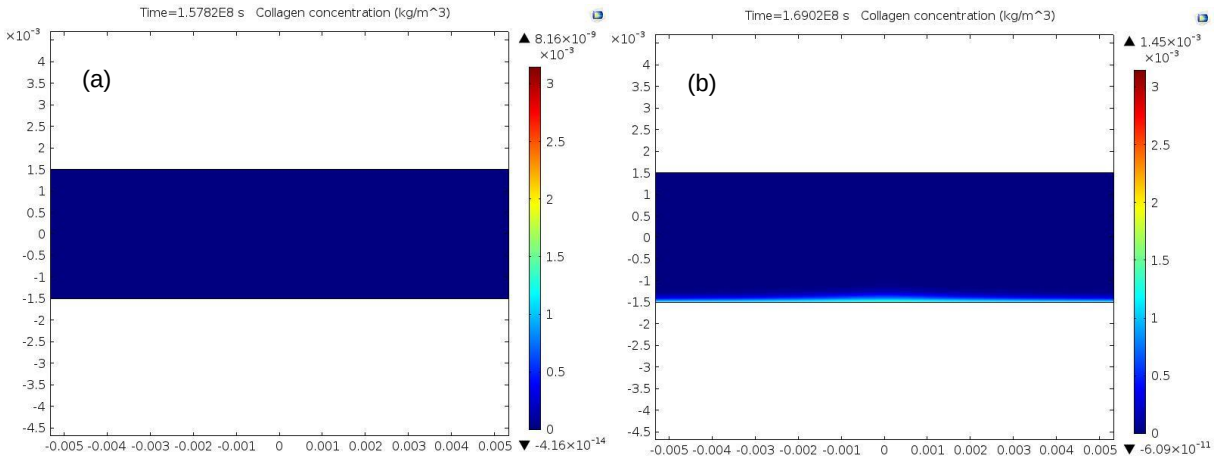

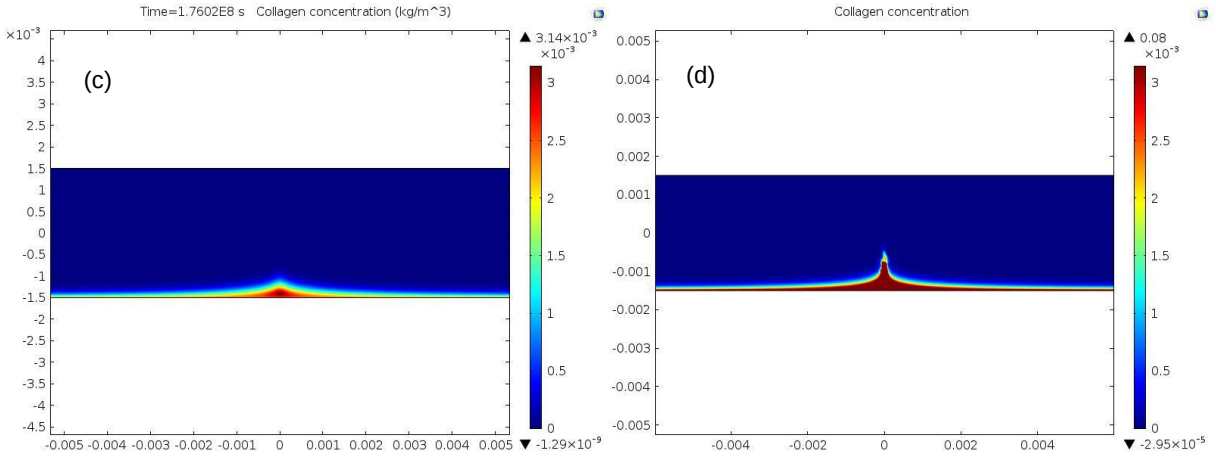

Figure 26 - Concentration evolution of collagen inside the intima for times $\boldsymbol{t = 157\,820\,000\ s}$, $\boldsymbol{t = 169\,020\,000\ s}$ and $\boldsymbol{t = 176\,020\,000\ s}$. For $\boldsymbol{t = 189\,320\,000\ s}$, the obtained collagen singularity is shown.

In conclusion, total simulation time constitutes a relevant limitation of this work. Moreover, we compared our results with previous authors on atherosclerosis modeling due to the lack of experimental data regarding intima concentrations of biological agents. In fact, currently, it is not possible to calculate intima concentrations yet, thus, the validation of our results with *in vivo* or *in vitro* experiments is not provided in this work, meaning that those might not be biologically reasonable.

4.2.3. More complex geometry

In this work, numerical simulations were also performed in a more realistic two-dimensional geometry which corresponds to an idealized left coronary artery bifurcation, where the lumen domain is coupled to the intima domain. In other words, in this model the simplified blood flow dynamics is attached to atherosclerosis complexity inside the thin innermost layer of the vessel wall.

According to literature, left anterior descending (LAD) artery is considered by many experts a high-risk lesion with restenosis approaching nearly 50% after percutaneous coronary intervention (PCI) [16]. Therefore, to yield results much closer to a real human stenosis, we chose to implement our model in the left main (LM) coronary artery bifurcation, which divides itself into LAD artery and left circumflex (LCx) artery. Dimensions and angles, represented in Figure 27, were taken from literature on human physiological dimensions (as reported in [126]), except for the intima layer, whose dimensions were already introduced in chapter 3. Note that blood enters at the LM inlet region and flows towards LCx and LAD outlets, as portrayed by the arrows.

In this complex geometry (idealized left coronary bifurcation), we consider a total number of $148\,451$ degrees of freedom, where $21\,174$ correspond to the lumen subdomain and $127\,277$ to the intima subdomain. Spatial discretization of both subdomains is portrayed in Figure 28.

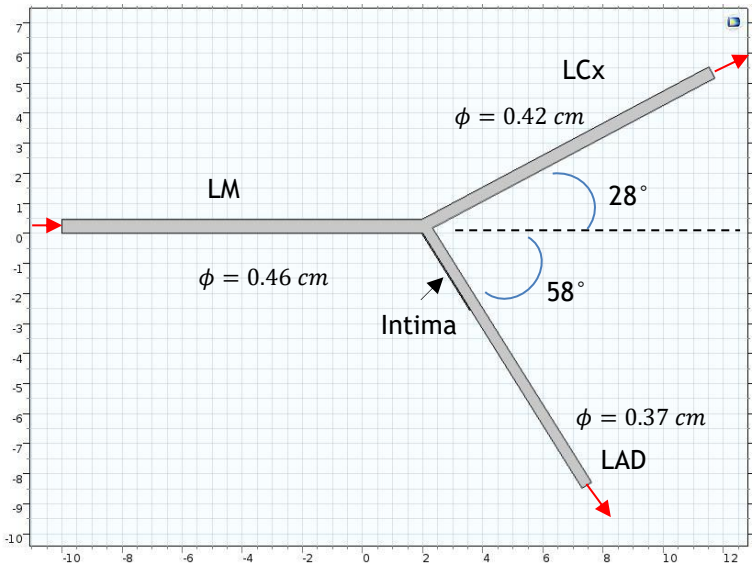

Figure 27 - Illustration of the LM coronary artery bifurcation into LAD and LCx arteries, where dimensions and angles were taken from[126]. The red arrows stand for blood flow direction; thus, the inlet boundary is placed at LM artery whereas the outlets are located at the end of LCx and LAD branches.

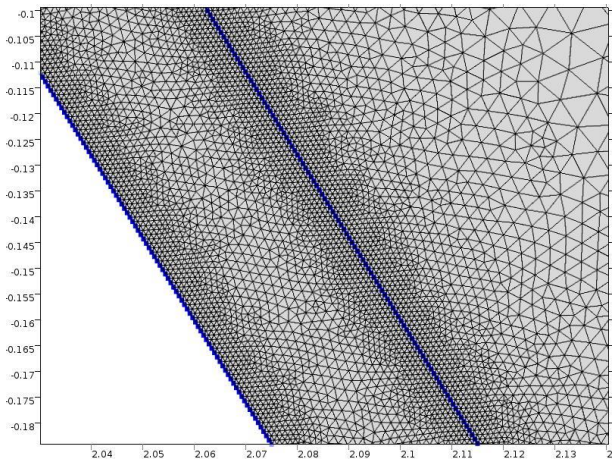

Figure 28 - Spatial discretization applied to the subdomains (**20 271** elements inside the lumen domain and **61 896** elements inside the intima domain).

Although we initially aimed at measuring plaque growth velocity with the consequent endothelial deformation applied to this geometry configuration, in the time we had we could only access wall shear stress distribution and its influence on the endothelial permeability to LDL and monocytes as well as the behaviour of atherosclerosis protagonists inside the intima layer during Stage II (Fatty Streak).

4.2.3.1. WSS influence on the endothelial permeability

According to literature, lower WSS values define atheroprone regions in arteries, that is, probable endothelial areas for LDL and monocytes entrance, thus, atherosclerosis initial inflammation [124]. This work assumes that the endothelial permeability to monocytes and LDL is increasing function of MCP-1 (as already described) and decreasing function of WSS. Therefore, to access its influence in our model, we computed WSS magnitude for a stationary study along the red endothelial region highlighted in

Figure 29 (a). The obtained results are shown in Figure 29 (b) and a zoom view is provided in Figure 30.

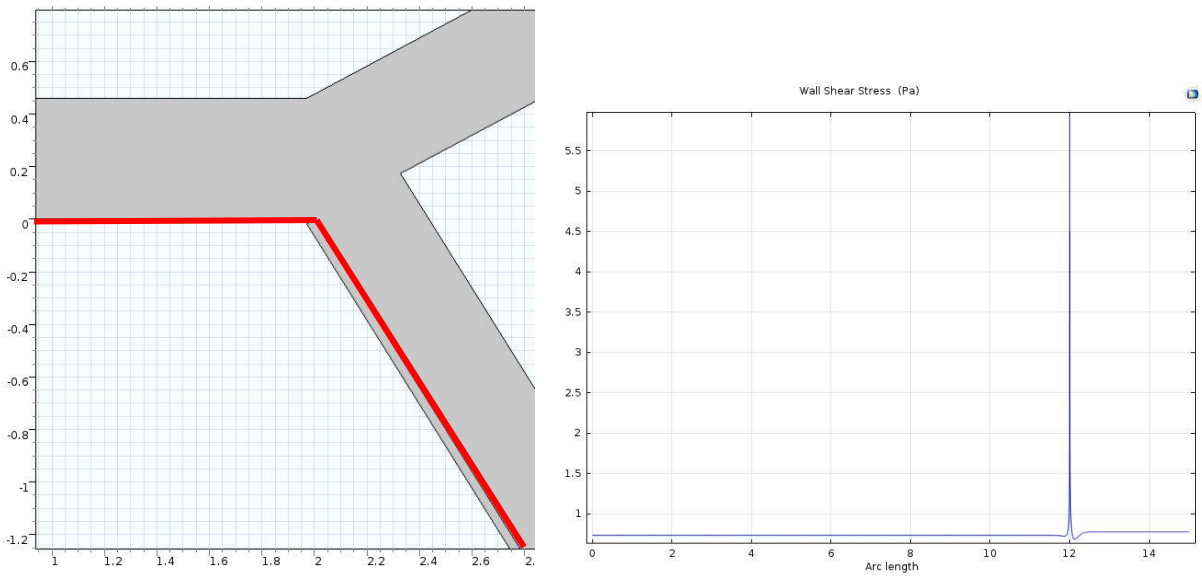

(a) (b)

Figure 29 - Representation of the endothelial region (highlighted in red) where WSS magnitude was computed (a) and WSS magnitude evolution along the given endothelial region (b).

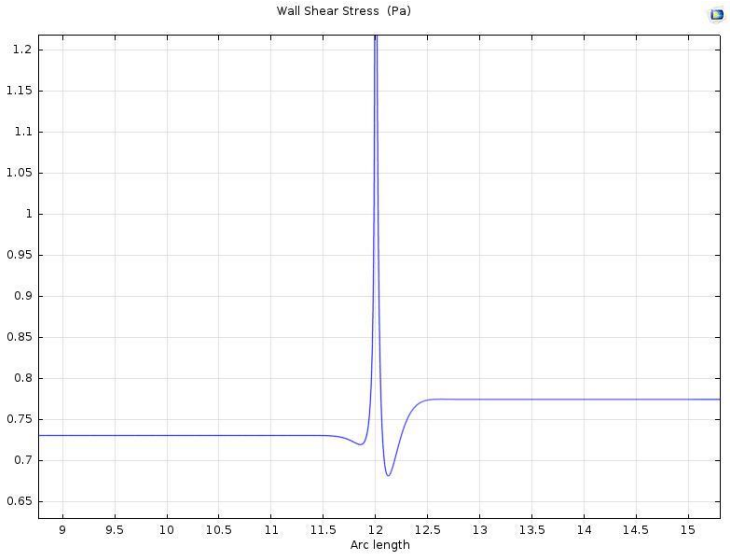

Figure 30 - Zoom view of WSS magnitude evolution along the given endothelial region.

Looking at our results, the clear conclusion is that hemodynamic shear stresses distribution is spatially nonuniform along the chosen endothelial region. Moreover, the lowest WSS magnitudes (around *arc length* 12, which corresponds to the 2 mm region in Figure 29 (a)) are near $0.68\ Pa$ and correspond to the endothelial LAD which is closest to the bifurcation site, a result that is in accordance with literature (see chapter 2).

Nonetheless, this physical quantity is not entirely described as expected. In fact, as reported by Silva et al. in [13], after the bifurcation region, WSS magnitude should return to its standard value (in our case, along the LM endothelium the WSS features $0.73\ Pa$). To obtain those accurate WSS patterns, future

work on the LM coronary artery bifurcation should couple the artery with highest caliber (LCx artery) with the intima domain (instead of LAD artery).

The obtained stationary result for blood velocity magnitude is provided in Figure 31 as well as the respective streamlines profile. Blood pressure inside the LM coronary bifurcation is, in turn, shown in Figure 32.

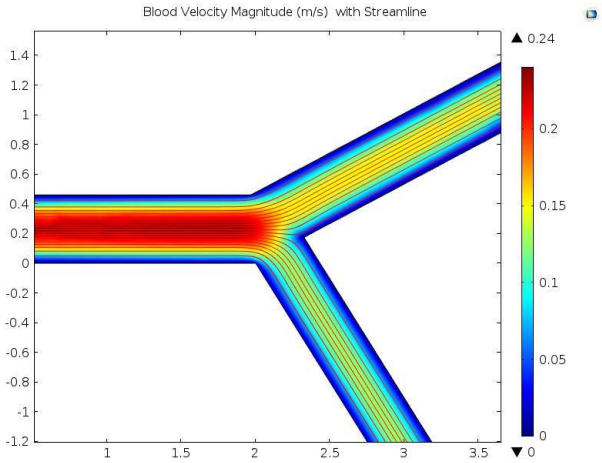

Figure 31 - Blood velocity magnitude inside LM coronary artery bifurcation with its streamlines profile.

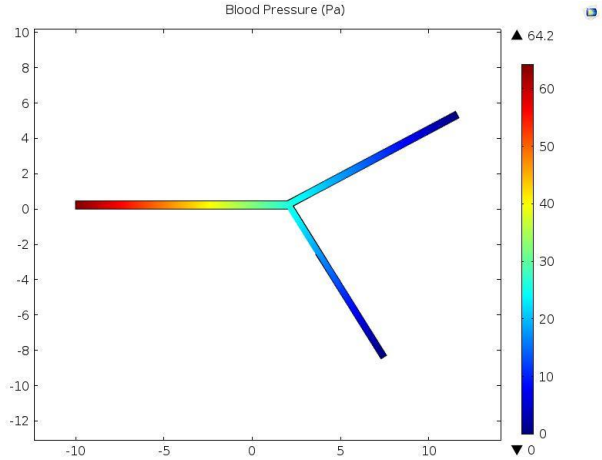

Figure 32 - Blood pressure inside the LM coronary artery bifurcation.

Furthermore, as predicted by our model assumptions and literature (see chapter 2), the decreased shear force caused by blood flow on the vessel wall rises the endothelial permeability to circulating LDL particles and monocytes, as shown in Figures 33 (a) and 33 (b), respectively. In fact, for lower WSS values, EP to LDL reaches $6.5 \times 10^{-9}\ cm/s$ while EP to monocytes reaches $1.5 \times 10^{-6}\ cm/s$, which are significantly higher than the corresponding standard values (as reported in chapter 3).

Consequently, we conclude that, according to our model, the highest EP regions would match with EC deformed areas thus, intima plaque growth would be expected to occur there. An interesting study in future work regards the comparison of higher EP regions with lower WSS regions.

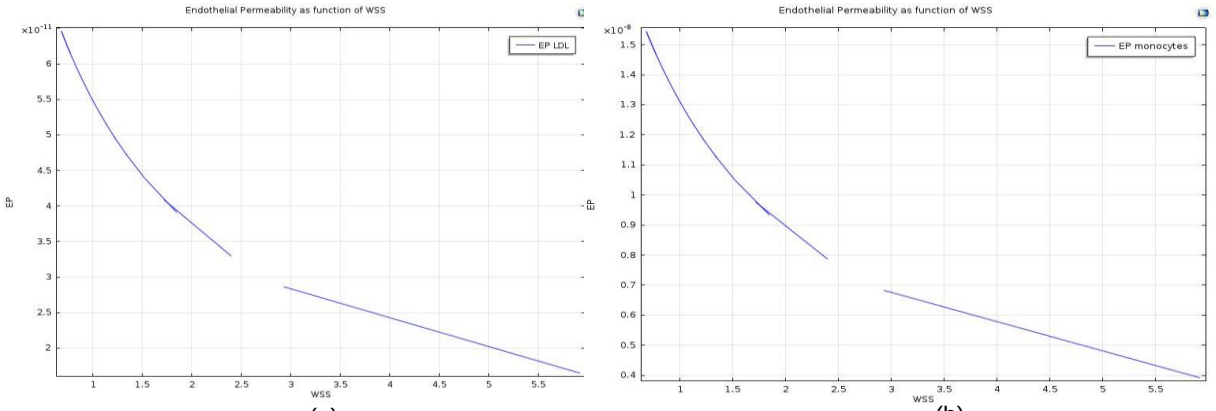

(a) (b)

Figure 33 - Influence of WSS on the endothelial permeability to circulating LDL particles (a) and monocytes (b).

After careful attention to Figure 4.23, a gap is visible on the EP lines for WSS values around $2.5\ N$. Looking back at Figure 30, when WSS reaches values closed to this, it displays a rapid growth, consequently, explaining the EP indetermination (see Equation (3.4)).

The lack of experimental data (WSS clinical patterns, for instance) prevents us from performing a valuable comparison of the obtained results with biologically reasonable measurements. Still, we believe that the observed WSS variations support the theory that endothelial surveillance through local hemodynamic forces monitorization is a useful tool for accessing the focal propensity of atherosclerotic lesions, thus, prevention strategies may focus on this systemic factor [11].

4.2.3.2. Atherosclerosis protagonists inside the intima layer

Although our initial goal regarded the complete implementation of our coupled model in an idealized coronary bifurcation, plaque growth inside LAD intima layer was not performed due to time constraints. Instead, a simplified model was computed for a one-year simulation, allowing the visualization of atherosclerosis protagonists inside the intima layer of LAD artery (see Figure 34). These results come from geometry shown in Figure 27 and correspond to Stage II of the disease (which goes from Equation (3.1.a) to (3.4)). Thus, we provide oxLDL, macrophages, MCP-1 and foam cells concentrations at the end of the simulation.

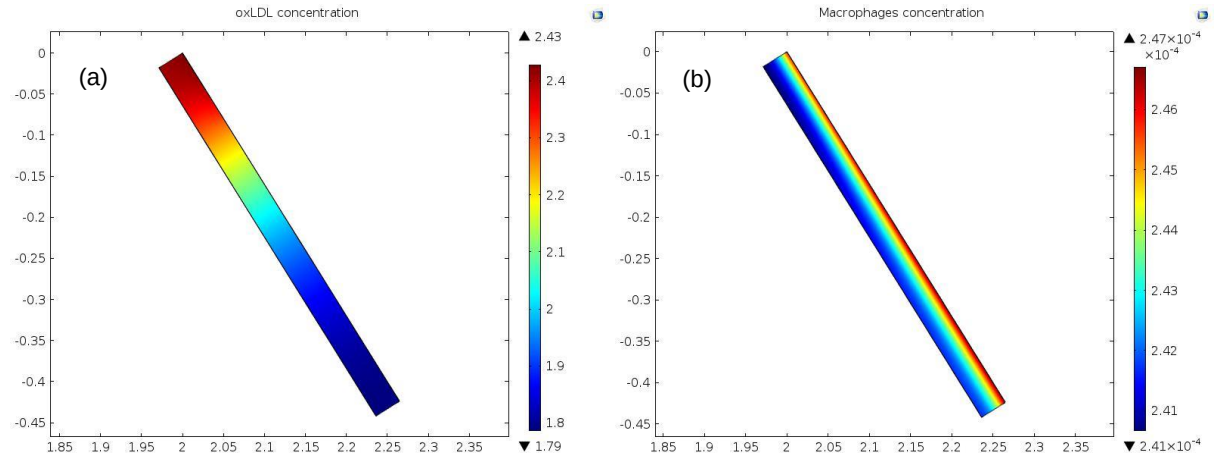

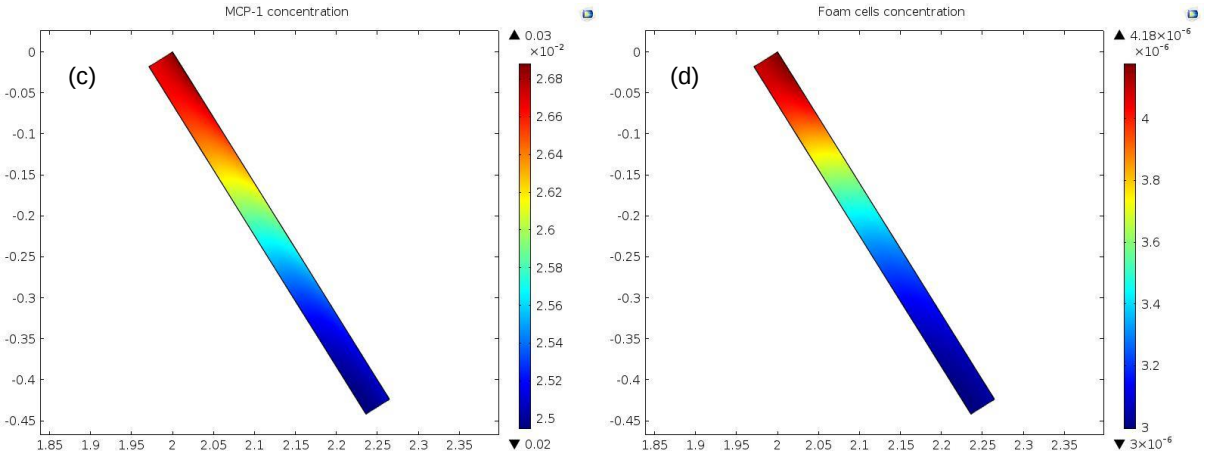

Figure 34 - LM coronary bifurcation displaying atherosclerosis intima protagonists until Stage II, that is, oxLDL (a), macrophages (b), MCP-1 (c) and foam cells (d) for time $t = 47\,304\,000\ s$.

As expected from literature, for one and a half years of simulation, the obtained results illustrate the atherosclerotic tendency for higher species concentrations at lower WSS endothelial regions, this is, closer to the bifurcation site (remember the red endothelial region highlighted in Figure 29 (a) and respective WSS pattern of Figure 30).

Moreover, foam cells LAD intima distribution (Figure 34 (d)) is clearly following oxLDL evolution (Figure 34 (a)) rather than macrophages concentration evolution (Figure 34 (b)), which is in accordance with previous results (see Figures 17, 18 and 20). In addition, macrophages proliferation is, again, a determinant event, leading to a more significant accumulation of these immune cells within higher WSS regions.

Although oxLDL concentration is not biologically reasonable (compare Figure 34 (a) with Figure 15, where we used the simplified rectangular model), we conclude that our study of species distribution within this complex geometry is quite satisfactory but, owing to time constraints, plaque growth into the LAD arterial lumen was not modeled in this work. Therefore, future work should start by coupling it with intima growth, also aiming to reach stage III (SMCs and PDGF intima dynamics).

4.3. Sensitivity Analysis

To critically analyze the obtained results, we accessed the robustness of our model providing parameters uncertainty. We performed a sensitivity analysis technique through *Sensitivity Interface* (present in COMSOL Multiphysics 5.0) by means of stationary studies, allowing parameters influence on the system determination, rather than analyzing the problem which results from temporal discretization in time-dependent studies.

As described in chapter 3 (from Equation (3.33) to (3.37)), the chosen method was *Forward Sensitivity* which, by varying parameters around an introduced value, provides mathematical models evaluation with respect to specific parameters. Hence, we aim at finding the most determinative (or influenceable) parameters included in the suggested model, that is, parameters whose variation causes significant effects on output variables and, consequently, on the obtained results.

For each parameter, a stationary sensitivity analysis was accomplished for the respective atherosclerosis stage. Thus, stage I includes sensitivity analysis of parameters present in the dynamics of oxLDL, macrophages and MCP-1. Stage II adds foam cells transport equation parameters and Stage III includes SMCs and PDGF dynamics. Stage IV, in turn, contains only one parameter from collagen dynamics. Finally, sensitivity analysis to the parameter present in Stokes system is also displayed.

To summarize our results, Table 3 lists the obtained sensitivity average values, correspondent parameters and their respective origin (experimental, estimated or adapted to our model). For consistent comparison among parameters with different units and magnitudes, the obtained sensitivity values were normalized[24]. It is relevant to mention, though, that whenever the same parameter was evaluated with respect to different variables, we assumed the highest computed value.

Table 3 - Summary of the obtained results from sensitivity analysis to our model parameters. Average normalized sensitivity values (in percentage) are provided as well as parameters respective origin (experimental, estimated or adapted). Critical parameters (minimum absolute sensitivity value of $\mathbf{50}\%$) are highlighted.

Parameter	Experimental/Estimated/Adapted	Average Sensitivity (%)
$d_{L_{ox}}$	Experimental	2.4868×10^{-4}
d_M	Experimental	3.0402×10^{-2}
$d_{M_{cp}}$	Experimental	24.71
d_{F_c}	Experimental	1.2724×10^{-4}
d_S	Experimental	-51.97
d_G	Experimental	-3138.10
$k_{M_{cp},M}$	Experimental	-2.8796×10^{-6}
k_{M_{cp},F_c}	Experimental	3.7924×10^{-10}
$k_{G,M}$	Experimental	3193.30
k_{G,F_c}	Experimental	1.4785×10^{-2}
k_{F_c}	Experimental	98.29
k_{col}	Experimental	103.94
$\lambda_{M_{cp}}$	Experimental	-24.71
λ_{F_c}	Experimental	-100.00
λ_G	Experimental	-13.15
r_{diff}	Experimental	101.52
r_{ox}	Experimental	-3.1917×10^{-2}
M_{pro}	Adapted	-100.03
$k_{L_{ox}}$	Experimental	-98.29
$k_{M_{cp}}$	Experimental	249.02
$k_{L_{ox},M}$	Estimated	3.1576×10^{-2}

[24]If p is a parameter and C a model unknown which depends on p, the performed normalization of sensitivity values was accomplished by multiplying the latter ones by p/C, along the entire spatial domain. This is a linear estimation of the percentage change in the output variable C [140].

$a_{M_{cp},L_{ox}}$	Adapted	-8.4484×10^{-5}
$\tilde{a}_S$	Estimated	-7.9857×10^{14}
C_{LDL}	Adapted	-3.1917×10^{-2}
C_m	Experimental	101.52
L_{ox}^{th}	Experimental	3.7503×10^{-7}
A	Experimental	-114.35
S_0	Experimental	51.99
P_0	Experimental	1.5658×10^{13}
G_0	Experimental	7.8291×10^{14}
χ_C	Adapted	1.8243
χ_M	Adapted	-5.1581×10^{-5}
P_{LDL}^{st}	Estimated	248.86
P_{LDL}^{max}	Experimental	-248.89
P_m^{st}	Estimated	-4.2449×10^{-2}
P_m^{max}	Experimental	105.17

Providing the general picture of high sensitivities, we assumed as critical parameters (highlighted in Table 3) those with a minimum absolute value of 50%. Positive sensitivity values indicate that increasing the parameter will increase the respective model unknown. As an example, MCP-1 degradation rate ($d_{M_{cp}}$) displayed the positive normalized sensitivity 24.71%, meaning that an increase of 1% on this parameter will increase MCP-1 intima concentration in 24.71%. On the other hand, negative values indicate that a decrease in the parameter will decrease the respective model unknown. For instance, foam cells degradation rate (λ_{F_c}) registered a normalized sensitivity of -100% which means that a decrease of 1% on its value decreases foam cells intima concentration in 100%. Similar explanation can be drowned for the other parameters.

From our study on parameters origins (previously addressed in Table 2), the expected model robustness (best scenario) would correspond to high sensitivities associated to experimentally obtained parameters since those are believed to be closer to human physiological values than estimated or adapted parameters. In fact, looking at Table 3, one verifies that high sensitivities were obtained for some experimental parameters such as foam cells formation rate, saturation rate of oxLDL by one macrophage and SMCs diffusion coefficient. Of course, there are inevitable limitations related to experiments and many parameters derived from animal models (not human), therefore, measuring errors might be portrayed in such cases. Future work could overcome this problem by performing tests with different values (within the previewed range) for those parameters.

However, three parameters clearly stand out from Table 3 owing to the colossal assigned sensitivity values (solution strongly depends on them): SMCs influx rate into the intima (estimated), PDGF influx concentration (experimental) and MCP-1 influx concentration (experimental). This outcome is not that surprising because those parameters are present in SMCs dynamics, which resulted in an unsolved

computational singularity (numerical instability). Evidently, at the interface between intima and media layers, these parameters are hardy measured in human models. From our results, we cannot draw any conclusion, so we strongly state that Stage III parameters remain an important focus for future experimental procedures. Apart from SMCs influx rate into the intima, other estimated parameters such as standard permeability to LDL, as well as adapted ones like macrophages proliferation rate, also displayed high sensitivities (see Table 3). This unexpected result suggests that solution highly depends on non-experimental (uncertain) parameters, compromising the robustness of the proposed system.

Moreover, the majority of low sensitivities was assigned to experimental parameters, such as oxLDL, macrophages and foam cells diffusion coefficients. Nevertheless, some estimated or adapted values are also framed within this set (e.g. chemotactic sensitivity parameters, MCP-1 activation rate and the rate of oxLDL uptake by macrophages). Our model is, therefore, robust towards variations of these non-certain parameters, that is, no significant effects on the solution are detected when their values change. Table 4 displays a clear overview of the performed sensitivity analysis by assigning parameters origin (experimental, estimated or adapted), according to the correspondent percentages of distribution, to one category of normalized average sensitivity values: low (<50%) or high (≥50%).

Table 4 - Distribution of each parameter origin (experimental, estimated or adapted) between two categories of normalized average sensitivity values: high (≥50%) and low (<50%).

Average Sensitivity Value	Experimental	Estimated	Adapted
Low	30,05%	5,56%	11,11%
High	44,44%	5,56%	2,78%

As already mentioned, there is a significant set of experimental parameters assigned high normalized average sensitivity values (44,44% of used model parameters) which is an indicative of model robustness. However, high sensitivities were also obtained for estimated and adapted values (in total, 8,34% of model parameters), arousing for the importance of future experimental procedures focusing on parameters determination.

Sensitivity analysis may uncover computational errors of mathematical models and experimental errors. Once the obtained mathematical inconsistency could derive from stationary PDEs (which might not be the most suitable to our PDEs system), time-dependent sensitivity studies were performed for five months and the obtained results are displayed in Appendix E (Figures show spatial sensitivity distributions for each parameter). Although we verified no variation tendency (the most influenceable results tended to remain the same over time), little modifications on most of used parameters considerably affected the obtained results. One way of improving our sensitivity study in future work regards increasing simulations time.

Despite some inconclusive results, sensitivity analysis contributes for the quality of the implemented model once it gives us an idea about which parameters we should focus on as we start to consider design changes. In fact, providing the current lack of experimental data regarding atherosclerosis mathematical modeling, sensitivity analysis finds the most important parameters, that is, those that significantly affect the model and, for that reason, should be topic of concern in future clinical and experimental trials. Moreover, sensitivity analysis helps increasing model accuracy when choosing the best values for parameters optimization studies.

5. Limitations and Future Work

5.1. Limitations of the proposed model

This thesis has been meant as an assembly document on mathematically modelling of atherosclerosis disease, particularly focused on advanced lesion mechanisms, including the fibrofatty formation and progression with the maturation and stabilization of the plaque. It puts forward many ideas, some original and some taken from the literature. However, the proposed model is incomplete for many reasons.

Firstly, mathematical analysis of our model was not performed, and it is required to prove existence and uniqueness of solutions as well as to validate these complex models, as claimed in [8]. Secondly, our simplified model does not address every atherosclerosis player or process, especially during earlier stages. In fact, LDL particles and monocytes motion were not computed inside both subdomains (lumen and intima). Monocytes adhesion and transmigration into the vessel wall, a critical event in atherosclerosis initiation, was also omitted. Furthermore, free oxygen radicals and non-oxidized LDL particles which leave the intima layer (re-entering in the luminal flow) were neglected. Besides, T-Cells, which are relevant activators of macrophages as reported in [14], have also been omitted, as well as SMCs migration due to ECM gradient (the so-called haptotaxis). In fact, SMCs motion was simplified to chemotaxis in response to PDGF and MCP-1 gradients. Moreover, our model does not address SMCs apoptosis, frequently considered by other authors (like Cilla et al.) an important event within the vasculature (due to various stimuli such as oxidative stress, high levels of intima oxLDL or inflammatory cytokines) since it usually leads to plaque vulnerability [69].

In addition, at the endothelial surface the biomechanical interaction between blood flow and the vessel wall was not considered in this work. As reported in [11], fluid-structure interaction problem is a current concern among researchers, owing not only to vessel changes of shape and mechanical properties but also to the key role of shear stress action, exerted by blood on the arterial wall, during vascular diseases. Apart from that, the endothelial remodeling, that is, the rapid recovery after mechanical endothelial injury, and neovascularization are also relevant processes during atherosclerosis illness (as concluded in [127] and [128]) which we disregarded. Finally, regarding the lumen domain, the theoretical simplification of blood as a Newtonian fluid also corresponds to a limitation of our work. Actually, many experimental studies have proved that blood flow shows non-Newtonian features, such as shear thinning viscosity behavior, thixotropy (time-dependent shear thinning property), viscoelasticity or yield stress. Numerous factors including plasma viscosity, hematocrit and erythrocytes capacity to form aggregates or to deform have an influence on blood rheology. Besides, no blood oscillations due to heartbeat were considered.

Furthermore, computational tools always portray some limitations since their performance is highly dependent on simulations time and geometry dimensionality. In fact, the idealized two-dimensional coronary artery adopted in our model undergoes more limitations over the numerical results than a three-dimensional geometry since the latter is a configuration much closer to a real artery (which eventually

allows personalized arterial geometry). In addition, our numerical simulations model the long process of atherosclerotic plaque growth for only one year and a half (which corresponds to 47 347 200 seconds) whereas, in reality, this pathological phenomenon needs decades to develop. This time discrepancy compromises our model parameters choice since some were manipulated to accelerate the inflammatory reaction and obtain faster computations, consequently, it limits our results accuracy.

As one major goal of the present thesis, the comparison of the obtained results with experimental data was performed. As clinical data on human evolution of plaques is scarce, we used several animal model parameters. However, during the available time we had, the ideal experimental procedure (using ApoE$^{-/-}$ mice, that is, atherosclerotic mice models) was not performed (see Appendix C), as already explained in chapter 3. Moreover, some experimental data taken from literature to access physiological parameters correspond to estimated orders of magnitude since no clinical data are yet available. In fact, it is difficult to obtain *in vivo* measures of certain physical variables. For instance, in clinical practice, there is no used technique to determine WSS or arterial mechanical properties, which renders it difficult to compare and interpret data (including parameters) between atherosclerosis studies [76].

Besides, clinical values of intima concentrations of the key players in our model inside the thin intima layer are quite small, thus, they are hardly experimentally obtained. In fact, the available parameters in literature correspond to plasma (or serum) quantifications, thus, no intima values are presented yet. Therefore, there is a significant discrepancy between literature values and the concentrations obtained in our simulations, and so comparison of results was only directed towards previous works on atherosclerosis modeling (such as Silva et al., Hao and Friedman, Cilla et al.) [14], [13], [8].

5.2. Plans for future work

One of the most current challenges regarding atherosclerosis modeling is related to plaque instability and (eventual) rupture, that is, mechanisms and key players during Stage V [75] , [129]. Thus, one interesting future step is to couple our model to plaque rupture and consequent release of its content (cellular debris and collagen fibres, for instance). Moreover, concerning our mathematical assumptions, we recommend here brief notes which could bring our model closer to real pathophysiological conditions (note that some have been mentioned by other authors too). Firstly, at the endothelial boundary, we did not assume the limitation on monocytes recruitment. Thus, future work should add factor $\frac{M_{cp}}{M_{cp}+1}$ on the boundary condition of macrophages dynamics. In fact, resorting to MCP-1 concentration (M_{cp}), it acts to limit monocytes recruitment since it yields:

$$\begin{cases} 0\ , & \text{if } M_{cp} = 0 \\ >0\ , & \text{if } M_{cp} > 0 \\ 1, & \text{if } M_{cp} \longrightarrow \infty \end{cases} \tag{5.1}$$

As already stated, future work should also couple monocytes and LDL dynamics (inside both lumen and intima subdomains) to our model. In addition, movement of cells from the intima into the lumen direction was not considered. During atherosclerosis progression, non-oxidized LDL particles and macrophages, eventually, leave the intima layer and re-enter in the arterial lumen.

Moreover, regarding Stokes equations, an extensive study of the pressure action should be performed. Although we assumed intima volume growth was due to formation of foam cells, macrophages proliferation and chemotaxis (in response to MCP-1), SMCs proliferation and migration (in response to MCP-1 and PDGF) and collagen synthesis, several inflammatory protagonists and phenomena were disregarded. Consequently, it is possible that important terms are missing (SMCs haptotaxis and oxLDL creation, for instance). Instead, it is also plausible that eventually some other terms should have not been considered. Finally, the pressure term was not written in the weak formulation but only in the classical form of the PDE equation.

Still on the theoretical side, alternatively to the boundary conditions assumed at the media surface, as suggested by Calvez and coauthors, we could have considered non-zero velocity on Γ_{med} [10]. In fact, both media and intima layers are porous media, thus, they are not tight which, implicitly, means that certain species (such as SMCs) do not have zero velocity at the media boundary. Nonetheless, this was no concern in this work because our simulations on intima plaque growth could be influenced by species movement within Γ_{med}, especially those happening in the y direction (the main direction of plaque growth velocity vector). Hence, future work on this topic should remove the stated simplification. Below, in Figure 35, we encourage this further investigation by suggesting the following Dirichlet boundary conditions for the intima domain that could be considered:

- inlet and outlet boundaries with periodic boundary conditions, where the intima growth velocity component in x direction is taken as zero ($\boldsymbol{u} = 0$);
- the media boundary with zero velocity component in the y direction ($\boldsymbol{v} = 0$).

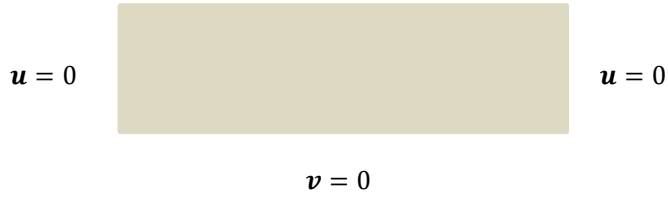

Figure 35 - Scheme of our suggestion for future work on media boundary conditions of Stokes equations.

Furthermore, in order to have a more realistic model of atherosclerotic plaque heterogeneity and complex composition, important phenomena should have been considered. Among those, endothelial remodeling could be implemented on the permeability function, defined for both LDL and monocytes. Linked to the endothelial repair, in early atherosclerotic stages the progression of the hypoxia environment, leads to the expression and release of angiogenic factors, such as vascular endothelial growth factor (VEGF) [130]. Thus, angiogenesis phenomenon occurs and, notably, neovascularization in atherosclerotic lesions plays a major role in plaque growth and instability. In fact, recent studies have shown that angiogenesis may take part in plaque destabilization and thromboembolic events, therefore, this process and its main protagonists could have been considered in this work [129]. Besides, calcification phenomenon is also relevant during advanced stages since calcium phosphates gradually form calcium cores which may, eventually, develop into big calcification centers inside the arterial wall, process orchestrated by SMCs.

Concerning future personalized computations, several variables are interesting to be considered. To state a few, one could study the influence of hypertension on the LDL transport and accumulation within the deformable vessel wall or even HDL dynamics impact on atherosclerosis possible treatment. The latter, in particular, was suggested by Hao and Friedman research in [14], where they concluded that HDL particles help preventing atherosclerosis since they also oxidize inside the intima (without being ingested by macrophages), thus, taking up free radicals that are otherwise available for LDLs. Moreover, HDL removes cholesterol from foam cells, the key promotors of the inflammatory reaction [68]. Further development should also investigate the influence of the heartbeat in blood flow (modeling of oscillations) as well as a non-Newtonian blood flow model. Additionally, future work should also aim at considering the effects of elastic behavior of the artery wall in the model and include fluid structure interaction in the simulations, as performed by Yang et al in [11]. Finally, longer simulation times should be accomplished to deepen the knowledge of atherosclerosis advanced stages, as well as more complex 3D geometries implementation, possibly, even real-patient specific arterial geometries (reconstructed from medical images), commonly seen as a potential benefit for vascular disease prediction using computer simulation [85].

To finish, clinical data are still needed to validate our model and obtain quantitatively reliable results, instead of using parameters from different animal models. Nevertheless, the latter ones, despite their inherent limitations, allow greater mechanistic insight into these cause-effect relationships. As a starting point, we performed an experimental procedure with one healthy mouse that should be accomplished in future work using $ApoE^{-/-}$ mice, the ideal mice models for atherosclerosis studies to obtain the accurate values of mice parameters. Thus, the crucial validation of our model with experimental results is allowed which, then, renders it easier to extrapolate for human atherosclerotic physiological conditions. In fact, as reported in Appendix C, Whitman studied the relation between $ApoE^{-/-}$ mice age, length of fed time and type of diet with the correspondent atherosclerosis stages of plaque development [89]. Once our interest of study was mainly focused on advances stages (III and IV), those pathological conditions are commonly obtained through standard diet given to 7 to 11 months (Stage III) and more than 10 months (Stage IV) mice. In a shorter time, it might also be achieved with mice following a Western diet for 12 to 16 weeks (Stage III) or for 18 to 20 weeks (Stage IV).

Hence, monitorization of time evolution of plaques in sacrificed mice consists on a suitable future path to access experimental parameters, such as monocytes endothelial adherence and transmigration, LDL serum levels, foam cells intima concentration (with posterior determination of the reaction coefficient between oxLDL and macrophages), arterial luminal radius, percentage of stenosis, velocity of atheroma plaque growth or even the influence of risk factors (obesity, diabetes, etc.) in plaque growth (by measuring LDL cholesterol levels or circulating oxLDL levels, as performed in [131]). Therefore, comparison with computational results is, posteriorly, viable [75]. In conclusion, a close cooperation with experts in medicine, biomechanics, mathematics, biophysics and biochemistry is highly required to set up new appropriate experimental procedures for parameters estimation, a task that remains challenging and larger and prospective clinical studies are underway.

References

[1] B. Z. Shao, B. Z. Han, Y. X. Zeng, D. F. Su, and C. Liu, “The roles of macrophage autophagy in atherosclerosis,” *Acta Pharmacol. Sin.*, vol. 37, no. 2, pp. 150–156, 2016.

[2] R. Ross, “Inflammation or Atherogenesis,” *N. Engl. J. Med.*, vol. 340, no. 2, pp. 115–126, 1999.

[3] O. W. in Data, “Share of Deaths by Cause,” 2016.

[4] “Ministério da Saúde (2018), Retrato da Saúde, Portugal.”

[5] T. I. Zohdi, G. A. Holzapfel, and S. A. Berger, “A phenomenological model for atherosclerotic plaque growth and rupture,” *J. Theor. Biol.*, 2004.

[6] P. Cullen, J. Rauterberg, and S. Lorkowski, “The Pathogenesis of Atherosclerosis,” vol. 1, pp. 3–70, 2005.

[7] M. A. Seidman, R. N. Mitchell, and J. R. Stone, “Pathophysiology of Atherosclerosis,” *Cell. Mol. Pathobiol. Cardiovasc. Dis.*, pp. 221–237, 2014.

[8] T. Andrade Freire da Silva Supervisor, A. da Costa Sequeira dos Ramos Silva, and R. B. Neves Ferreira Santos, “Mathematical Modeling of the Atherosclerosis Physiopathology,” 2016.

[9] V. Calvez, A. Ebde, N. Meunier, and A. Raoult, “Mathematical and Numerical Modeling of the Atherosclerotic Plaque Formation,” *ESAIM Proc.*, vol. 28, pp. 1–12, 2009.

[10] V. Calvez, J. G. Houot, N. Meunier, A. Raoult, and G. Rusnakova, “Mathematical and numerical modeling of early atherosclerotic lesions,” 2010.

[11] Y. Yang, W. Jäger, M. Neuss-Radu, and T. Richter, “Mathematical modeling and simulation of the evolution of plaques in blood vessels,” *J. Math. Biol.*, 2015.

[12] M. A. K. Bulelzai and J. L. A. Dubbeldam, “Long time evolution of atherosclerotic plaques,” *J. Theor. Biol.*, vol. 297, pp. 1–10, 2011.

[13] M. Cilla, E. Peña, and M. A. Martínez, “Mathematical modelling of atheroma plaque formation and development in coronary arteries,” 2013.

[14] W. Hao and A. Friedman, “The LDL-HDL profile determines the risk of atherosclerosis: A mathematical model,” *PLoS One*, 2014.

[15] P. M. Winter *et al.*, “Endothelial αvβ3integrin-targeted fumagillin nanoparticles inhibit angiogenesis in atherosclerosis,” *Arterioscler. Thromb. Vasc. Biol.*, vol. 26, no. 9, pp. 2103–2109, 2006.

[16] S. Kasturi, S. Bandimida, N. Gajiwala, and A. Thakkar, “Case Report A Challenging Case of Bifurcation Lesion in Left Anterior Descending Artery : Managed Successfully with Everolimus-Eluting Bioresorbable Vascular Scaffold and Kissing Balloon Technique under Optical Coherence Tomography Guidance,” no. June, pp. 114–116, 2015.

[17] R. E. Klabunde, *Cardiovascular Physiology Concepts*, 2nd ed. 2012.

[18] K. Barrett, H. Brooks, S. Boitano, and S. Barman, *Ganong’s Review of Medical Physiology*. 2010.

[19] A. J. Pappano and W. G. Wier, *Cardiovascular Physiology*, 10th ed. 2013.

[20] K. Rogers, *The Cardiovascular System*, 1st ed. Britannica Educational, 2011.

[21] G. S. Hoffman, C. M. Weyand, C. A. Langford, and J. Goronzy, Eds., *Inflammatory Disease of Blood Vessels*. Wiley-Blackwell, J., 2012.

[22] S. Mitrovska, S. Jovanova, I. Matthiesen, and C. Liebermans, *Atherosclerosis: Understanding pathogenesis and challenge for treatment*. 2009.

[23] O. Kocher *et al.*, “Phenotypic features of smooth muscle cells during the evolution of experimental carotid artery intimal thickening. Biochemical and morphologic studies.,” *Lab. Invest.*, vol. 65, no. 4, pp. 459–70, Oct. 1991.

[24] G. Wick and C. Grundtman, Eds., *Inflammation and Atherosclerosis*. 2012.

[25] M. Simionescu and A. V. Sima, “Morphology of Atherosclerotic Lesions,” in *Inflammation and Atherosclerosis*, Vienna: Springer Vienna, 2012, pp. 19–37.

[26] A. N. Orekhov, Y. V. Bobryshev, and D. A. Chistiakov, “The complexity of cell composition of the intima of large arteries: focus on pericyte-like cells,” *Cardiovasc. Res.*, vol. 103, no. 4, pp. 438–451, Sep. 2014.

[27] Lloyd-Jones D et al., “Heart disease and stroke statistics--2009 update: a report from the American Heart Association Statistics Committee and Stroke Statistics Subcommittee.,” *Circulation*, 2009.

[28] WHO. World Heart Federation. World Stroke Organization, “Global Atlas on Cardiovascular disease prevention and control,” *Publ. by World Heal. Organ. Collab. with World Hear. Fed. World Hear. Fed. World Stroke Organ.*, p. 155, 2011.

[29] H. F. Galley and N. R. Webster, “Physiology of the endothelium,” *Br. J. Anaesth.*, vol. 93, no. 1, pp. 105–113, Jul. 2004.

[30] J. Seebach *et al.*, “Endothelial barrier function under laminar fluid shear stress.,” *Lab. Invest.*, vol. 80, no. 12, pp. 1819–31, Dec. 2000.

[31] J. Seebach *et al.*, “Regulation of endothelial barrier function during flow-induced conversion to an arterial phenotype,” *Cardiovasc. Res.*, vol. 75, no. 3, pp. 596–607, 2007.

[32] S. Y. Yuan and R. R. Rigor, *Regulation of Endothelial Barrier Function*. 2010.

[33] A. Hartsock and W. J. Nelson, “Adherens and tight junctions: Structure, function and connections to the actin cytoskeleton,” *Biochim. Biophys. Acta - Biomembr.*, vol. 1778, no. 3, pp. 660–669, Mar. 2008.

[34] D. Mehta and A. B. Malik, “Signaling Mechanisms Regulating Endothelial Permeability,” *Physiol. Rev.*, vol. 86, no. 1, pp. 279–367, Jan. 2006.

[35] G. Egawa, S. Nakamizo, Y. Natsuaki, H. Doi, Y. Miyachi, and K. Kabashima, “Intravital analysis of vascular permeability in mice using two-photon microscopy,” *Sci. Rep.*, vol. 3, no. 1, p. 1932, Dec. 2013.

[36] E. D. Frohlich and D. Susic, “Blood Pressure, Large Arteries and Atherosclerosis,” in *Atherosclerosis, Large Arteries and Cardiovascular Risk*, Basel: KARGER, 2006, pp. 117–124.

[37] T. Hirase and K. Node, “Endothelial dysfunction as a cellular mechanism for vascular failure.,” *Am. J. Physiol. Heart Circ. Physiol.*, vol. 302, no. 3, pp. H499-505, Feb. 2012.

[38] J. Davignon and P. Ganz, “Role of endothelial dysfunction in atherosclerosis.,” *Circulation*, vol. 109, no. 23 Suppl 1, pp. III27-32, Jun. 2004.

[39] N. Chhabra, “Endothelial dysfunction – A predictor of atherosclerosis,” *Internet J. Med. Updat.*, vol. 4, no. 1, 2009.

[40] P. Kerr, R. Tam, and F. Plane, *Endothelium in Mechanisms of Vascular Disease*. 2011.

[41] J. Ohayon *et al.*, “Is arterial wall-strain stiffening an additional process responsible for atherosclerosis in coronary bifurcations?: an in vivo study based on dynamic CT and MRI,” *Am. J. Physiol. Circ. Physiol.*, vol. 301, no. 3, pp. H1097–H1106, Sep. 2011.

[42] P. F. Davies, “Hemodynamic shear stress and the endothelium in cardiovascular pathophysiology.,” *Nat. Clin. Pract. Cardiovasc. Med.*, vol. 6, no. 1, pp. 16–26, Jan. 2009.

[43] A. M. Malek, S. L. Alper, and S. Izumo, “Hemodynamic shear stress and its role in atherosclerosis.,” *JAMA*, vol. 282, no. 21, pp. 2035–42, Dec. 1999.

[44] D. G. Meyers, “The iron hypothesis--does iron cause atherosclerosis?,” *Clin. Cardiol.*, vol. 19, no. 12, pp. 925–9, Dec. 1996.

[45] P. H. Stone *et al.*, “Prediction of sites of coronary atherosclerosis progression: In vivo profiling of endothelial shear stress, lumen, and outer vessel wall characteristics to predict vascular behavior.,” *Curr. Opin. Cardiol.*, vol. 18, no. 6, pp. 458–70, Nov. 2003.

[46] C. Cheng *et al.*, “Shear stress – induced changes in atherosclerotic plaque composition are modulated by chemokines,” vol. 117, no. 3, 2007.

[47] X. Xie *et al.*, “In vitro and in vivo investigations on the effects of low-density lipoprotein concentration polarization and haemodynamics on atherosclerotic localization in rabbit and zebrafish.,” *J. R. Soc. Interface*, vol. 10, no. 82, p. 20121053, May 2013.

[48] M. Colic, S. Pantovic, M. Jeremic, V. Jokovic, Z. Obradovic, and M. Rosic, “Transport of Low-Density Lipoprotein Into the Blood Vessel Wall During Atherogenic Diet in the Isolated Rabbit Carotid Artery.,” *Circ. J.*, vol. 79, no. 8, pp. 1846–52, 2015.

[49] G. Kostner, Ed., *Lipoproteins - Role in Health and Diseases*. InTech, 2012.

[50] C. A. Cobbold, J. A. Sherratt, and S. R. J. Maxwell, “Lipoprotein oxidation and its significance for atherosclerosis: a mathematical approach.,” *Bull. Math. Biol.*, vol. 64, no. 1, pp. 65–95, Jan. 2002.

[51] A. N. Orekhov, Y. V Bobryshev, I. A. Sobenin, A. A. Melnichenko, and D. A. Chistiakov, “Modified low density lipoprotein and lipoprotein-containing circulating immune complexes as diagnostic and prognostic biomarkers of atherosclerosis and type 1 diabetes macrovascular disease.,” *Int. J. Mol. Sci.*, vol. 15, no. 7, pp. 12807–41, Jul. 2014.

[52] S. J. Lin, K. M. Jan, and S. Chien, “Role of dying endothelial cells in transendothelial macromolecular transport.,” *Arterioscler. An Off. J. Am. Hear. Assoc. Inc.*, vol. 10, no. 5, pp. 703–709, Sep. 1990.

[53] L. M. Cancel and J. M. Tarbell, “The role of apoptosis in LDL transport through cultured endothelial cell monolayers.,” *Atherosclerosis*, vol. 208, no. 2, pp. 335–41, Feb. 2010.

[54] H. J. Guretzki, K. D. Gerbitz, B. Olgemöller, and E. Schleicher, “Atherogenic levels of low density lipoprotein alter the permeability and composition of the endothelial barrier.,” *Atherosclerosis*, vol. 107, no. 1, pp. 15–24, May 1994.

[55] J. M. Tarbell, “Shear stress and the endothelial transport barrier,” *Cardiovasc. Res.*, vol. 87, no.

2, pp. 320–330, Jul. 2010.

[56] D. A. Cox and M. L. Cohen, “Effects of oxidized low-density lipoprotein on vascular contraction and relaxation: clinical and pharmacological implications in atherosclerosis.,” *Pharmacol. Rev.*, vol. 48, no. 1, pp. 3–19, Mar. 1996.

[57] D. P. Ramji and T. S. Davies, “Cytokines in atherosclerosis: Key players in all stages of disease and promising therapeutic targets,” *Cytokine Growth Factor Rev.*, vol. 26, no. 6, pp. 673–685, Dec. 2015.

[58] A. Zlotnik and O. Yoshie, “Chemokines: A New Classification Review System and Their Role in Immunity,” *Immunity*, vol. 12, pp. 121–127, 2000.

[59] T. B. Barrett and E. P. Benditt, “Platelet-derived growth factor gene expression in human atherosclerotic plaques and normal artery wall.,” *Proc. Natl. Acad. Sci. U. S. A.*, vol. 85, no. 8, pp. 2810–4, Apr. 1988.

[60] D. F. Bowen-Pope, T. W. Malpass, D. M. Foster, and R. Ross, “Platelet-derived growth factor in vivo: levels, activity, and rate of clearance.,” *Blood*, vol. 64, no. 2, pp. 458–69, Aug. 1984.

[61] S. Y. Wang, K. L. Mak, L. Y. Chen, M. P. Chou, and C. K. Ho, “Heterogeneity of human blood monocyte: two subpopulations with different sizes, phenotypes and functions.,” *Immunology*, vol. 77, no. 2, pp. 298–303, Oct. 1992.

[62] A. Ghattas, H. R. Griffiths, A. Devitt, G. Y. H. Lip, and E. Shantsila, “Monocytes in coronary artery disease and atherosclerosis: where are we now?,” *J. Am. Coll. Cardiol.*, vol. 62, no. 17, pp. 1541–51, Oct. 2013.

[63] R. van Furth, “Production and migration of monocytes and kinetics of macrophages,” in *Mononuclear Phagocytes*, Dordrecht: Springer Netherlands, 1992, pp. 3–12.

[64] Z. Mamdouh, A. Mikhailov, and W. A. Muller, “Transcellular migration of leukocytes is mediated by the endothelial lateral border recycling compartment.,” *J. Exp. Med.*, vol. 206, no. 12, pp. 2795–808, Nov. 2009.

[65] W. A. Muller, “How endothelial cells regulate transmigration of leukocytes in the inflammatory response.,” *Am. J. Pathol.*, vol. 184, no. 4, pp. 886–96, Apr. 2014.

[66] Y. L. Chen, K. M. Jan, H. S. Lin, and S. Chien, “Ultrastructural studies on macromolecular permeability in relation to endothelial cell turnover.,” *Atherosclerosis*, vol. 118, no. 1, pp. 89–104, Nov. 1995.

[67] K. Ley, C. Laudanna, M. I. Cybulsky, and S. Nourshargh, “Getting to the site of inflammation: the leukocyte adhesion cascade updated.,” *Nat. Rev. Immunol.*, vol. 7, no. 9, pp. 678–89, Sep. 2007.

[68] C. Mckay *et al.*, “Towards a Model of Atherosclerosis.”

[69] M.-L. Bochaton-Piallat and M. Bäck, “Novel concepts for the role of smooth muscle cells in vascular disease: towards a new smooth muscle cell classification,” *Cardiovasc. Res.*, vol. 114, no. 4, pp. 477–480, Mar. 2018.

[70] J. H. Campbell and G. R. Campbell, “Smooth muscle phenotypic modeling--a personal experience.,” *Arterioscler. Thromb. Vasc. Biol.*, vol. 32, no. 8, pp. 1784–9, Aug. 2012.

[71] H. Wolinsky and S. Glagov, “A lamellar unit of aortic medial structure and function in

mammals.," *Circ. Res.*, vol. 20, no. 1, pp. 99–111, Jan. 1967.

[72] M. R. Bennett, S. Sinha, and G. K. Owens, "Vascular Smooth Muscle Cells in Atherosclerosis," *Circ. Res.*, vol. 118, no. 4, pp. 692–702, Feb. 2016.

[73] P. Libby, P. M. Ridker, G. K. Hansson, and Leducq Transatlantic Network on Atherothrombosis, "Inflammation in atherosclerosis: from pathophysiology to practice.," *J. Am. Coll. Cardiol.*, vol. 54, no. 23, pp. 2129–38, Dec. 2009.

[74] J. M. May and Z.-C. Qu, "Ascorbic acid prevents increased endothelial permeability caused by oxidized low density lipoprotein.," *Free Radic. Res.*, vol. 44, no. 11, pp. 1359–68, Nov. 2010.

[75] M. Bulelzai, *Mathematical models for atherosclerotic plaque evolution*, no. december. 2013.

[76] T. G. Papaioannou and C. Stefanadis, "Vascular wall shear stress: basic principles and methods," *Hell. J Cardiol*, vol. 46, no. 1, pp. 9–15, 2005.

[77] B. Mompeo, D. Popov, A. Sima, E. Constantinescu, and M. Simionescu, "Diabetes-induced structural changes of venous and arterial endothelium and smooth muscle cells.," *J. Submicrosc. Cytol. Pathol.*, vol. 30, no. 4, pp. 475–84, Oct. 1998.

[78] T. Quillard and P. Libby, "Molecular imaging of atherosclerosis for improving diagnostic and therapeutic development.," *Circ. Res.*, vol. 111, no. 2, pp. 231–44, Jul. 2012.

[79] C. Hahn and M. A. Schwartz, "Mechanotransduction in vascular physiology and atherogenesis.," *Nat. Rev. Mol. Cell Biol.*, vol. 10, no. 1, pp. 53–62, Jan. 2009.

[80] M. Simionescu and A. V Sima, "Inflammation and Atherosclerosis," pp. 19–38, 2012.

[81] R. Virami, "Lessons from Sudden Coronary Death," *Arter. Thromb Biol*, pp. 1262–1275, 2000.

[82] C. L. Lendon, M. J. Davies, G. V Born, and P. D. Richardson, "Atherosclerotic plaque caps are locally weakened when macrophages density is increased.," *Atherosclerosis*, vol. 87, no. 1, pp. 87–90, Mar. 1991.

[83] S. Chung and K. Vafai, "Low-density lipoprotein transport within a multi-layered arterial wall-Effect of the atherosclerotic plaque/stenosis," *J. Biomech.*, 2013.

[84] N. El Khatib, S. Génieys, and V. Volpert, "Atherosclerosis Initiation Modeled as an Inflammatory Process," *Math. Model. Nat. Phenom*, vol. 2, no. 2, pp. 126–141, 2007.

[85] N. Filipovic *et al.*, "Computer simulation of three-dimensional plaque formation and progression in the coronary artery," *Comput. Fluids*, 2013.

[86] N. Faust, F. Varas, L. M. Kelly, S. Heck, and T. Graf, "Insertion of enhanced green fluorescent protein into the lysozyme gene creates mice with green fluorescent granulocytes and macrophages.," *Blood*, vol. 96, no. 2, pp. 719–726, 2000.

[87] a S. Silva, C. Saldanha, and J. Martins e Silva, "Effects of velnacrine maleate in the leukocyte-endothelial cell interactions in rat cremaster microcirculatory network.," *Clin. Hemorheol. Microcirc.*, vol. 36, no. 3, pp. 235–246, 2007.

[88] P. Kubes and S. M. Kerfoot, "Leukocyte recruitment in the microcirculation: the rolling paradigm revisited.," *News Physiol. Sci.*, vol. 16, no. April, pp. 76–80, Apr. 2001.

[89] S. C. Whitman, "A practical approach to using mice in atherosclerosis research.," *Clin. Biochem. Rev.*, vol. 25, no. 1, pp. 81–93, 2004.

[90] A. Datta and V. Rakesh, *An introduction to modeling of transport processes: Applications to*

biomedical systems. Cambridge University Press, 2009.

[91] T. Silva, J. Tiago, and A. Sequeira, “Mathematical Analysis and Numerical Simulations for a Model of Atherosclerosis.”

[92] B. Hokland, a J. Mendez, and J. F. Oram, “Cellular localization and characterization of proteins that bind high density lipoprotein.,” *J. Lipid Res.*, vol. 33, no. 9, pp. 1335–42, 1992.

[93] L. Formaggia, A. Quarteroni, and A. Veneziani, Eds., *Cardiovascular Mathematics*. Milano: Springer Milan, 2009.

[94] “COMSOL Multiphysics,” 2014.

[95] A. Quarteroni and A. Valli, *Numerical Approximation of Partial Differential Equations*, vol. 23. Berlin, Heidelberg: Springer Berlin Heidelberg, 1994.

[96] D. Kuzmin, *A Guide to Numerical Methods for Transport Equations*. 2010.

[97] P. Brown, A. Hindmarsh, and L. Petzold, “Using Krylov Methods in the Solution of Large-Scale Differential-Algebraic Systems,” *Numer. Math. Gr.*, vol. 39, no. 5, pp. 561–563, 1993.

[98] J. T. Dodge, B. G. Brown, E. L. Bolson, and H. T. Dodge, “Lumen diameter of normal human coronary arteries. Influence of age, sex, anatomic variation, and left ventricular hypertrophy or dilation.,” *Circulation*, vol. 86, no. 1, pp. 232–246, Jul. 1992.

[99] R. N. MacAlpin, A. S. Abbasi, J. H. Grollman, and L. Eber, “Human Coronary Artery Size During Life,” *Radiology*, vol. 108, no. 3, pp. 567–576, Sep. 1973.

[100] U. Olgac, V. Kurtcuoglu, and D. Poulikakos, “Computational modeling of coupled blood-wall mass transport of LDL: effects of local wall shear stress.,” *Am. J. Physiol. Heart Circ. Physiol.*, vol. 294, no. 2, pp. H909-19, Feb. 2008.

[101] H. H. Lipowsky, S. Usami, and S. Chien, “In vivo measurements of ‘apparent viscosity’ and microvessel hematocrit in the mesentery of the cat,” *Microvasc. Res.*, vol. 19, no. 3, pp. 297–319, May 1980.

[102] D. C. Schwenke and T. E. Carew, “Initiation of atherosclerotic lesions in cholesterol-fed rabbits. II. Selective retention of LDL vs. selective increases in LDL permeability in susceptible sites of arteries.,” *Arteriosclerosis*, vol. 9, no. 6, pp. 908–18.

[103] C. Bell, *Clinical Guide to Laboratory Tests.*, 3rd ed., vol. 35, no. 11. 2009.

[104] C. Chen and D. B. Khismatullin, “Oxidized Low-Density Lipoprotein Contributes to Atherogenesis via Co-activation of Macrophages and Mast Cells,” *PLoS One*, vol. 10, no. 3, p. e0123088, Mar. 2015.

[105] W. R. Milnor, “Hemodynamics,” *Clin. Cardiol.*, vol. 13, no. 11, p. 821a–821a, Nov. 1989.

[106] M. Prosi, P. Zunino, K. Perktold, and A. Quarteroni, “Mathematical and numerical models for transfer of low-density lipoproteins through the arterial walls: a new methodology for the model set up with applications to the study of disturbed lumenal flow,” *J. Biomech.*, vol. 38, no. 4, pp. 903–917, Apr. 2005.

[107] M. Chaplain and A. Matzavinos, “Mathematical modelling of spatio-temporal phenomena in tumour immunology: Tutorials in mathematical biosciences III: cell cycle, proliferation, and cancer.,” Springer Berlin Heidelberg, Berlin, Heidelberg, 2006.

[108] M. R. Owen and J. A. Sherratt, “Pattern formation and spatiotemporal irregularity in a model for

macrophage-tumour interactions.," *J. Theor. Biol.*, vol. 189, no. 1, pp. 63–80, Nov. 1997.

[109] Y. Kim, S. Roh, S. Lawler, and A. Friedman, "miR451 and AMPK mutual antagonism in glioma cell migration and proliferation: a mathematical model.," *PLoS One*, vol. 6, no. 12, p. e28293, 2011.

[110] C. Xue, A. Friedman, and C. K. Sen, "A mathematical model of ischemic cutaneous wounds.," *Proc. Natl. Acad. Sci. U. S. A.*, vol. 106, no. 39, pp. 16782–7, Sep. 2009.

[111] P. Siogkas *et al.*, "Multiscale - Patient-Specific Artery and Atherogenesis Models," *IEEE Trans. Biomed. Eng.*, vol. 58, no. 12, pp. 3464–3468, Dec. 2011.

[112] B. Vesosky, D. K. Flaherty, and J. Turner, "Th1 cytokines facilitate CD8-T-cell-mediated early resistance to infection with Mycobacterium tuberculosis in old mice.," *Infect. Immun.*, vol. 74, no. 6, pp. 3314–24, Jun. 2006.

[113] H. Zahedmanesh, H. Van Oosterwyck, and C. Lally, "A multi-scale mechanobiological model of in-stent restenosis: deciphering the role of matrix metalloproteinase and extracellular matrix changes," *Comput. Methods Biomech. Biomed. Engin.*, vol. 17, no. 8, pp. 813–828, Jun. 2014.

[114] W. Zhao, C. A. Oskeritzian, A. L. Pozez, and L. B. Schwartz, "Cytokine Production by Skin-Derived Mast Cells: Endogenous Proteases Are Responsible for Degradation of Cytokines," *J. Immunol.*, vol. 175, no. 4, pp. 2635–2642, Aug. 2005.

[115] A. Friedman, J. Turner, and B. Szomolay, "A model on the influence of age on immunity to infection with Mycobacterium tuberculosis.," *Exp. Gerontol.*, vol. 43, no. 4, pp. 275–85, Apr. 2008.

[116] H. Esterbauer, G. Striegl, H. Puhl, and M. Rotheneder, "Continuous Monitoring of in Vztro Oxidation of Human Low Density Lipoprotein," *Free Radic. Res. Commun.*, vol. 6, no. 1, pp. 67–75, Jan. 1989.

[117] D. A. Rahdert, W. L. Sweet, F. O. Tio, C. Janicki, and D. M. Duggan, "Measurement of density and calcium in human atherosclerotic plaque and implications for arterial brachytherapy," *Cardiovasc. Radiat. Med.*, vol. 1, no. 4, pp. 358–367, Oct. 1999.

[118] D. C. Miller, A. Thapa, K. M. Haberstroh, and T. J. Webster, "Endothelial and vascular smooth muscle cell function on poly(lactic-co-glycolic acid) with nano-structured surface features.," *Biomaterials*, vol. 25, no. 1, pp. 53–61, Jan. 2004.

[119] J. Rhodes, J. Sharkey, and P. Andrews, "Serum IL-8 and MCP-1 concentration do not identify patients with enlarging contusions after traumatic brain injury.," *J. Trauma*, vol. 66, no. 6, p. 1591–7; discussion 1598, Jun. 2009.

[120] Y. Kim and A. Friedman, "Interaction of tumor with its micro-environment: A mathematical model.," *Bull. Math. Biol.*, vol. 72, no. 5, pp. 1029–68, Jul. 2010.

[121] Y. Kim, S. Lawler, M. O. Nowicki, E. A. Chiocca, and A. Friedman, "A mathematical model for pattern formation of glioma cells outside the tumor spheroid core.," *J. Theor. Biol.*, vol. 260, no. 3, pp. 359–71, Oct. 2009.

[122] J. Glod *et al.*, "Monocytes form a vascular barrier and participate in vessel repair after brain injury.," *Blood*, vol. 107, no. 3, pp. 940–6, Feb. 2006.

[123] S. Marino, I. B. Hogue, C. J. Ray, and D. E. Kirschner, "A methodology for performing global

uncertainty and sensitivity analysis in systems biology.," *J. Theor. Biol.*, vol. 254, no. 1, pp. 178–96, Sep. 2008.

[124] M. Molavi Zarandi, R. Mongrain, and O. F. Bertrand, "Determination of Flow Conditions in Coronary Bifurcation Lesions in the Context of the Medina Classification," *Model. Simul. Eng.*, vol. 2012, pp. 1–10, 2012.

[125] P. Sjogren *et al.*, "Measures of oxidized low-density lipoprotein and oxidative stress are not related and not elevated in otherwise healthy men with the metabolic syndrome.," *Arterioscler. Thromb. Vasc. Biol.*, vol. 25, no. 12, pp. 2580–6, Dec. 2005.

[126] Y. Cui *et al.*, "Quantification of left coronary bifurcation angles and plaques by coronary computed tomography angiography for prediction of significant coronary stenosis: A preliminary study with dual-source CT," *PLoS One*, vol. 12, no. 3, p. e0174352, 2017.

[127] L. Tilling, J. Hunt, A. Donald, B. Clapp, and P. Chowienczyk, "Arterial injury and endothelial repair: Rapid recovery of function after mechanical injury in healthy volunteers," *Cardiol. Res. Pract.*, vol. 2014, 2014.

[128] C. Camaré, M. Pucelle, A. Nègre-Salvayre, and R. Salvayre, "Angiogenesis in the atherosclerotic plaque," *Redox Biol.*, vol. 12, no. January, pp. 18–34, 2017.

[129] M. Guo, Y. Cai, X. Yao, and Z. Li, "Mathematical modeling of atherosclerotic plaque destabilization: Role of neovascularization and intraplaque hemorrhage," *J. Theor. Biol.*, vol. 450, pp. 53–65, Aug. 2018.

[130] S. E. Heinonen *et al.*, "The effects of VEGF-A on atherosclerosis, lipoprotein profile, and lipoprotein lipase in hyperlipidaemic mouse models," *Cardiovasc. Res.*, vol. 99, no. 4, pp. 716–723, 2013.

[131] S. Toshima *et al.*, "Circulating oxidized low density lipoprotein levels. A biochemical risk marker for coronary heart disease.," *Arterioscler. Thromb. Vasc. Biol.*, vol. 20, no. Ldl, pp. 2243–2247, 2000.

[132] T. Hillen and K. J. Painter, "A user's guide to PDE models for chemotaxis," *J. Math. Biol.*, vol. 58, no. 1–2, pp. 183–217, Jan. 2009.

[133] H. C. Stary *et al.*, "A definition of advanced types of atherosclerotic lesions and a histological classification of atherosclerosis. A report from the Committee on Vascular Lesions of the Council on Arteriosclerosis, American Heart Association.," *Arterioscler. Thromb. Vasc. Biol.*, vol. 15, no. 9, pp. 1512–31, Sep. 1995.

[134] B. M. Gumbiner, "Cell adhesion: the molecular basis of tissue architecture and morphogenesis.," *Cell*, vol. 84, no. 3, pp. 345–57, Feb. 1996.

[135] Y. Abebe, G. Bhardwaj, and M. Habtamu, "Physiology Part I, Lecture Notes for Health Science Students," 2006.

[136] G. Cesarman-Maus and K. A. Hajjar, "Molecular mechanisms of fibrinolysis.," *Br. J. Haematol.*, vol. 129, no. 3, pp. 307–21, May 2005.

[137] S. F. Wilson, *Perfusion in Concepts for Nursing Practice*. Division, Elsevier Science Health Science, 2012.

[138] C. O'Connor, "Cell Division: Stages of Mitosis," *Nat. Educ.*, vol. 1, no. 1, p. 188, 2008.

[139] A. Sequeira, “Hemorheology: Non-Newtonian Constitutive Models for Blood Flow Simulations,” 2018, pp. 1–44.

[140] M. a Atherton, R. Bates, M. Perry, M. Oldfield, and H. Wynn, “Sensitivity analysis modelling for microscale multiphysics robust engineering design,” no. October 2014, pp. 1–8, 2008.

Appendix A

Advection-Reaction-Diffusion Equations

Our mathematical model considers advection-reaction-diffusion (A-R-D) equations written as:

$$\frac{\partial C}{\partial t} + \nabla \cdot (-D\nabla C) + \nabla \cdot (\boldsymbol{v}C) = F \tag{A.1}$$

where $C = C(x, y, t) \in \mathbb{R}$ denotes the concentration of a substance per unit volume, $\frac{\partial C}{\partial t}$ represents the evolution of that concentration, $\nabla \cdot (-D\nabla C)$ stands for the diffusion term and $\nabla \cdot (\boldsymbol{v}C)$ for the advection term (with transport velocity $\boldsymbol{v}$). The latter can be simplified to $\boldsymbol{v} \cdot \nabla C$ when $\nabla \cdot \boldsymbol{v} = 0$ (for incompressible fluids). Finally, F is the influx term, that is, the reaction term.

In this work, we assume that diffusion coefficients are known (constants). However, when it comes to real life problems, it usually depends on many factors such as the substance concentration.

In the limit of pure diffusion ($\boldsymbol{v} = 0$), one obtains a reaction-diffusion (R-D) model, whereas in the limit of pure advection ($D = 0$) it leads to advection-reaction (A-R) model. One may also have a advection-diffusion model by deleting the reaction term ($F = 0$).

Furthermore, when substance C moves in response to a certain stimulus (S), the advection term is replaced by the chemotactic term, $\nabla \cdot (\chi_C \, \mathrm{C} \, \nabla S)$, that is, the chemotactic motion due to a chemical gradient. Then, the resulting equation is called chemotaxis-reaction-diffusion (χ -R-D) equation [132].

Once the type of model is chosen, boundary and initial conditions have to be defined. The nomenclature in a bounded domain consists of the domain (Ω), its boundary ($\partial\Omega$), an inflow part ($\Gamma_{in} = x \in \partial\Omega | \boldsymbol{v} \cdot \boldsymbol{n} < 0$) and an outflow part ($\Gamma_{out} = x \in \partial\Omega | \boldsymbol{v} \cdot \boldsymbol{n} > 0$), and a solid wall ($\Gamma_0 = x \in \partial\Omega | \boldsymbol{v} \cdot \boldsymbol{n} = 0$) with $\boldsymbol{n}$ denoting the unit outward normal to the boundary at point $x \in \partial\Omega$.

On the one hand, if values of C are known on a certain boundary Γ_D, a Dirichlet boundary condition (the so-called no slip BC) is imposed:

$$C = C(x, y, t) = C_D(x, y, t), \qquad \forall x \in \Gamma_D, \forall t \in [0, T] \tag{A.2}$$

On the other hand, Neumann boundary conditions are defined as:

$$(-D\nabla C + \boldsymbol{v}C) \cdot \boldsymbol{n} = g(x, t, C), \qquad \forall x \in \Gamma_N, \forall t \in [0, T] \tag{A.3}$$

where the right-hand side term stands for a given normal flux on Γ_N.

Appendix B

Atherosclerosis Mathematical Model by El Khatib et al. (2007)

As precursors of atherosclerosis inflammation modeling, El Khatib et al. described a model for the inflammation period (during the early stage of atherosclerosis) through one and two-dimensional simple models [84]. In their work, reaction-diffusion equations were used for both variables: the density of immune cells (B) and the density of inflammatory cytokines, secreted by those cells (A).

Thus, the one-dimensional model was defined as

$$\frac{\partial B}{\partial t} - d_B \frac{\partial^2 B}{\partial x^2} = f_1(A) - \lambda_B B \tag{B.1}$$

$$\frac{\partial A}{\partial t} - d_A \frac{\partial^2 A}{\partial x^2} = f_2(A)\, B - \lambda_A A \tag{B.2}$$

for $x \in [0, L]$, where L stands for the intima's length. In both equations, the last term refers to the degradation of immune cells ($-\lambda_B B$) and cytokines ($-\lambda_A A$), whereas their respective diffusions are represented by $d_B \frac{\partial^2 B}{\partial x^2}$ and $d_A \frac{\partial^2 A}{\partial x^2}$ (d_B and d_A stand for the immune cells diffusion coefficient and the cytokines diffusion coefficient, respectively).

Besides, the function $f_1(A)$ models the immune cells recruitment from the lumen (which is promoted by the cytokines) while the term $f_2(A)\, B$ models the cytokines production rate. Their respective expressions are given by:

$$f_1(A) = \frac{\alpha_1 + \beta_1 A}{1 + \frac{A}{t_1}} \tag{B.3}$$

$$f_2(A) = \frac{\alpha_2 A}{1 + \frac{A}{t_2}} \tag{B.4}$$

where $\alpha_1 = f_1(0)$, representing the beginning of the inflammation, β_1 corresponds to the auto-amplification phenomenon of the recruitment of monocytes and $1 + \frac{A}{t_1}$ represents the saturation in the recruitment of B, with t_1 being the characteristic time for the fibrous cap formation. In Equation (B.4), the term $\alpha_2 A$ represents the secretion of proinflammatory cytokines and $1 + \frac{A}{t_2}$ represents the inhibition of those, with t_2 being the necessary time for this inhibition to act. Regarding the boundary conditions, homogeneous Neumann conditions were imposed for both variables.

The two-dimensional model, in turn, was defined as

$$\frac{\partial B_\varepsilon}{\partial t} - d_B \Delta B_\varepsilon = -\lambda_B B_\varepsilon \tag{B.5}$$

$$\frac{\partial A_\varepsilon}{\partial t} - d_A \Delta A_\varepsilon = f_2(A_\varepsilon)\, B_\varepsilon - \lambda_A A_\varepsilon \tag{B.6}$$

in $\Omega_\varepsilon = [0, L] \times [0, \varepsilon]$, where L is the intima's length and ε its height. For A_ε, homogeneous Neumann boundary conditions were imposed for each boundary, while for B_ε those were defined as

$$\frac{\partial B_\varepsilon}{\partial x}(0, y) = \frac{\partial B_\varepsilon}{\partial x}(L, y) = 0 \tag{B.7}$$

for $y \in [0, \varepsilon]$ and

$$\frac{\partial B_\varepsilon}{\partial y}(x, 0) = 0 \;;\; \frac{\partial B_\varepsilon}{\partial y}(x, \varepsilon) = \frac{f_1(A_\varepsilon)}{d_B} \tag{B.8}$$

for $x \in [0, L]$.

Through this analytic study followed by numerical simulations, the authors reached the conclusion that, inside the tunica intima, initial conditions such as oxLDL and monocytes concentration determine the inflammatory reaction level, thus, the atherosclerotic pathology development.

Appendix C

Mice as an Atherosclerosis Model

In 2004, Whitman published a review article where he discussed the use of mice in atherosclerosis studies. In his work, the author describes several available mouse models and experimental procedures, specially focusing on apolipoprotein E deficient (ApoE $^{-/-}$) and low-density lipoprotein receptor deficient (ldlr $^{-/-}$) mice. He concluded that the expected atherosclerotic lesions, associated with a specific stage of development, depend on mice age, length of fed time and type of diet [89]. Accordingly, ApoE $^{-/-}$ mice stayed as the most accurate in what advanced atherosclerotic plaques are concerned (our interest of study). Therefore, Table C.1 summarizes the results of the mentioned paper for ApoE $^{-/-}$ mice (with lesions obtained in the ascending aorta), where the division of human atherosclerosis stages was adapted (from the American Heart Association) to match with ours (see chapter 2) [133].

Table C.1 - Lesion Stage and timeframe for atherosclerosis development in ApoE $^{-/-}$ mice. Adapted from [89].

	Atherosclerosis Stage			
Mouse Model (diet)	I	II	III	IV
[a]ApoE $^{-/-}$ ([c]standard diet)	1-2 months	4-5 months	7-11 months	10> months
[b]ApoE $^{-/-}$ ([d]Western diet)	4-6 weeks	8-10 weeks	12-16 weeks	18-20 weeks

[a] Time refers to the mouse age (in months).

[b] Time refers to the fed time of Western diet, starting when they are between 4-8 weeks of age.

[c] Standard chow diet generally consists of 20% (wt/wt) protein from plant and animal sources, 4.5%(wt/wt) fat, 0.02% (wt/wt) cholesterol, no casein, no sodium cholate.

[d] Two common sources of Western Diet are from Harlan Teklad (#88137; Madison, Wisconsin, USA) and Dyets Inc. (#112286; Bethlehem, Pennsylvania, USA). Both consist of 21% (wt/wt) fat (butterfat) and 0.15% (wt/wt) cholesterol, 19.5% (wt/wt) casein and no sodium cholate.

Providing these results, it is verified that atherosclerosis lesions in Stage I (Endothelial Dysfunction) can be experimentally obtained with one- or two-months mice following a standard diet, as well as through mice undergoing a Western diet for 4 to 6 weeks. Secondly, Stage II (Fatty Streak) can be achieved by means of standard diet to mice with 4 to 5 months of age or a Western diet during 8 to 10 weeks. Finally, moving to our interest of study, Stages III (Fibrofatty Lesion) and IV (Fibrous and Mature Plaque) are commonly obtained through standard diet given to 7 to 11 months (third stage) and more than 10 months (fourth stage) mice. In a shorter time, these latter stages might also be achieved with mice following a Western diet for 12 to 16 weeks (Stage III) or for 18 to 20 weeks (Stage IV).

Appendix D

Numerical Simulations - Workflow

Table D.1 – Simulations workflow with atherosclerosis key players, respective computational time and COMSOL extension.

Protagonists	Computational Time	COMSOL Extension
oxLDL	1,5 years	https://meocloud.pt/link/888dffc1-01f2-46f0-bfca-86dd19f0b5ba/1%20-%20Modelo%20de%20transporte_Param_oxLDL.mph/
oxLDL, Macrophages, MCP-1	1,5 years	https://meocloud.pt/link/069f40bc-7791-48e6-b977-62d865a6bc64/ModeloSimples_malha_chemotaxis.mph/
oxLDL, Macrophages, MCP-1, Stokes, endothelial deformation	1,5 years	https://meocloud.pt/link/3c9ab7b4-79d4-4533-a3e3-8f5a2c8b749a/1%20-%20Endo%20Dysf%20_%20Stokes%20%2B%20Deform.mph/
oxLDL, Macrophages, MCP-1, Stokes, endothelial deformation, foam cells	6 years	https://meocloud.pt/link/cd6c5bc5-7a96-4ce7-8c90-897f6fe72453/II_fatty_streak_crescimento5anos.mph/
oxLDL, Macrophages, MCP-1, foam cells, PDGF, SMCs	6 years	https://meocloud.pt/link/9f3f29f3-9605-450c-9046-fc84e6817bec/III%20-%20fibrofatty_lesion.mph/
oxLDL, Macrophages, MCP-1, foam cells, PDGF, SMCs, collagen	5 years	https://meocloud.pt/link/30323bea-7c0e-4a2f-b897-aac40b26a217/bioquimica_5anos.mph/
Left coronary bifurcation with intima layers at all branches	(Future work)	https://meocloud.pt/link/5da32662-5909-41db-82e7-84130d0a5f71/Bifurcation%20_%20Navier%20Stokes%20%2B%20Intimas.mph/

Appendix E

Time Dependent Sensitivity Analysis

Although our general total simulation time corresponds to five years, time dependent sensitivity analysis was only possible to perform for $13\,000\,000\ s$ (approximately, 5 months) for Stages I and II (both including plaque growth analysis). Regarding Stages III and IV, owing to the previously explained numerical instability, it was not possible to obtain reasonable solutions for time dependent sensitivity analysis neither.

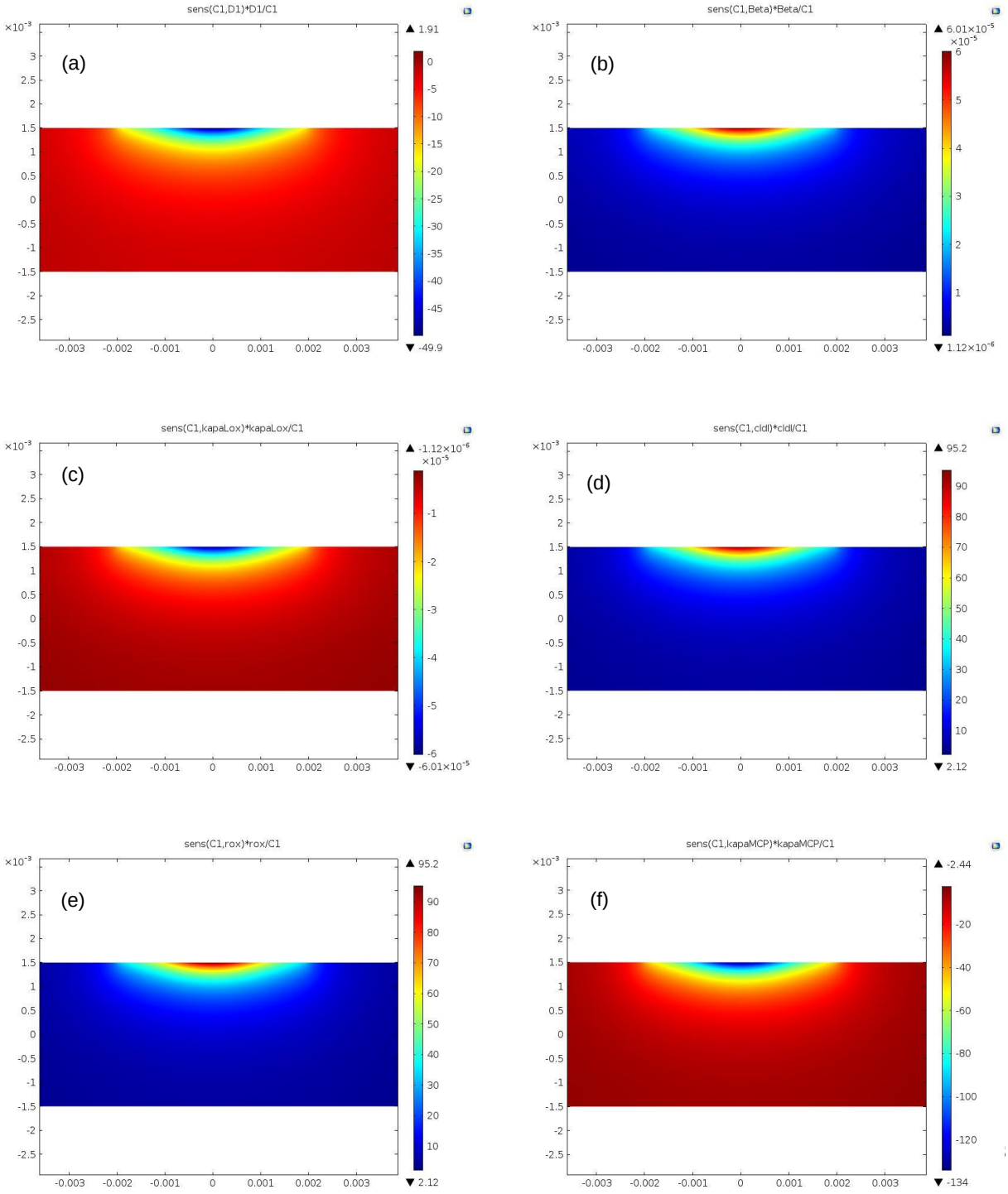

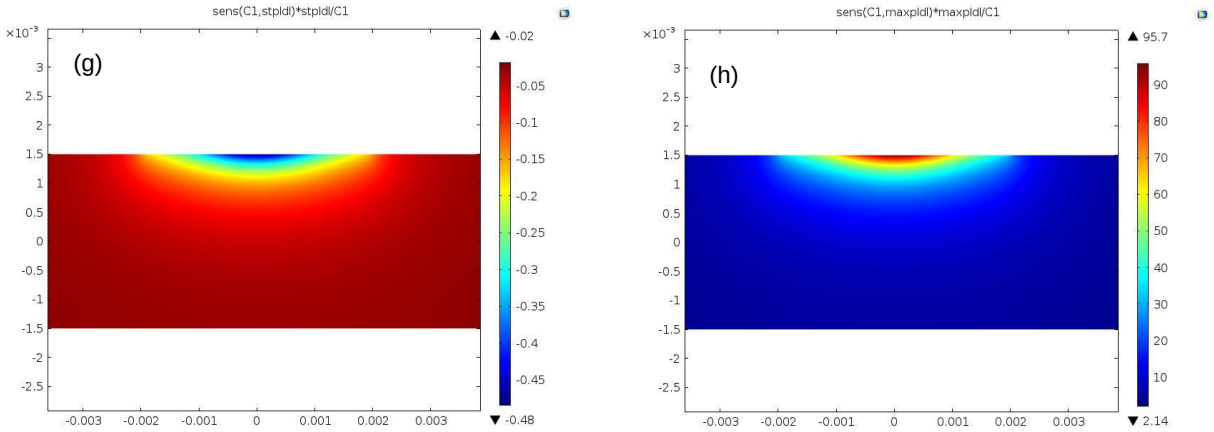

Figure E.1 – Normalized sensitivity values of oxLDL intima concentration with respect to oxLDL diffusion coefficient (a), rate of oxLDL uptake by macrophages (b), saturation rate of oxLDL uptake by one macrophage (c), LDL endothelial influx (d), LDL oxidation rate (e), saturation rate of MCP-1 due to ingestion by macrophages (f), standard endothelial permeability to LDL (g) and maximum endothelial permeability to LDL (h).

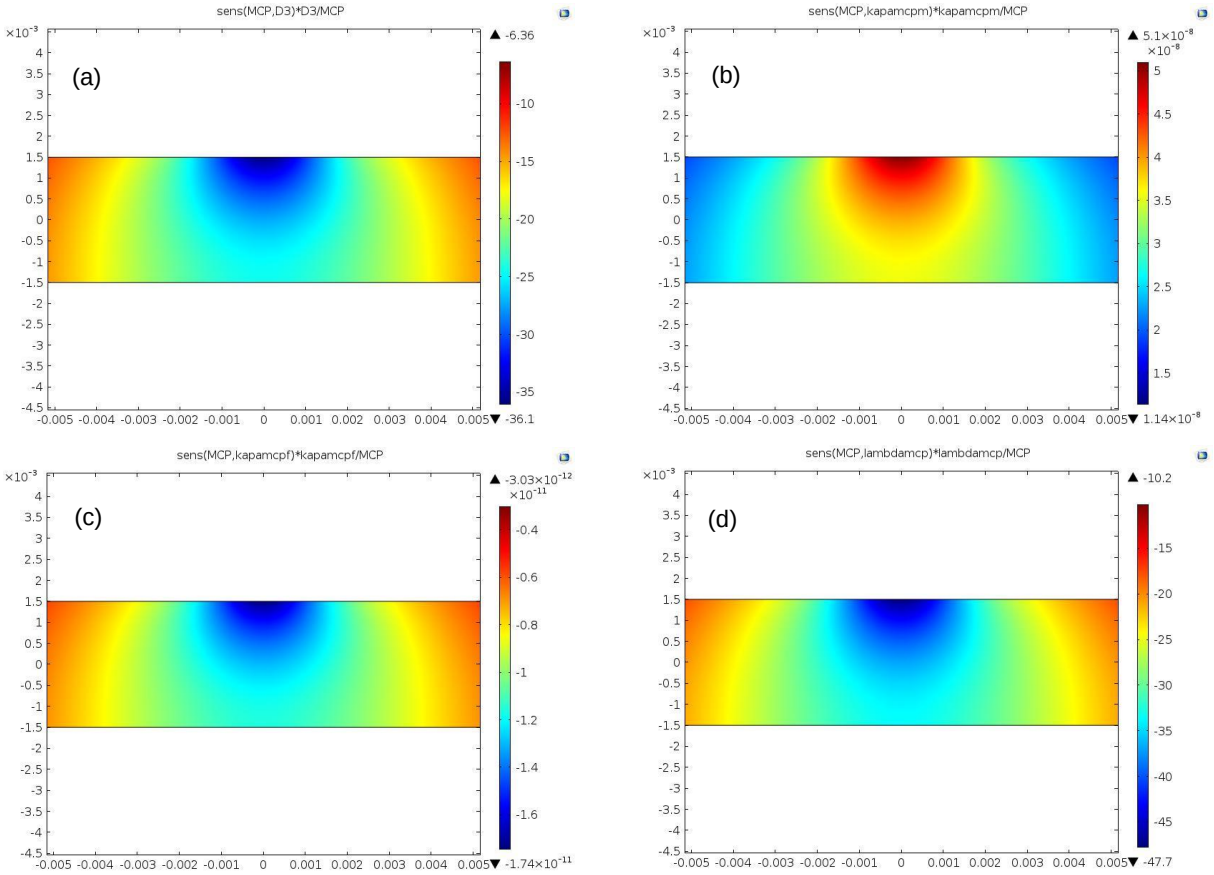

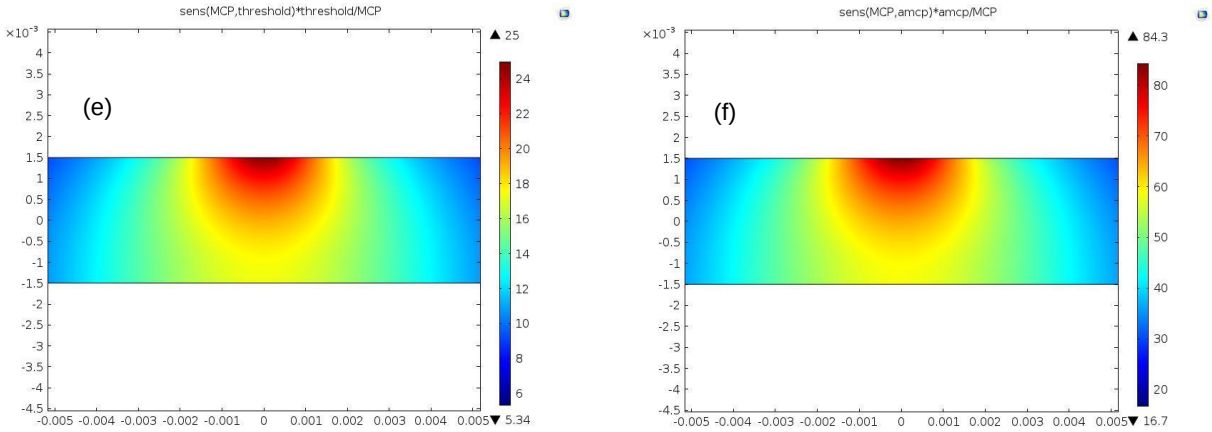

Figure E.2 – Normalized sensitivity values of MCP-1 intima concentration with respect to MCP-1 diffusion coefficient (a), MCP-1 production rate by macrophages (b) and by foam cells (c), MCP-1 degradation rate (d), threshold oxLDL concentration (e) and rate of MCP-1 activation (f).

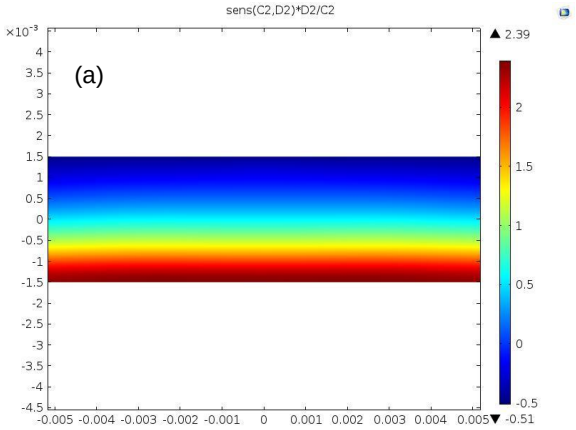
sens(C2,D2)*D2/C2
(a)
▲ 2.39
▼ -0.51

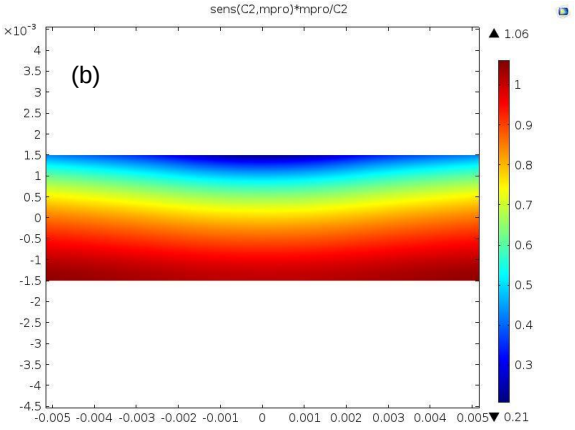
sens(C2,mpro)*mpro/C2
(b)
▲ 1.06
▼ 0.21

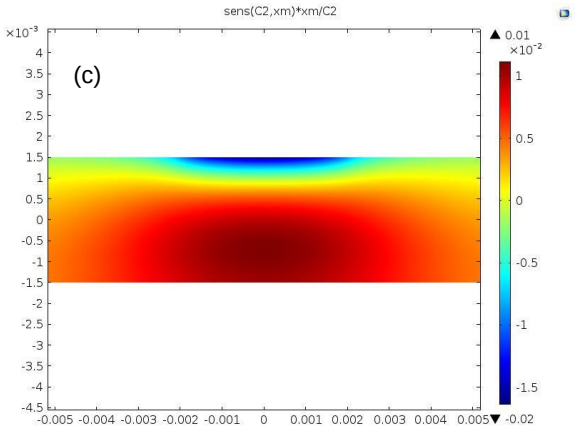
sens(C2,xm)*xm/C2
(c)
▲ 0.01
▼ -0.02

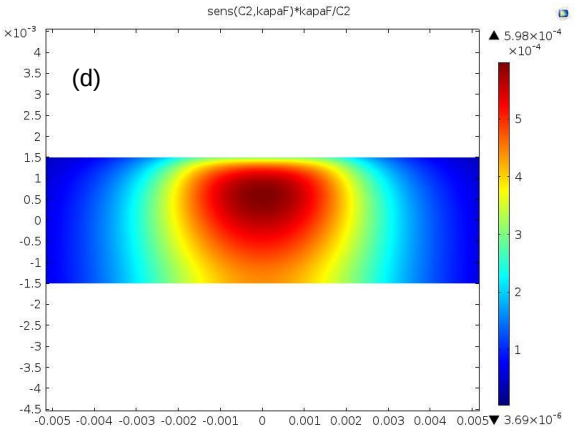
sens(C2,kapaF)*kapaF/C2
(d)
▲ 5.98×10⁻⁴
▼ 3.69×10⁻⁶

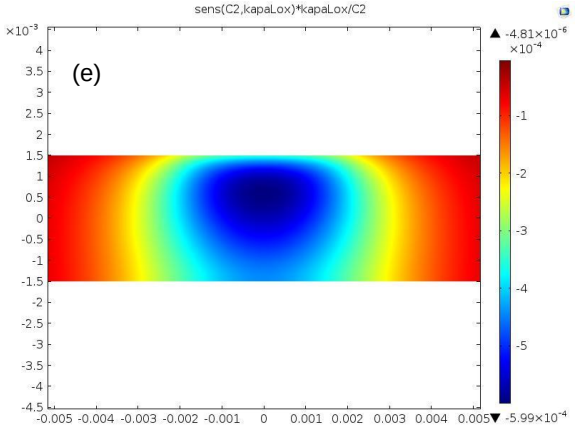
sens(C2,kapaLox)*kapaLox/C2
(e)
▲ -4.81×10⁻⁶
▼ -5.99×10⁻⁴

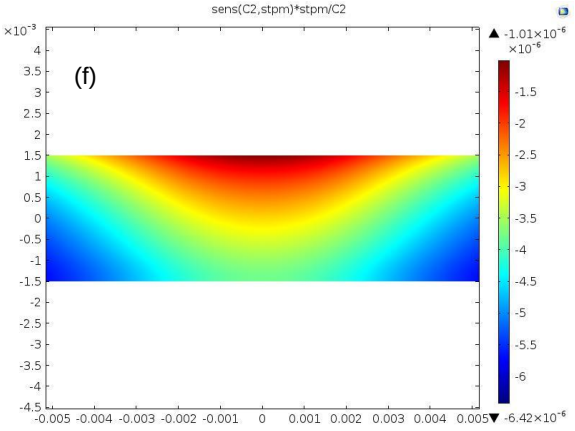
sens(C2,stpm)*stpm/C2
(f)
▲ -1.01×10⁻⁶
▼ -6.42×10⁻⁶

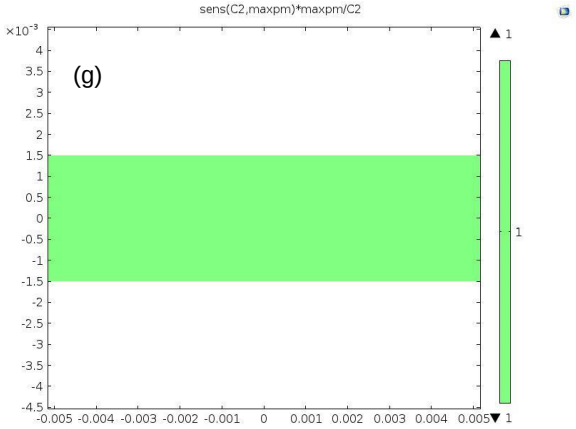
sens(C2,maxpm)*maxpm/C2
(g)
▲ 1
▼ 1

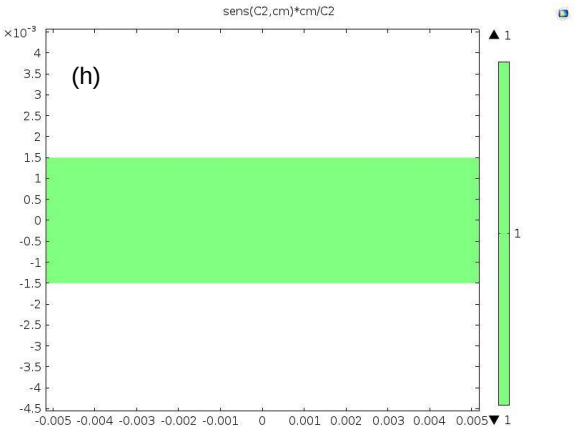
sens(C2,cm)*cm/C2
(h)
▲ 1
▼ 1

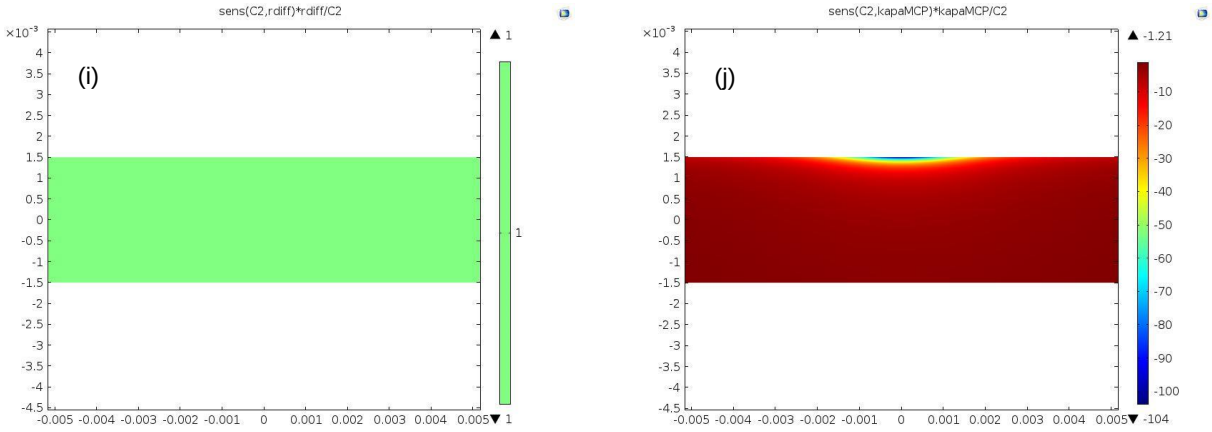

Figure E.3 – Normalized sensitivity values of macrophages intima concentration with respect to macrophages diffusion coefficient (a), proliferation rate inside the intima (b), chemotactic parameter (c), rate of foam cells formation (d), saturation rate of oxLDL uptake by one macrophage (e), standard endothelial permeability to monocytes (f), maximum endothelial permeability to monocytes (g), monocytes endothelial influx (h), monocytes differentiation rate into macrophages (i) and saturation rate of MCP-1 due to ingestion by macrophages (j).

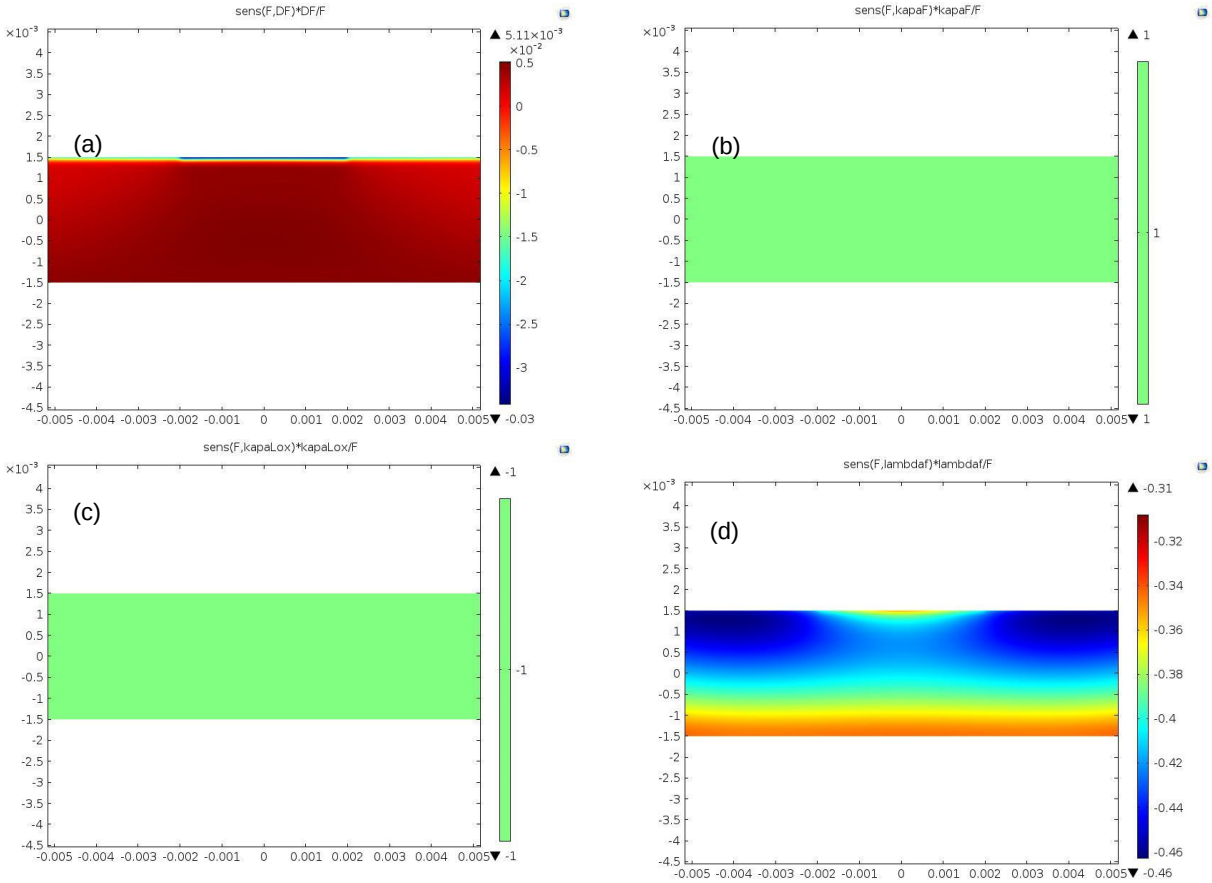

Figure E.4 – Normalized sensitivity values of foam cells intima concentration with respect to foam cells diffusion coefficient (a), rate of foam cells formation (b), saturation rate of oxLDL uptake by one macrophage (c) and foam cells degradation rate (d).

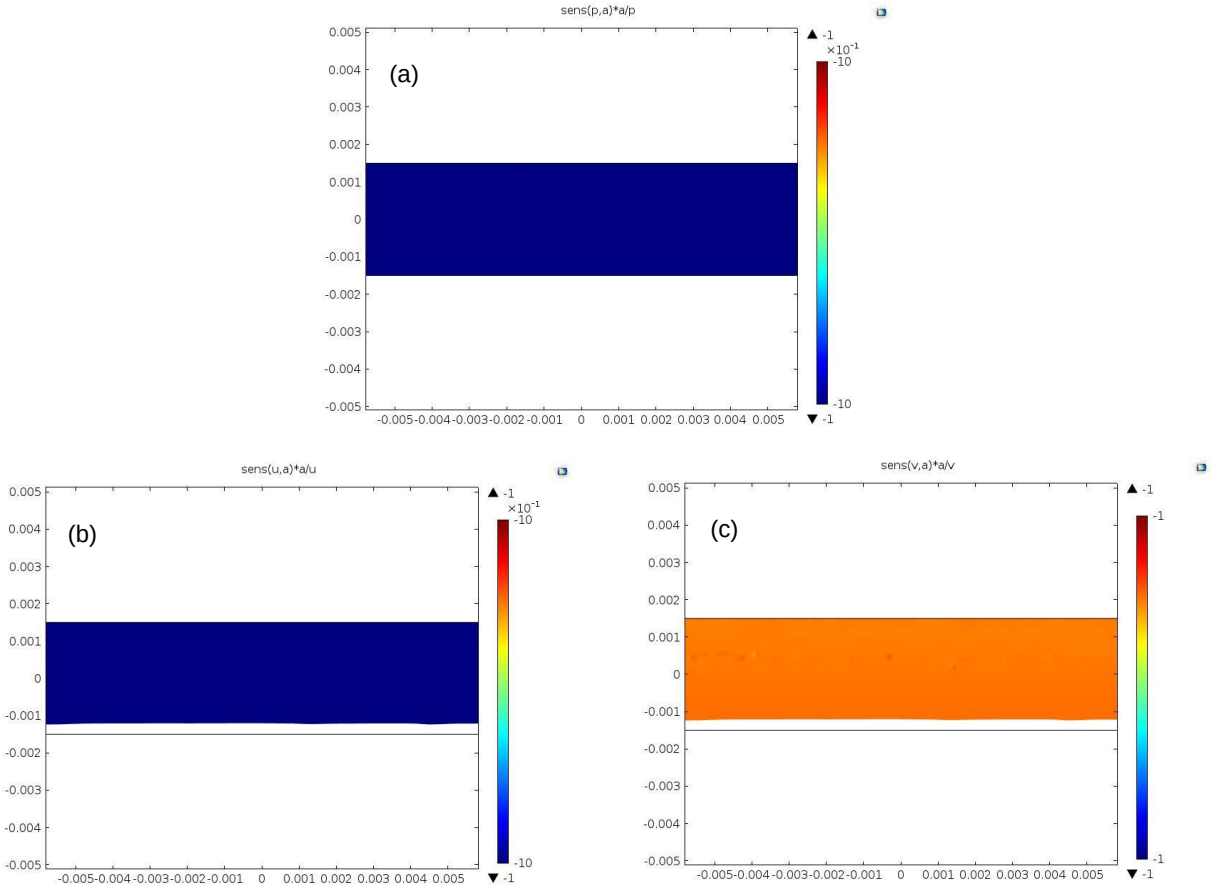

Figure E.5 – Normalized sensitivity values of plaque growth with respect to the average density inside the intima. This influence was accessed with respect to intima pressure (a) and plaque growth velocity vector, both horizontal direction (b) and vertical direction (c).